

WIND-TUNNEL INVESTIGATION OF PLUME
DISPERSION AND TRANSPORT OVER COMPLEX
TERRAIN FOR COLSTRIP POWER PLANT--
STABLE STRATIFICATION

by

R. L. Petersen¹ and J. E. Cermak²

for

Montana Power Company
40 East Broadway
Butte, Montana 59707

February 1979

CER78-79RLP-JEC39

¹Research Assistant Professor, Department of Civil Engineering, Colorado State University, Fort Collins, Colorado.

²Professor-in-Charge, Fluid Mechanics and Wind Engineering Program, Department of Civil Engineering, Colorado State University, Fort Collins, Colorado.

ABSTRACT

A wind tunnel test over a 1:5000 scale model of the terrain in the vicinity of the Colstrip Power Plant, Rosebud County, Montana was performed. The tests were conducted under stable stratification and a tracer gas was released at two effective plume altitudes (381 and 476 m prototype) approximately 5.2 m (26 km prototype) upwind of Badger and Garfield Peaks. The resulting ground level concentration patterns were measured to assess the validity of the EPA Valley Model assumption of plume impaction on elevated terrain.

The results of the study showed the Valey Model overpredicts ground level concentrations at Badger and Garfield Peaks by a factor ranging from 1.7 to 98.0 for the wind tunnel tests corresponding to Pasquill Gifford Stability Category E. Comparison of the Plume Dispersion Characteristics with the Pasquill Gifford Curves showed that the horizontal plume spread (σ_y) was one category more stable than the vertical plume spread (σ_z) and both dispersion parameters were indicative of a stable plume.

ACKNOWLEDGEMENTS

The authors wish to thank Mr. Dan Berube and Dr. Carlton Grimm from Montana Power Company for their support during this project as well as the timely suggestions by Mr. Loren Crow.

During the course of this research several graduate and undergraduate students helped on the data collection and processing phases of the projects. Special thanks go to 1) Evan Twombly for his assistance in the computer programming phase of the program, and to 2) Dave Graham and Tom Zook for their assistance in processing the data.

The authors also appreciate the help of the following Colorado State University staff members: Mr. J. A. Garrison for managing the photographic and model construction phases of the project; Mr. Jim Maxton for equipment trouble shooting and assistance in the data collection; Mrs. Eunice Felton for coordinating the typing of this report; Ms. Hanae Akari for coordinating the drafting; and Mr. Bob Beazley for data collection and reduction assistance.

TABLE OF CONTENTS

<u>Chapter</u>		<u>Page</u>
1 INTRODUCTION		1
2 SUMMARY AND CONCLUSIONS		3
3 WIND-TUNNEL SIMILARITY REQUIREMENTS		6
4 EXPERIMENTAL PROGRAM		15
4.1 Summary		15
4.2 Scale Models and Wind Tunnel		16
4.3 Flow Visualization		19
4.4 Gas Tracer Technique		20
4.5 Velocity and Temperature Measurements		23
5 STABLE BOUNDARY-LAYER RESULTS		29
5.1 General		29
5.2 Analysis of Velocity and Temperature Measurements		32
6 ANALYSIS OF PLUME DISPERSION PATTERNS		40
6.1 Wind Tunnel Results.		40
6.2 Modification of Numerical Model.		49
REFERENCES.		54
TABLES.		56
FIGURES		85
APPENDIX A: Tabulation of Concentration Measurements		127
APPENDIX B: Error Analysis		148
APPENDIX C: Valley Model Computer Outputs		154

LIST OF TABLES

<u>Table</u>	<u>Page</u>
4.1 Summary of Model Parameters for Wind-Tunnel Test.	57
4.2 Summary of Prototype Parameters for Colstrip Power Plant.	57
4.3 Summary of Wind-Tunnel Tests.	58
4.4 Sampling Grid Coordinates for:	
a) Flat terrain runs at site L with $Fr_T = 4.6$	59
b) Flat terrain runs at site G for $Fr_T = 1.8$ and 4.6 and at site L' with $Fr_T = 1.8$	59
c) 325° wind direction runs at site L with $Fr_T = 3.3$	60
d) 325° wind direction runs at site G with $Fr_T = 3.3$	60
e) 349° wind direction runs at site M' with $Fr_T = 1.9$ and 6.5	61
f) 349° wind direction runs at site G' with $Fr_T = 1.9$ and 6.5	61
5.1 EPA Stability Criteria for Colstrip Power Plant	62
5.2 Revised Stability Criteria Based on Froude Number for Colstrip Power Plant.	62
5.3 Example of Power Law Exponent Variation with Stability from a) Touma, 1967) and b) Sutton, 1953.	63
5.4 Velocity Profiles for 352° Wind Direction and $Fr_T = 3.3$	64
5.5 Summary of Similarity Theory Analysis of Velocity Profiles for the 325° Wind Direction and an Fr at 10 cm (Location A) of 2.0	66
5.6 Velocity Profiles for 349° Wind Direction and $Fr_T = 1.0$	67
5.7 Summary of Similarity Theory Analysis of Velocity Profiles for the 349° Wind Direction and an Fr at 10 cm (Location A) of 1.5	69

<u>Table</u>	<u>Page</u>
5.8 Velocity Profiles for 349° Wind Direction and $Fr_T = 6.5$	70
5.9 Summary of Similarity Theory Analysis of Velocity Profiles for the 349° Wind Direction and an Fr at 10 cm (Location A) of 3.9	72
5.10 Flat Terrain Velocity Profiles for $Fr_T = 1.9$	73
5.11 Summary of Similarity Theory Analysis of Velocity Profiles for Flat Tunnel and an Fr at 10 cm (Location A) of 2.2	74
5.12 Flat Terrain Velocity Profiles for $Fr_T = 4.6$	75
5.13 Summary of Similarity Theory Analysis of Velocity Profiles for Flat Tunnel and an Fr at 10 cm (Location A) of 2.7	76
6.1 Summary of Concentration Measurements.	77
6.2 Height of Plume (h) Relative to Release Height (H) at Locations G and L	78
6.3 Ratio of Maximum Aerial Concentration (K_H) to Maximum Ground-Level Concentration (K_g) and the Associated Model and Full-scale Conditions	79
6.4 Predicted Correction Factor (K_o/K_g) for Ground Level Measurements as a Function of σ_z , z_g and h	80
6.5 Ratio of Maximum Ground Level Concentrations (Dimensionless) with and without Terrain for Similar Stabilities (Froude Numbers)	81
6.6 Comparison of Maximum Observed Dimensionless Concentration with that Predicted Using the Gaussian Model	82
6.7 Valley Model Computed Concentrations with Associated Model Inputs and the Corrected Concentration Based on Wind-Tunnel Results for E Stability (Gas Temperature Equals 361°K)	83
6.8 Valley Model Computed Concentrations with Associated Model Inputs and the Corrected Concentration Based on Wind-Tunnel Results for D Stability (Gas Temperature Equals 361°K; $\sigma_z = 240$ m)	84

LIST OF FIGURES

<u>Figure</u>		<u>Page</u>
4.2-1	Topographic Map of the Area Modeled in the Wind Tunnel for the 349° Wind Direction (Badger Peak)	86
4.2-2	Topographic Map of the Area Modeled in the Wind Tunnel for the 325° Wind Direction (Garfield Peak)	87
4.2-3	Picture of Wood Frame and Attached Fans to which the Aluminum Sheets were Fixed that Conform with the Topography	88
4.2-4	Picture of Probe from which Smoke and Trace Gas were Released	89
4.2-5	Meteorological Wind Tunnel, Fluid Dynamics and Diffusion Laboratory, Colorado State University	90
4.2-6	Three-Dimensional Sketch of Wind-Tunnel Configuration for the Stable Boundary-Layer Tests	91
4.3-1	Camera Setup for the Stable Boundary-Layer Tests of Colstrip Power Plant	92
4.4-1	Photograph of Sampling Rake used to Withdraw Gas from the Wind Tunnel	93
4.4-2	Photograph of Flame Ionization Gas Chromatograph and Gas Sampling System	94
4.5-1	Typical Calibration Curves for Hot-Film Sensor (Matheson Linear Flow Meter was used as Calibration Standard)	95
4.5-2	Values and Location of Surface Temperature (°C) on the Aluminum Shell Model for Wind Tunnel Conditions Set During Runs 3 and 4	96
5.2-1	Dimensionless Velocity Profiles for the 325° Wind Direction (Garfield Peak) and a Fr_T of 3.3	97
5.2-2	Vertical Profiles of Longitudinal Turbulence Intensity for the 325° Wind Direction (Garfield Peak) and Fr_T of 3.3	98
5.2-3	Vertical Profile of Froude Number for the 325° Wind Direction (Garfield Peak) and a Fr_T of 3.3	99

<u>Figure</u>		<u>Page</u>
5.2-4	Dimensionless Velocity Profiles for the 349° Wind Direction (Badger Peak) and a Fr_T of 1.9	100
5.2-5	Vertical Profiles of Longitudinal Turbulence Intensity for the 349° Wind Direction (Badger Peak) and a Fr_T of 1.9	101
5.2-6	Vertical Profiles of Froude Number for the 349° Wind Direction (Badger Peak) and a Fr_T of 1.9	102
5.2-7	Dimensionless Velocity Profile for the 349° Wind Direction (Badger Peak) and a Fr_T of 6.3	103
5.2-8	Vertical Profiles of Longitudinal Turbulence Intensity for the 349° Wind Direction (Badger Peak) and Fr_T of 6.3	104
5.2-9	Vertical Profiles of Froude Number for the 349° Wind Direction (Badger Peak) and a Fr_T of 6.3	105
5.2-10	Dimensionless Velocity Profiles for the Flat Terrain Case and a Fr_T of 1.8	106
5.2-11	Vertical Profile of Longitudinal Turbulence Intensity for the Flat Terrain Case and a Fr_T of 1.8	107
5.2-12	Vertical Profile of Froude Number for the Flat Terrain Case and a Fr_T of 1.8	108
5.2-13	Dimensionless Velocity Profiles for the Flat Terrain Case and a Fr_T of 4.6	109
5.2-14	Vertical Profiles of Longitudinal Turbulence Intensity for the Flat Terrain Case and a Fr_T of 4.6	110
5.2-15	Vertical Profile of Froude Number for the Flat Terrain Case and a Fr_T of 4.6	111
6.1-1	Plume Visualization for 325° Wind Direction (Badger Peak). $Fr_T = 3.3$ and a Release Height of a) 7.6 cm (381 m prototype), b) 9.5 cm (476 m prototype)	112

<u>Figure</u>		<u>Page</u>
6.1-2	Plume Visualization for the 349° Wind Direction (Garfield Peak), $Fr_T = 1.9$ and a Release Height of a) 7.6 cm (381 m prototype), b) 9.5 cm (476 m prototype)	113
6.1-3	Plume Visualization for 349° Wind Direction (Badger Peak), $Fr_T = 6.5$ and a Release Height of a) 7.6 cm (381 m prototype), b) 9.5 cm (476 m prototype)	114
6.1-4	Plume Visualization for Flat Terrain, $Fr_T = 4.6$ and a Release Height of a) 7.6 cm (381 m prototype), b) 9.5 cm (476 m prototype)	115
6.1-5	Plume Visualization for Flat Terrain, $Fr_T = 1.8$ and a Release Height of a) 7.6 cm (381 m prototype), b) 9.5 cm (476 m prototype)	116
6.1-6	Plot of Observed σ_z Values in Comparison to the Pasquill-Gifford Curves for Low Fr Cases	117
6.1-7	Plot of Observed σ_z Values in Comparison to Pasquill-Gifford Curves for High Fr Cases	118
6.1-8	Plot of Observed σ_y Values in Comparison to Pasquill-Gifford Curves for Low Fr Cases	119
6.1-9	Plot of Observed σ_y Values in Comparison to Pasquill-Gifford Curves for High Fr Cases	120
6.1-10	Isopleths of $\sigma_z(z_0)/\sigma_z(z_0 = 10 \text{ cm})$, Virtually Independent of Heat Flux Based on Pasquill (1974)	121
6.1-11	Plot of Plume Height Range ($Z_{\max} \rightarrow \bar{Z}$) versus Downwind Distance for the 349° Wind Direction and an Fr_T of 1.8	122
6.1-12	Plot of Plume Height Range ($\bar{Z} \rightarrow Z_{\max}$) versus Downwind Distance for the 349° Wind Direction and an Fr_T of 6.3	123

<u>Figure</u>	<u>Page</u>
6.1-13 Plot of Plume Height Range ($Z_{\max} \rightarrow \bar{Z}$) versus Downwind Distance for the 325° Wind Direction and an Fr_T of 1.9	124
6.1-14 Plot of Plume Height Range ($\bar{Z} \rightarrow Z_{\max}$) versus Downwind Distance for the Flat Terrain Case with an Fr_T of 1.8	125
6.1-15 Plot of Plume Height Range ($\bar{Z} \rightarrow Z_{\max}$) versus Downwind Distance for the Flat Terrain Case with Fr_T of 4.6	126

LIST OF SYMBOLS

<u>Symbol</u>	<u>Definition</u>	<u>Units</u>
A	Hot film calibration constant	(-)
B	Hot film calibration constant	(-)
C_p	Specific heat at constant pressure	($\text{m}^2 \text{s}^{-2} \text{°K}^{-1}$)
d	Diameter of hot film	(m)
D	Stack diameter	(m)
E	Hot-film voltage	(V)
E_c	Eckert number $[u_o^2 / (C_{p_o} \Delta T_o)]$	(-)
F_L	Lagrangian spectral function	(s)
Fr	Ambient Froude number $\left[\frac{u(z)}{\sqrt{\frac{g}{T} \frac{\Delta \theta}{\Delta z}} z} \right]$	(-)
Fr_a	Stack Froude number $\left[\frac{u_a}{\sqrt{g \gamma D}} \right]$	(-)
Fr_T	Froude number at top of meteorological tower	$\left[\frac{u_T}{\sqrt{\frac{g}{T} \frac{\Delta \theta}{\Delta z}} z_T} \right]$ (-)
g	Acceleration due to gravity	(ms^{-2})
Gr	Grashof number $\left[\frac{g d^3 (T_w - T_g)}{\nu^2 T_g} \right]$	(-)
h	Height of plume above ground-level	(m)
H	Effective plume altitude and release height	(m)
i_x	Turbulence intensity in x direction [u'/u]	(-)
I	Current through wire	(a)
k	Thermal conductivity	($\text{Wm}^{-1} \text{°K}^{-1}$)
K	Dimensionless concentration $\left[\frac{x u_H H^2}{x_o V} \right]$	(-)

<u>Symbol</u>	<u>Definition</u>	<u>Units</u>
ℓ	Length of hot film	(m)
L	Length scale or Monin Obukhov Length Scale	(m)
n	Frequency, power law exponent or Kings Law exponent	(varies)
Nu	Nusselt number	(-)
P	Pressure	(Pa)
Pr	Prandtl number $\left[\frac{v_o \rho_o C_p o}{k_a} \right]$	(-)
Q_m	Emission rate	(g/s)
R	Velocity ratio $[u_s / u_H]$	(-)
R_c	Hot resistance at calibration conditions	(Ω)
Re	Reynolds number $\left[\frac{L_o u_o}{v_o} \right]$	(-)
R_H	Film hot resistance	(Ω)
Ri	Richardson number $\frac{g}{T} \left[\frac{\frac{\partial \theta}{\partial z}}{\left(\frac{\partial u}{\partial z} \right)^2} \right]$	(-)
Ro	Rossby number $\left[\frac{L_o \Omega_o}{u_o} \right]$	(-)
R_o	Film resistance at reference conditions	(-)
$R(\tau)$	Autocorrelation	(-)
t, τ, ξ	Time or time scales	(s)
T, θ	Temperature or potential temperature	(°K)
t_1	Center of gravity of autocorrelation curve	(s)
t_o	Integral time scale	(s)
u	Ambient velocity	(m/s)
u_H	Ambient velocity at release height, H	(m/s)
u_s	Stack exit velocity	(m/s)

<u>Symbol</u>	<u>Definition</u>	<u>Units</u>
u_T	Ambient velocity at top of meteorological tower	(m/s)
u_*	Friction velocity	(m/s)
V	Volume flow	($m^3 s^{-1}$)
w	Uncertainty interval	(varies)
x, y, z	Cartesian coordinates	(m)
z_m	Matching height $\left(\frac{z_2 - z_1}{\ln z_2/z_1} \right)$	(m)
\bar{z}	Center of mass	(m)
z_{max}	Height of maximum concentration above ground level	(m)

Greek Symbols

α	Thermal coefficients of resistance	($\Omega / {}^\circ K$)
χ	Concentration	(ppm)
χ_o	Source strength	(ppm)
γ	Density ratio $\left[\frac{\rho_a - \rho_s}{\rho_a} \right]$	(-)
Λ	Length scale	(m)
ν	Kinematic viscosity or angle between plume axis and a horizontal plane	($m^2 s^{-1}$)
Ω	Angular velocity	(s^{-1})
Φ^*	Dissipation term	(-)
ρ	Density	($g m^{-3}$)
σ_z, σ_y	Vertical and horizontal standard deviation of concentration distribution	(m)

<u>Symbol</u>	<u>Definition</u>
<u>Subscripts</u>	
a	Pertaining to ambient conditions
H	Pertaining to reference height H
i,j,k	Tensor or summation indices
m	Model
o	General reference quantity or initial condition
p	Prototype
r	Reference quantity
s	Pertaining to stack exit conditions
wo	Without terrain present
w	With terrain present
∞	Free stream
<u>Superscripts</u>	
'	Root-mean-square of quantity
*	Dimensionless parameter

Wind-Tunnel Investigation of Plume Dispersion
and Transport over Complex Terrain
for Colstrip Power Plant--Stable Stratification

1 INTRODUCTION

The Colstrip Power Plant (CPP) is located in Rosebud County, Montana about 20 km north of the Northern Cheyenne Indian Reservation. At the present time Montana Power Company (MPC) and Puget Sound Power and Light (PSPL) have a coal-fired power plant with two units operating for a total capacity of 716 MW (gross). MPC, PSPL, Washington Water Power, Portland General Electric and Pacific Power and Light have requested permission to build and operate two new units at Colstrip with an added capacity of 1400 MW (net). In order for construction of these new units to be permitted these companies have had to demonstrate that ambient air quality would not be significantly deteriorated and also that air quality standards would be met.

A numerical modeling effort by Region VIII EPA (Denver, Colorado) showed that the Class I increment for SO_2 of $25 \mu\text{g}/\text{m}^3$ would be exceeded on Badger and Garfield Peaks under stable stratification unless very stringent emission reductions were effected by the utility group. The model used by EPA which is referred to as the Valley Model (Burt, 1976) is recognized as being conservative (i.e., predicts high) since it assumes that the plume centerline does not rise with the terrain but remains at a constant altitude and impinges on encountered high terrain for stable stratification. In spite of the conservativeness of the numerical model MPC has tentatively agreed to meet the emission limitations as estimated with this model with the option to revise the emission limits based on the results of a more sophisticated modeling effort which is the subject of this report.

Hence, it is the purpose of this study to evaluate the validity of the Valley Model assumption of plume impaction on elevated terrain through physical modeling in a wind tunnel and develop appropriate correction factors for the Valley Model. Specifically the goal is to simulate Pasquill Stability Class E and measure the resulting concentrations at Badger and Garfield Peaks on a 1:5000 scale model of the terrain in the vicinity of CPP. The results desired are: 1) determine whether the plume impinges on or goes over the terrain, and 2) determine a correction factor to modify the Valley Model prediction to account for enhanced dispersion in rugged terrain and/or added plume rise due to streamline movement over the terrain.

Included in this report are 1) summary and conclusions, 2) description of the similarity requirements for modeling the stable boundary layer, 3) experimental methods, 4) discussion of the results of the stable boundary-layer simulation, and 5) evaluation of the plume transport and diffusion patterns over the scale model.

2 SUMMARY AND CONCLUSIONS

Wind-tunnel tests of the transport and diffusion of plumes released at two effective plume altitudes (381 and 476 m, AGL--prototype) were conducted using 1:5000 scale models of the terrain for two wind directions (325 and 349°). The terrain model was constructed of aluminum sheets so that the surface could be cooled and thereby generate a stable boundary layer. In addition to cooling the terrain surface, the approach boundary layer was developed naturally over a 10.4 m upwind fetch of cooling plates. A second series of tests were conducted without the terrain model with a flat tunnel floor. These cases were to be used to compare the transport and dispersion patterns with and without the terrain.

To document the flow field a series of velocity and temperature profiles were taken along and lateral to the center of the wind-tunnel test section over the modeled terrain. The flow stability was measured by computing a Froude number which relates full-scale and model conditions.

A series of ground level and aerial concentration measurements were obtained at the location of Badger and Garfield Peaks in addition to another series of measurements at an intermediate location between the plant site and the high terrain. Photographs of all simulated conditions were obtained to document the plume transport characteristics.

The following summarizes the results of the study.

- The velocity and temperature profiles were indicative of a stable boundary layer. Each test condition was categorized by a Pasquill-Gifford Stability Class. The method of categorization entailed equating Froude numbers in model and prototype over an equivalent layer and assigning a stability class to the wind-tunnel results based on

Froude number categories for the atmosphere. Two cases of Pasquill-Gifford E and one of D stability were simulated when the modeled terrain was present. Without the terrain both cases were classed as an E stability with one case on the borderline of D.

- The plume dispersion parameters (σ_y and σ_z) were dependent on the Froude number and hence the simulated stability class. The horizontal dispersion values (σ_y) for those cases classed as E stability clustered around the Pasquill-Gifford E and F lines whereas the corresponding vertical dispersion results (σ_z) fell along the Pasquill-Gifford D and E lines. The σ_y values for the cases classed as D stability (or close to D) fell along the Pasquill-Gifford E and F lines whereas the σ_z values fell along the D line. In general, the vertical dispersion coefficients were found to be one stability category less stable than the horizontal dispersion coefficients. This result is expected since the roughness in the model and prototype will enhance vertical mixing.

- The plume rise, as measured by the average of the center of mass and height above ground of the peak value, did not remain at a constant altitude with respect to mean sea level but tended to rise with the terrain. The ratio (h/H) of plume height above ground level (h) to initial release height (H) ranged from 0.36 to 0.71 for the 7.6 cm (381 m prototype) releases and 0.65 and 0.82 for the 9.5 cm (476 m prototype) releases. For the same cases the Valley Model would have used ratios for respective release heights of 7.6 and 9.5 cm equal to 0.06 and 0.25 for the Badger Peak predictions and 0.14 and 0.32 for the Garfield Peak predictions.

- The ratio of maximum centerline concentration to maximum ground level concentration ranged from 1.0 to 3.75 for the 7.6 cm

(381 m prototype) releases and from 1.5 to 98.0 for the 9.5 cm (476 m prototype) releases. As expected, the lowest ratios (1.0 and 1.5) were observed for the case that was classed as D stability. For neutral conditions the vertical spread rate is greater and the plume becomes uniformly mixed. Using Brigg's (1974) plume equations respective wind speeds of 15.2 and 9.7 m/s are required to obtain plume altitudes of 381 and 476 m. At these speeds the concentration levels on Badger and Garfield Peaks are less than $1 \mu\text{g}/\text{m}^3$. For the stable cases (E stability) the ratio of maximum centerline to maximum ground level concentration as predicted by the Valley Model would be nearly equal to 1 for the Badger and Garfield Peak predictions. The observed ratios in the wind tunnel varied from 1.7 to 98.0.

In conclusion the results of this study show that the Valley Model overestimates ground-level concentrations for E stability on Badger Peak by a factor of 1.7 for a 381 m effective plume altitude and 5.34 for a 476 m effective plume altitude. For the Garfield Peak predictions (E stability) the Valley Model overpredicts by a factor of 3.75 for a 381 m effective plume altitude and 98.0 for a 476 m effective plume altitude.

3 WIND-TUNNEL SIMILARITY REQUIREMENTS

The basic equations governing atmospheric and plume motion (conservation of mass, momentum and energy) may be expressed in the following dimensionless form (Cermak, 1974):

$$\frac{\partial \rho^*}{\partial t} + \frac{\partial (\rho^* u_i^*)}{\partial x_i^*} = 0, \quad 3.1$$

$$\begin{aligned} \frac{\partial u_i^*}{\partial t^*} + u_j^* \frac{\partial u_i^*}{\partial x_j^*} - \left[\frac{L_o \Omega_o}{u_o} \right] 2\epsilon_{ijk} \Omega_j^* u_k^* &= \\ - \frac{\partial p^*}{\partial x_i^*} - \left[\frac{\Delta T_o L_o g_o}{T_o u_o^2} \right] \Delta T^* g^* \delta_{i3} & \\ + \left[\frac{v_o}{u_o L_o} \right] \frac{\partial^2 u_i^*}{\partial x_k^* \partial x_k^*} + \frac{\partial}{\partial x_i^*} - \overline{u'_i u'_j} & \end{aligned} \quad 3.2$$

and

$$\begin{aligned} \frac{\partial T^*}{\partial t^*} + u_i^* \frac{\partial T^*}{\partial x_i^*} &= \left[\frac{k_o}{\rho_o C_p v_o} \right] \left[\frac{v_o}{L_o u_o} \right] \frac{\partial^2 T^*}{\partial x_k^* \partial x_k^*} \\ + \frac{\partial}{\partial x_i^*} \overline{\theta' u'_i} + \left[\frac{v_o}{u_o L_o} \right] \left[\frac{u_o^2}{C_p (\Delta T)_o} \right] \phi^* &. \end{aligned} \quad 3.3$$

The dependent and independent variables have been made dimensionless (indicated by an asterisk) by choosing appropriate reference values.

For exact similarity, the bracketed quantities and boundary conditions must be the same in the wind tunnel and in the plume as they are in the corresponding full-scale case. The complete set of requirements for similarity is:

- 1) Undistorted geometry
- 2) Equal Rossby number: $\text{Ro} = u_o / (L_o \Omega_o)$
- 3) Equal gross Richardson number: $\text{Ri} = \Delta T_o g L_o / T_o u_o^2$

- 4) Equal Reynolds number: $Re = u_o L_o / v_o$
- 5) Equal Prandtl number: $Pr = (v_o \rho_o C_{p_o}) / k_o$
- 6) Equal Eckert number: $Ec = u_o^2 / [C_{p_o} (\Delta T)_o]$
- 7) Similar surface-boundary conditions
- 8) Similar approach-flow characteristics.

All of the above requirements cannot be simultaneously satisfied in the model and prototype. However, some of the quantities are not important for the simulation of many flow conditions. The parameters which can be neglected for this study and those which are important will now be discussed in detail.

- Neglected Parameters

For this study equal Reynolds number for model and prototype is not possible since the viscosities of the transport fluids are at most different by a factor of ten and the length scaling is 1:5000. This inequality is not a serious limitation. The Reynolds number related to the stack exit is defined by

$$Re_s = \frac{u_s D}{v_s} .$$

Hoult and Weil (1972) reported that plumes appear to be fully turbulent for exit Reynolds numbers greater than 300. Their experimental data show that the plume trajectories are similar for Reynolds numbers above this critical value. In fact, the trajectories appear similar down to $Re_s = 28$ if only the buoyancy dominated position of the plume trajectory is considered. Hoult and Weil's study was in a laminar cross flow (water tank) with low ambient turbulence levels and hence the rise and dispersion of the plume would be predominantly dominated by the plume's

own self-generated turbulence. These arguments for Reynolds number independence only apply to plumes in low ambient turbulence or to the initial stage of plume rise where the plume's self-generated turbulence dominates.

For similarity in the region dominated by ambient turbulence consider Taylor's (1921) relation for diffusion in a stationary homogeneous turbulence

$$\sigma_z^2(t) = \overline{w'^2} \int_0^\xi \int_0^t R(\xi) d\xi dt \quad 3.4$$

which can be simplified to (see Csanady, 1973)

$$\sigma_z^2(t) \approx \overline{w'^2} t^2 \approx i_z^2 x^2 \quad 3.5$$

for short travel times; or,

$$\sigma_z(t) = \sqrt{\overline{w'^2}} t_o(t-t_1); \quad 3.6$$

for long travel times where

$$t_o = \int_0^\infty R(\tau) d\tau \quad 3.7$$

is an integral time scale and

$$t_1 = \frac{1}{t_o} \int_0^\infty \tau R(\tau) d\tau \quad 3.8$$

is the center of gravity of the autocorrelations curve. Hence for geometric similarity at short travel times,

$$\frac{[\sigma_z^2]_m}{[\sigma_z^2]_p} = \frac{[L^2]_m}{[L^2]_p} = \frac{[i_z^2 x^2]_m}{[i_z^2 x^2]_p}$$

or,

$$[i_z]_m = [i_z]_p .$$

3.9

For similarity at long travel times

$$\begin{aligned} \frac{L_m^2}{L_p^2} &= \frac{[\sigma_z^2]_m}{[\sigma_z^2]_p} = \frac{\overline{w'^2 t_o(t-t_1)}_m}{\overline{w'^2 t_o(t-t_1)}_p} \\ &= \frac{[i_z^2]_m}{[i_z^2]_p} \frac{[t_o(t-t_1)/u^2]_m}{[t_o(t-t_1)/u^2]_p} = \frac{[Li_z^2 \Lambda]_m}{[Li_z^2 \Lambda]_p} \end{aligned}$$

if it is assumed $t_1 \ll t$, $t_o/u = \Lambda$ and $t/u = L$. Thus the turbulence length scales must scale as the ratio of the model to prototype length scaling if $(i_z)_m = (i_z)_p$ or,

$$\frac{L_m}{L_p} = \frac{\Lambda_m}{\Lambda_p} . \quad 3.10$$

An alternate way of evaluating the similarity requirement is by putting 3.4 in spectral form or (Snyder, 1972),

$$\sigma_z^2 = \overline{w'^2 t^2} \int_0^\infty F_L(n) \left[\frac{\sin \pi n t}{\pi n t} \right]^2 dn = \overline{w'^2 t^2} I \quad 3.11$$

where

$$I = \int_0^\infty F_L(n) \left[\frac{\sin \pi n t}{\pi n t} \right]^2 dn$$

F_L = Langrangian spectral function.

The quantity in brackets is a filter function the form of which can be seen in Pasquill (1974). In brief for $n > \frac{1}{t}$ the filter function is very small and for $n < \frac{1}{10t}$ virtually unity.

For geometric similarity of the plume the following must be true:

$$\frac{L_m^2}{L_p^2} = \frac{[\sigma_z^2]_m}{[\sigma_z^2]_p} = \frac{\overline{[w'^2 t^2 I]}_m}{\overline{[w'^2 t^2 I]}_p} = \frac{[L^2 i_z^2 I]_m}{[L^2 i_z^2 I]_p}$$

or

$$\frac{[i_z^2 I]_m}{[i_z^2 I]_p} = 1 \quad 3.12$$

If $[i_z]_m = [i_z]_p$ the requirement is $I_m = I_p$. For short travel times the filter function is essentially equal to one; hence, $I_m = I_p = 1$ and the same similarity requirement as previously deduced for short travel times is obtained (equation 3.9).

For long travel times the larger scales (smaller frequencies) of turbulence progressively dominate the dispersion process. If the spectra in the model and prototype are of a similar shape then similarity would be achieved. However for a given turbulent flow a decrease in Reynolds number (hence wind velocity) decreases the range (or energy) of the high frequency end of the spectrum. Fortunately, due to the nature of the filter function, the high frequency (small wavelength) components do not contribute significantly to the dispersion. There would be, however, some critical Reynolds number below which too much of the high frequency turbulence is lost. If a study is run with a Reynolds number in this range similarity may be impaired. To evaluate whether geometric similarity of the plumes was achieved for this study the σ_y and σ_z values obtained in the wind tunnel were compared with those quoted as being representative of atmospheric dispersion rates (Slade, 1968). If the model σ_y and σ_z values compare well for the corresponding atmospheric flow the inference is that Reynolds number independence was achieved.

The ambient flow field affects the plume trajectories and consequently similarity of this field between model and prototype is required. The mean flow field will become independent of Reynolds number if the flow is fully turbulent. The critical Reynolds number for this criteria to be met is based on the work of Nikuradse as summarized by Schlichting (1968) and Sutton (1953) and is given by

$$(Re)_{k_s} = \frac{k_s u^*}{v} > 75.$$

or assuming $k_s = 30 z_o$

$$Re_{z_o} = \frac{z_o u^*}{z} > 2.5.$$

In this relation k_s is a uniform sand grain height and z_o is the surface roughness factor. Re_{z_o} values were computed and will be discussed in section 5.

The Rossby number Ro is a quantity which indicates the effect of the earth's rotation on the flow field. In the wind tunnel equal Rossby numbers between model and prototype cannot be achieved. The effect of the earth's rotation becomes significant if the distance scale is large. Snyder (1972) puts a conservative cutoff point at 5 km for diffusion studies. For length scales above this value the Rossby number should be considered. For this particular study, the maximum range over which the plume is transported is 26 km in the horizontal and 1.0 km in the vertical. Hence the earth's rotation may effect plume transport and dispersion but was neglected for this study. Since the purpose of this study was to evaluate the validity of the Valley Model calculations on elevated terrain and the Valley Model does not consider Ro influences, neglecting this parameter is justified.

When equal Richardson numbers are achieved, equality of the Eckert number between model and prototype cannot be attained. This is not a serious compromise since the Eckert number is equivalent to a Mach number squared. Consequently, the Eckert number is small compared to unity for laboratory and atmospheric flows.

- Relevant Parameters

Since air is a transport medium in the wind tunnel and the atmosphere, near equality of the Prandtl number is assured. The stack Froude number is defined by

$$Fr_a = \frac{u_a}{\sqrt{g\gamma D}}$$

where

$$\gamma = \frac{\rho_a - \rho_s}{\rho_a} .$$

Although Fr_a does not specifically appear in the list of similarity parameters it can be thought of as a modified Richardson number for the stack gas. Thus, if Fr_a is set equal for model and prototype, the following relation between model and prototype velocity is obtained:

$$\frac{(u_a)_m}{(u_a)_p} = \frac{(D\gamma)_m^{1/2}}{(D\gamma)_p^{1/2}}$$

From this equation it can be seen that for typical atmospheric flows (on the order of 5-10 m/sec) low speeds (0.1-0.2 m/sec) in the wind tunnel will be required (assuming $D_m/D_p = 1/5000$ and $\gamma_m/\gamma_p = 2.7$). Quantitative measurements at these speeds especially of the turbulence quantities are difficult to obtain. Consequently it was decided to not model the plume rise for this study. Instead the gas was released at two effective plume altitudes as specified by MPC.

For simulating stable atmospheric conditions equality of the Richardson number between model and prototype is required. The bulk Richardson number is defined by

$$R_i = \frac{g}{\bar{T}} \frac{\left(\frac{\Delta T}{\Delta z} + \Gamma \right)}{\left(\frac{\Delta u}{\Delta z} \right)^2} .$$

However since measurements of Δu at low wind speeds are subject to large errors a better similarity parameter is the gross Richardson number which is the square of the reciprocal of an atmospheric Froude number defined by

$$Fr = \frac{u(z)}{z \sqrt{\frac{g}{\bar{T}} \left(\theta(z) - \theta_0 \right)}}$$

where

$u(z)$ = velocity at height z

$\theta(z)$ = potential temperature at z

θ_0 = potential temperature at $z = 0$

\bar{T} = average temperature between z and $z = 0$

For similarity of two stable flow fields

$$Fr_m = Fr_p .$$

The Fr categories used to define stability classes in the wind tunnel which correspond to those in the atmosphere are discussed in section 5.

To summarize, the following criteria were applied for the stable boundary-layer simulation:

- 1) $Fr_m = Fr_p$
- 2) Similar geometric dimensions

- 3) Sufficiently high Reynolds number to insure fully turbulent flow field and scaled plume geometry
- 4) Equality of dimensionless boundary condition (i.e., velocity and temperature profiles).

4 EXPERIMENTAL PROGRAM

4.1 Summary

The objective of this study is to evaluate the transport and diffusion of a plume released upwind of Garfield and Badger Peaks for Pasquill stability E. To meet this objective a 1:5000 scale model of the terrain extending from the Colstrip plant site (approximately 3 km upwind) beyond the peak in question was constructed. A stable boundary layer was developed naturally over the scale topography and tracer gas releases were made in the wind tunnel at two effective plume altitudes (381 m and 476 m in the prototype). The initial stage of plume rise was not simulated because 1) a direct simulation would have required unreasonably low tunnel operating speeds, 2) the model stack exit Reynolds number would have been below the critical value for similarity, and 3) the initial stage of plume rise was deemed unimportant since the peaks are 26 km from the source.

The model operating conditions are given in Table 4.1 and for reference the full-scale plant conditions are numerated in Table 4.2. A total of 10 tests were conducted in the wind tunnel. The run numbers, terrain configurations, Froude numbers, Richardson numbers, and release heights for each test are given in Table 4.3. The results from Runs 1 and 2 will not be discussed or presented since they were exploratory in nature and as such, inconsistencies in the data were observed.

All tests were conducted in a similar manner. A stable boundary layer was established over the model or flat tunnel floor and measurements of velocity and temperature were made directly upwind of the source. The profiles were analyzed to assess whether the desired Richardson number had been achieved. Once the desired value was obtained

numerous velocity and temperature profiles were made along the center of the test section and lateral to the test section centerline.

After completing the velocity measurements a metered quantity of gas mixed to be neutrally buoyant (density of air) was allowed to flow from a release probe at a speed close to the ambient wind speed. Aerial and ground level distributions of the resulting plume were made at two locations, one about half way between the source (12 km) and the other on the high terrain.

To qualitatively document the flow pattern the plume was made visible by passing the gas mixture through titanium tetrachloride prior to emission from the release probe. Stills (color and black and white) and motion pictures of the tests in Table 4.3 were obtained.

A more detailed description of every facet of the study will now be given.

4.2 Scale Models and Wind Tunnel

- Scale Model

A 1:5000 scale model of the topography in the vicinity of the Colstrip Power Plant (CPP) for two wind directions (349 and 325°) was constructed to be positioned in the meteorological wind tunnel. The topographic strips that were constructed are shown in Figures 4.2-1 and 4.2-2. Also shown in the Figures are various reference points from which velocity and concentration measurements were obtained. These points will be referred to in the results section of the report.

Construction of the topographic model entailed a two-step process. The first step involved constructing a styrofoam model out of 1.3 cm thick styrofoam sheets (corresponds to a 61 m full-scale contour interval). United States Geological Survey maps were enlarged and used

as patterns from which the styrofoam was cut. The roughness elements on the styrofoam terrain model consisted of the 1.3 cm contour interval steps. The second phase of construction entailed constructing a wood-ribbed frame as shown in Figure 4.2-3. The frame had wood supports approximately every 30.5 cm which were cut to conform with the terrain elevation. Next, thin aluminum foil was placed on the styrofoam model and molded in 30.5 cm wide strips to fit the terrain contours. Once a strip was molded it was placed onto the wood frame and fastened. This procedure was repeated until a 1.22 x 1.83 cm section was complete. A picture of a completed section is shown in Figure 4.3-2. As can be seen, holes were cut in the ribs at the bottom to allow for circulation of air underneath the aluminum topographic simulated surface. Next, fans were positioned underneath the aluminum surface to enhance the airflow beneath the model. This is also shown in Figure 4.2-3. This hollow platform was then placed on the cooling plates that are permanently installed in the wind tunnel and the fans were activated to enhance the heat transfer from the surface and thereby keep a fairly uniform surface temperature distribution along the aluminum topographic surface of the model.

Since a scale model of the power plant and stacks were not constructed for this study, no scale model was required. The release probe that was used to emit the tracer gases is shown in Figure 4.2-4. A thermistor was built into the probe in addition to a thermistor fastened to the upwind side of the probe. This was done so that the temperature difference of the gas exiting the probe and approaching the probe could be monitored to assure that a neutrally buoyant plume was being released. As an additional check on this neutral buoyancy, visual

observation of the gas being emitted from the probe was made. If the gas was positively or negatively buoyant, an upward or downward initial trajectory to the plume was immediately evident.

- Wind Tunnel

The meteorological wind tunnel (MWT) shown in Figure 4.2-5 was used for this study. This wind tunnel especially designed to study atmospheric flow phenomena (Cermak, 1958; Plate and Cermak, 1963), incorporates special features such as an adjustable ceiling, a rotating turntable, temperature controlled boundary walls, and a long test section to permit adequate reproduction of micrometeorological behavior. Mean wind speeds of 0.1 to 39.6 m/s in the MWT can be obtained. Boundary layer thicknesses up to 1.2 m can be developed naturally over the downstream 6.1 m of the MWT test section. Thermal stratification in the MWT is provided by the heating and cooling systems in the section passage in the test-section floor.

For this study no vortex generators or boundary-layer trips were installed at the entrance since a very shallow boundary layer was desired. To develop the stable boundary layer a set of 12 Roll-Bond aluminum panels were placed approximately 10 cm above the tunnel floor 10.4 m directly upwind of the terrain model. The plates were positioned high enough such that they were at the same altitude as the aluminum shell model. This enabled a smooth transition from the aluminum plates to the model to be maintained. One of the Roll-Bond plates was used as a ramp at the beginning of the test section. A three-dimensional sketch of the tunnel configuration is shown in Figure 4.2-6.

The Roll-Bond aluminum panels and the permanently installed cooling plates were connected to the facility refrigeration system and cooled to

approximately -8.3°C for all tests. The free-stream air (air entering the test section) temperature was varied to obtain the desired thermal stratification. During all tests the fans which were built into the terrain model were running to enhance the heat transfer from the model surface insuring that a stable boundary layer would be maintained.

4.3 Flow Visualization

The purpose of this phase of study is to visually assess the transport of the plumes released from two effective plume altitudes over the terrain downwind of the CPP. The data collected consist of a series of photographs of the smoke emitted from the probe for the different release heights and stratifications set in the tunnel. The photographic tests are numerated in Table 4.3

The smoke from the release probe was produced by passing the required gas mixture through a container of titanium tetrachloride located outside the wind tunnel and transported through the tunnel wall by means of a tygon tube terminating at the probe inlet. The plume was illuminated with high intensity lamps and a visible record was obtained by means of black and white photographs taken with a supergraphic camera (lens focal length 135 mm) and color slides taken with a Pentax camera (focal length 50 mm). The shutter speed for the black and white photographs was 1/20 of a second and for the color slides 1/30 of a second. The black and white and color photographs were taken at an angle perpendicular to the tunnel such that the field of view would show the plume being transported over Garfield or Badger Peak. The camera setup for each camera is shown in Figure 4.3-1. A series of 16 mm motion pictures were taken of all tests. A Bolex movie camera was used with a speed of 24 ft per second. The movies consisted of taking an

initial close-up of the smoke release after which the camera was moved parallel to the tunnel from the smoke release down to the high terrain.

4.4 Gas Tracer Technique

The purpose of this phase of the experimental study is to provide quantitative information on the transport and dispersion of the plume emitted from the probe over the elevated terrain and at an intermediate location. To meet this goal a comprehensive set of concentration measurements were taken. The data obtained included ground level samples, a horizontal array of samples elevated above the ground and an array of samples along the center of the tunnel in the vertical direction. In total approximately 25 samples were obtained in one complete crosswind pattern. For each run the sampling rake which had attached to it all of the sampling ports previously described was positioned at two locations, one intermediate to the high terrain and one on the high terrain. A photo of the sampling rake is shown in Figure 4.4-1. The test procedure consisted of: 1) setting the proper tunnel wind speed, 2) releasing a metered mixture of tracer gas (ethane) and nitrogen of the required density (that of air) from the release probe, 3) withdraw samples of air from the tunnel at the locations designated in the sampling rakes, and 4) analyze the samples with a flame ionization gas chromatograph (FIGC). A photograph of the sampling system and gas chromatograph is shown in Figure 4.4-2. The location of the various sampling positions relative to ground level and the position at which the rake is placed is listed in Table 4.4.

The procedure for analyzing air samples from the tunnel was as follows: 1) a 2 cc sample volume drawn from the wind tunnel is introduced into the flame ionization detector (FID), 2) the output from the

electrometer (in millivolts) is sent to the Fluid Dynamics and Diffusion Laboratory (FDDL) dedicated minicomputer system, 3) the analog signal is converted to a digital record at a rate of 208 values per second which are then averaged in groups of 16, 4) a digital record is integrated and an ethane concentration determined by multiplying the integrated signal (mvs) times a calibration factor (ppm/mvs), 5) the ethane concentration is stored in the computer for subsequent use, and 6) a summary of the computer analysis (ethane concentration, peak height, integrated voltage, etc.) is printed out on the remote terminal at the wind tunnel. Prior to any data collection a known concentration of ethane is introduced into the FID to determine the calibration factor. This factor is input into the computer for use in converting the data.

The FID operates on the principal that the electrical conductivity of a gas is directly proportional to the concentration of charged particles within the gas. The ions in this case are formed by the effluent gas being mixed in the GC with hydrogen and then burned in air. The ions and electrons formed enter an electrode gap and decrease the gap resistance. The resulting voltage drop is amplified by an electrometer and fed to the FDDL computer. When no effluent gas is flowing, a carrier gas (nitrogen) flows through the FID. Due to certain impurities in the carrier some ions and electrons are formed creating a background voltage or zero shift. When the effluent gas enters the FID the voltage increases above this zero shift in proportion to the degree of ionization or correspondingly the amount of tracer gas present. Since the chromatograph used in this study features a temperature control on the flame and electrometer there is very low zero drift. In case of any zero drift the computer program which integrates the effluent peak also subtracts out the zero drift.

The total system error will be discussed in Appendix B. The lower limit of measurement (approximately 2 ppm) is imposed by the instrument sensitivity and the background concentration of ethane within the air in the wind tunnel. Background concentrations were measured and assumed to be the values at the extreme edges of the plume. These values were subtracted from all data quoted herein.

The wind-tunnel concentration data for all tests in this report are presented in the following dimensionless form

$$K = \frac{x u_H^2}{x_0 V}$$

where x is the observed concentration and x_0 is the source strength of the tracer gas. The tracer gas source strength was measured during the period of measurement and the appropriate observed value was used in tabulating the data.

The concentration data was computer processed to obtain the center of mass (\bar{z}) and the standard deviation (σ_z or σ_y). The parameters were determined by numerically integrating the following equations over the height (and width, where appropriate) of the concentration profiles:

$$Q = \int_0^h K dz$$

$$\bar{z} = 1/Q \int_0^h z K dz$$

$$\sigma_z^2 = 1/Q \int_0^h (z - \bar{z})^2 K dz$$

The numerical integration was obtained using the trapezoidal rule.

When interpreting model concentration measurements it is important to remember that there can be a considerable difference between the instantaneous concentration in the plume and the average concentration due to horizontal meandering in the atmosphere. In the wind tunnel, a plume does not generally meander due to the absence of large-scale eddies. Thus, it is found that field measurements of peak concentrations which effectively eliminate horizontal meandering should correlate with the wind-tunnel data (Hino, 1968). Since the primary purpose of this study is to compare plume characteristics either with or without terrain or maximum aerial and ground level values, the question of time averaging is not important. This assumes that these ratios do not vary when large-scale eddies are added to the plume motion.

4.5 Velocity and Temperature Measurements

Mean and turbulent velocity measurements were performed to 1) quantitatively assess the flow patterns over the simulated terrain and flat tunnel floor, 2) monitor and set flow conditions, and 3) document the approach conditions in the wind tunnel. Temperature measurements were also taken so that the characteristics of the thermal boundary layer could be obtained. Instrumentation used for this study included 1) one Thermo-Systems, Inc. (TSI) 1050 series anemometer, 2) a TSI Model 1210 hot-film sensor, 3) a Model 1800 LV Datametric Linear Flow Meter and Probe, 4) a Matheson Linear Mass Flow Meter and Controller for velocity calibration, and 5) a Yellow Springs, Inc. Precision Thermistor and telethermometer. Since all tests were conducted under stable stratification detailed temperature measurements were required. The techniques used to obtain the velocity data with this assortment of equipment and the data processing techniques will now be discussed in more detail.

- Hot-film Anemometry--Principle of Operation and Calibration Technique

The transducer used for measuring velocities for this study was a Model 1210 hot-film sensor. The sensor consists of a platinum film on a single quartz fiber. The diameter of the sensor is 0.0025 cm. The sensor has the capability of resolving one component of velocity in turbulent flow fields.

The basic theory of operation is based on the physical principle that the heat transfer from the wire equals the heat supplied to the wire by the anemometer or in equation form (see Hinze, 1975),

$$I^2 R_H = \pi \ell k_g (T_w - T_g) \text{ Nu} \quad 4.1$$

where

I = current through wire

k_g = heat conductivity of gas

ℓ = length of wire

T_w = temperature of wire

T_g = temperature of gas

Nu = Nusselt number

$$= F(\text{Re}, \text{Pr}, \text{Gr} \frac{T_w - T_g}{T_g}, \frac{\ell}{d})$$

$$\text{Re} = \frac{ud}{\nu' g}$$

$$\text{Pr} = \frac{C_p \mu_g}{k_g}$$

$$\text{Gr} = \frac{gd^3(T_w - T_g)}{\nu'^2 T_g}$$

d = diameter of wire

R_H = operating resistance of wire

For most wind-tunnel applications an empirical equation evolved by Kramers as reported in Hinze (1975) is adequate for representing Nu for a Reynolds number range $0.01 < Re < 1000$, or

$$Nu = 0.42 Pr^{0.2} + 0.56 Pr^{0.33} Re^{0.5}.$$

Free convection from the wire can be neglected for $Re > 0.5$ when

$$GrPr < 10^{-4}.$$

Alternately buoyancy may be neglected when

$$Gr < Re^3.$$

The temperature dependence of the electric resistance of the wire is assumed to follow the ensuing relation

$$R_H = R_o [1 + b_1(T_w - T_o) + b_2(T_w - T_o)^2 + \dots]$$

where b_i are temperature coefficients. Normally the higher order terms are neglected and

$$R_w = R_o [1 + b_1(T_w - T_o)].$$

Substituting the appropriate relations yield the following equation

$$\frac{I^2 R_w}{R_w - R_c} = A + B(\rho_c u)^n \quad 4.2$$

where

R_c = resistance of wire at calibration temperature

ρ_c = density of air at calibration temperature

$$A = \frac{\pi \ell k_f}{b_1 R_o} 0.42(Pr)^{0.2}$$

$$B = \frac{\pi \ell k_f}{b_1 R_o} 0.57(Pr)^{0.33} \left(\frac{d}{\mu}\right)^{0.5}.$$

For this study A, B, and u were obtained by calibrating the wire over a range of known velocities and determining A, B and n by a least-squares analysis. Since the wire is calibrated at fixed temperature and the wire will be placed in a stratified environment a method for correcting the voltage output of the wire was developed. At each measurement point in the wind tunnel the ambient temperature and resistance of the wire were measured. The instantaneous velocity was then calculated using the inverse of equation 4.2, or

$$u = \frac{T_a}{T_c} \left[\frac{\frac{I^2 R_w}{R_w - R_a} - A}{B} \right]^{1/n} \quad 4.3$$

where

T_a = the measured ambient temperature

R_a = the measured wire resistance at ambient temperature.

Calibration of the hot film was performed with the Matheson Linear Flow Meter (MLFR). A special flow chamber was attached to the MLFR with a specially constructed orifice which gave a uniform velocity profile upon exit. With this device velocities over the range of 0.09 to 2 m/s could be obtained. Accuracy of this system is quoted to be 1 percent of full-scale range or ± 0.02 m/s. Typical calibration curves are shown in Figure 4.5-1. A calibration was performed at the beginning of each day's measurement. The errors due to drift in the wire are assessed in Appendix B.

After the wire was calibrated, the desired flow condition was set in the wind tunnel. The free-stream velocity was monitored with the Model 800 LV Datametric Flow Meter and Probe. Once the desired

condition at the reference height was obtained the Datametric setting was recorded and used to monitor and set the tunnel conditions for all remaining tests. During all subsequent velocity measurements care was taken to ensure the Datametric probe reading remained constant.

- Data Collection

Velocity and temperature profiles were measured at various locations with and without the terrain. The number and exact location varied from test to test. For the initial series of tests, profiles were taken at locations A, B, C, D, G, H, I, J, K, L, M, N, and at O (see Figure 4.2-6). This series of profiles consisted of four profiles across the approach to the model and four at the end of the test section lateral to the test section. It also included six profiles down the center of the tunnel. This series of data was not collected for each run because the approach flow and lateral variation was deemed to be invariant when the model was changed to the various wind directions. Hence, the most detailed information was collected for the first wind direction. The manner of collecting the data was as follows: 1) the hot film was attached to a carriage along with a yellow spring thermistor, 2) the bottom height of the profile was set to be 0.64 cm, and 3) a vertical traversing mechanism which gave a voltage output corresponding to the height of the wire and thermistor above the ground, 4) the signals from the hot film and potentiometer device indicating height were fed directly to a Hewlett-Packard Series 1000 Real Time Executive Data Acquisition System, 5) samples were stored digitally in the computer at a rate of 500 samples/second, and 6) the computer program converted each voltage into a velocity (m/s) using the equation 4.3. Also, input was the cold

resistance and temperature at the level so that the appropriate correction as discussed above could be made. At this point the program computes several useful quantities using the following equations:

$$\bar{u} = 1/N \sum_{i=1}^N u_i$$

$$\overline{u'^2} = \frac{1}{N-1} \sum_{i=1}^N (u_i - \bar{u})^2$$

where N is the number of velocities considered (typically a 15-second average was taken, hence 7500 samples were obtained). The mean velocity and turbulence intensity at each measurement height were stored on a file in addition to being returned to the operator at the wind tunnel on a remote terminal. The temperature data were recorded by typing the indicated temperature from the Yellow Springs thermistor on the computer sheet at the remote terminal. To compute Richardson and Froude numbers a program had not been developed prior to conducting the test. Hence, this data were entered manually into the file for subsequent analysis.

To check the temperature distribution on the surface of the aluminum shell model a thermistor was placed at 16 points on the model. The temperature of each point and the relative location is shown in Figure 4.5-2. The mean temperature for the 16 points is 12.2°C , the high value 15.0°C , the low value 9.0°C and the standard deviations 1.7°C . All measured temperatures were within two standard deviations of the mean.

5 STABLE BOUNDARY-LAYER RESULTS

5.1 General

A stable boundary layer was developed over the simulated terrain and flat tunnel floor as described in Section 4. As discussed in Section 3 the requirements for similarity of the flow between laboratory and field are equality of the Froude number (or Richardson number), a sufficiently high Reynolds number, undistorted length scaling, and equality of dimensionless boundary conditions. To assess whether similarity was achieved measurements in the field are desirable to compare with the wind-tunnel results. Froude number data can be obtained from an on-site meteorological tower which is instrumented with wind speed and direction at 93.3 and 34 m and temperature at 90.6 and 31.4 m, AGL. Boundary conditions such as approach temperature and velocity profiles are not available and thus representative data from other locations must be considered when assessing these similarity parameters.

The goal of this study was to simulate in a wind tunnel Pasquill E-stability for two effective plume altitudes. Hence a criteria relating Froude number (or Richardson number) to Pasquill category is needed. The method used to classify stability at the CPP (D, E, or F) is shown in Table 5.1 and is similar to that recommended in AEC Safety Guide 23. The method shown is based primarily on a temperature difference with critical wind speed cutoffs. In the wind tunnel temperature difference alone is not a good indicator of stability (this probably holds true for the atmosphere also). Hence a Froude number categorization was derived from Table 5.1 using the limit of temperature difference and

wind speed. For example for E stability the highest $Fr_T^{1)}$ would be obtained using a $\frac{\Delta\theta}{\Delta z}$ of $1^\circ C/100 m$ and a wind speed of 10 m/s or,

$$Fr_T = \frac{10}{\sqrt{\frac{9.8}{293} \cdot 01}} \cdot 93.3 = 5.9.$$

The categories are presented in Table 5.2 and were obtained by insuring that Fr_T categories for each stability do not overlap.

For velocity and temperature profiles collected in the wind tunnel Fr_T was calculated over the scaled interval of field measurement (93.3 and 34 m) to compare with Table 5.2 and to give an indication of the equivalent Pasquill category simulated.

The bulk Richardson number is also an indicator of stability and is defined by

$$Ri = \frac{g}{T} \frac{\Delta T \Delta z}{(\Delta u)^2} \quad 5.1$$

where

ΔT = the temperature difference between the level Δz

Δu = the wind speed difference between the level Δz

Δz = the height difference between measurement points

\bar{T} = the average temperature over Δz .

To estimate the relation between Pasquill categories and the bulk Richardson number the work of Golden (1972) was employed. Golden

¹⁾ For atmospheric flows the Fr_T is defined by

$$\frac{u_T}{\sqrt{\frac{g}{T} \frac{\Delta\theta}{\Delta z}}} \cdot z_T$$

where $\frac{\Delta\theta}{\Delta z}$ is potential temperature, u_T the velocity at the top of the tower, and z_T the height above ground level of u_T .

presents curves which relate the Pasquill category to surface roughness (z_o) and Monin-Obukhov length scale (L). The bulk Richardson number range for E stability can then be estimated using the following definition for Ri

$$Ri = \frac{z_m}{L} \frac{\phi_H}{\phi_m^2} \quad 5.2$$

where

$$z_m = \frac{z_2 - z_1}{\ln z_2/z_1}$$

z_2, z_1 = top and bottom height of velocity and temperature measurement at meteorological tower

L = Monin-Obukhov length scale

$$\phi_H = 0.74 + 4.7 z_m/L$$

$$\phi_m = 1.0 + 4.7 z_m/L.$$

If it is assumed that the surface roughness (z_o) around CPP is equal to 0.5 m, the curve in Golden relating Pasquill category as a function of z_o and L shows the range of $1/L$ for E stability is approximately $0.005 < 1/L < 0.015$.

From equation 5.2 the equivalent Ri range for E stability becomes

$$0.11 < Ri < 0.16.$$

The Ri was calculated as a function of z_m for all velocity profiles collected in the wind tunnel. Thus two methods are available for relating the wind tunnel stratification to a corresponding Pasquill-Gifford category. The Fr_T values are the most reliable in that experimental errors influence the values the least (see Appendix B--Error Analysis).

To assess the flow characteristics in the wind tunnel the velocity profiles were analyzed to obtain z_o , u^* , $1/L$, n and Re_{z_o} . The

values of z_0 , u^* and $1/L$ for each profile were estimated by finding the z_0 , u^* , and $1/L$ which gave the best fit (by least squares) to the following equation which is characteristic of atmospheric (Businger, 1972) and wind-tunnel flows (Cermak, 1974):

$$\frac{u}{u_*} = \frac{1}{k} \ln \frac{z}{z_0} + \frac{4.7z}{L} .$$

The root-mean-square error (\hat{e}) between predicted and observed velocity was computed to assess the goodness of fit.

The power law exponent was computed by fitting the data by least squares to the following equation:

$$(\frac{u}{u_r}) = (\frac{z}{z_r})^n .$$

The power law exponent varies with stability in the atmosphere as given in Table 5.3. For assessing the similarity of the velocity profiles in the tunnel and field for corresponding stabilities this table should be referred to.

The turbulent Reynolds number Re_{z_0} was computed for each profile and was used to assess whether the flow was fully turbulent. For fully turbulent flows $Re_{z_0} > 2.5$ (Schlichting, 1968; Sutton, 1953). The u_* and z_0 values used for computing Re_{z_0} were obtained from the least squares analysis as discussed above.

5.2 Analysis of Velocity and Temperature Measurements

This section will discuss the velocity and temperature measurements obtained for each test enumerated in Table 4.3.

- 325° Wind Direction and $Fr_T = 3.3$

For this test the plate temperature in the wind tunnel was approximately $-8.3^\circ C$ and the free-stream air temperature (air entering

the test section) was 40°C. The Datametrics setting was 160 SFPM. Table 5.4 summarizes the mean velocity, turbulence intensity, temperature, Froude number and bulk Richardson number versus height for each profile. The profiles at locations A, B, C, and D were taken directly upwind of the model lateral to the flow over Roll Bond cooling plates (see Figure 4.2-6) and profiles L, M, N, and O were taken lateral to the flow at the end of terrain model.

Table 5.5 gives a summary of the analysis of each profile. The estimated values for z_0 , $1/L$, u^* , Re_{z_0} and n for each profile are tabulated and were computed using the equations discussed in Section 5.1. The surface roughness ranged from 0.07 cm to 22.2 cm with a mean value of 0.3 cm. The extreme values occurred on the high terrain at the end of the model where the assumption of horizontal homogeneity is least valid and is a necessary requirement for the log-linear relationship for velocity profiles to be valid. The average friction velocity (u^*) was computed to be 4.2 cm/s. The average turbulent Reynolds number is 9.0, well above the limit of 2.5 for fully turbulent flows to exist. The power law exponent (n) for the profiles ranged from 0.36 to 0.62 with an average value of 0.50. These high values of n are characteristic of a stable boundary layer and such values have been observed in the atmosphere(Touma, 1977 and Sutton, 1953).

To visually assess the flow characteristics over the model, Figures 5.2-1 through 5.2-3 were prepared. Figure 5.2-1 shows the dimensionless velocity profiles along the center of the model. As can be seen the upper-level velocity was nearly constant for all profiles and ranged from 0.95 to 1.0 m/s. A speed-up in velocity close to the ground is noticed at site L--taken on Garfield Peak.

The turbulence intensity profiles are shown in Figure 5.2-2. Close to the model surface the turbulence levels are highest. Overall the turbulence intensity values are low and range between 1.5 and 7.8 percent. The Froude number, Fr , was plotted versus height in Figure 5.2-3 for the profiles taken along the center of the tunnel. Near the surface the Fr values are largest indicating a less stable layer exists than aloft. This less stable layer is created by enhanced mixing due to the roughness of the surface which would also be characteristic of the prototype conditions. Above 5-8 cm the Fr values become nearly constant and approach a value of 2 at all locations. Using Fr_T as a stability indicator this case would be classified as a Pasquill E using the criteria adopted in Section 5.1 (Table 5.2).

- 325° Wind Direction and an $Fr_T = 1.9$

For this test the plate temperature in the wind tunnel was set at -8.3°C and air entering the test section was maintained at 40°C . The Datametrics setting was 167 SFPM. Table 5.6 gives the mean velocity, turbulence intensity, temperature, Froude number and bulk Richardson number versus height for each profile. A total of ten profiles were obtained for this test; three lateral to the flow immediately upwind of the terrain model (locations A, B, and D); three lateral to the flow at the end of the terrain model (locations K, L, and M), and the remainder along the center of the model (G, H, I, and J). The profiles taken at locations A and M were also along the center of the test section.

Table 5.7 gives a summary of each profile. The surface roughness computations gave values of z_0 ranging from 0.05 to 0.70 cm with a mean value of 0.36 cm. The Monin-Obukhov length-scale values are

all positive with an average value of 0.63 m. The friction velocity ranged from 3.2 to 8.1 cm/s with an average of 4.8 cm/s and the turbulent Reynolds number ranged from 1.1 to 27.7 with an average of 13.0 (above the critical value of 2.5 for fully turbulent flow). The power law exponent ranged from 0.32 to 0.67 with an average of 0.50. This range is indicative of a stable boundary layer.

The velocity profiles taken along the center of the model are plotted in Figure 5.2-4 and show a similar pattern to those discussed for the 325° wind direction. The upper level velocity ranged from 0.82 at the approach to the terrain and increased to 1.15 m/s upwind of Badger Peak. The turbulence intensity versus height is plotted in Figure 5.2-5 for the profiles taken along the center of the model. Above 10 cm the turbulence levels are low (~2 percent) for all locations whereas below 10 cm values as high as 15 percent are observed. The high turbulence near the ground is created by the mechanical mixing induced by the rough surface features.

The Fr variation with height along the center of the test section is shown in Figure 5.2-6. Fr profiles at A', H', and I' show a nearly constant value (~2) above 2 cm. At the higher terrain locations (J' and L') the Fr values increase at all heights but the greatest increase is near the ground. Based on Fr this case would be classed as Pasquill E on the border of a Pasquill F.

- 349° Wind Direction and $Fr_T = 6.3$

The wind tunnel conditions for this test were a -8.3°C plate temperature, a 57°C temperature for the air entering the test section and a Datametrics setting of 230 SFPM. Table 5.8 lists the mean velocity, turbulence intensity, temperature, Froude number and

Richardson numbers versus height for all profiles. A total of eight profiles were obtained for this test: six along the center of the test section (A' , G' , H' , I' , J' , and M') and two off the centerline on either side of M' (profiles K' and L'). Figure 4.2-6 shows the relative location of each profile. Table 5.9 summarizes the computed values of z_0 , $1/L$, u^* , Re_{z_0} and n for each profile.

The surface roughness ranges from 0.01 to 0.47 cm with an average of 0.25 cm. The Monin-Obukhov length scale values are all positive with an average value of 0.7 m. The average value for u^* is 8.3 cm and for Re_{z_0} 17.2 (above the critical value of 2.5). The power law exponent ranged from 0.31 to 0.52 with an average of 0.39. The exponents are lower than the other two cases previously discussed suggestions this case is less stable as the Fr and Ri data confirm.

Figure 5.2-7 shows the velocity profiles along the center of the tunnel at locations G' , H' , I' , J' , and L' . The upper level velocity u_∞ varies from 1.7 m/s at G' to 1.4 at I' and J' . The variation is due in part to a slight drift in the tunnel conditions during the test (i.e., the Datametrics was reading high for the profile taken at G' and H'). Figure 5.2-8 shows the turbulence intensity values plotted versus height for each profile. Close to the ground i_x is high (10-15 percent) whereas aloft i_x is significantly lower (1-3 percent).

The Froude number variation with height is plotted in Figure 5.2-9. As can be seen the Fr values for this case are significantly higher than the previous two cases with upper level (10-40 cm) values ranging from 2.4 to 4.7. At lower levels (< 10 cm) values as high as 15 are observed. Based on Fr and the discussion in Section 5.1 this case is on the borderline of being a Pasquill D. In fact, the Fr_T

values for this case range from 5.4 to 11.3 with most being above the cutoff of 5.9 for E stability.

- Flat Terrain and $Fr_T = 1.8$

For this test the floor temperature was approximately -6.7°C and the air entering the test section was maintained at 56.7°C . The Data-metrics setting was 190 SFPM. Table 5.10 gives the mean velocity, turbulence intensity, temperature, Froude number and Richardson number versus elevation for the profiles collected at sites A', G', I', and L'. These profiles were located along the center of the tunnel.

Table 5-11 summarizes the results of the z_0 , $1/L$, u^* , Re_{z_0} and n calculations for each profile. The surface roughness for this case ranged from 0.86 to 1.5 cm with a mean of 0.92 cm. The mean values for L , u^* , Re_{z_0} , and n were respectively 2.7 m, 8.9 cm/s, 56.7 and 0.27. In general, the L and z_0 values seem unrealistic and may be caused by a stagnate zone or flow reversal region over the plate surface. The stagnate region caused the velocity profiles to exhibit an irregular shape as shown in Figure 5.2-10 and hence the log-linear equation would not fit the velocity data well. If the profiles are carefully inspected an uncharacteristic decrease in velocity near the tunnel floor is evident particularly at sites I' and L'. A flow reversal may have occurred at I' and L' but would not be recorded on a single hot-film sensor. This reversal was not noticed while testing was in progress but, if present, will effect the dispersion patterns close to the surface of the tunnel.

The turbulence intensity versus height is shown in Figure 5.2-11. A slightly higher level of turbulence is noted near the ground but overall the values are low and above 10 cm range from 1.3 to 2.4 percent.

The Fr variation with height is shown in Figure 5.2-12. Overall the Fr values are almost constant with height and range from 0.5 to 3.1. Based on the Fr_T value, this case would be classed as Pasquill E but the flow irregularities near the tunnel floor may produce unreasonable ground level concentrations.

- Flat Terrain and $Fr_T = 4.6$

The tunnel floor was set at -6.7°C and the air entering the test section was 56.7°C for this test. The Datametrics setting was 215 SFPM. Table 5.12 gives the mean velocity, turbulence intensity, temperature, Froude number and Richardson number versus height for the profile collected at locations A', G', I', and L'. The results of the detailed analysis of each profile are given in Table 5.13. The estimated surface roughness (z_0) ranged from 0.2 to 1.4 cm with an average of 0.7 cm. The average values for L , u^* , Re_{z_0} and n were 1.7 m, 8.7 cm/s, 45, and 0.70. The z_0 and L values again seem unrealistic and are explained by the shape of velocity profiles plotted in Figure 5.1-13. A stagnate air layer of about 2 cm depth is prevalent at location L'. The remaining profiles show no stagnate layer but the profiles at G' and I' have uncharacteristic shapes. Above 5 cm the profiles are almost linear and below 5 cm they are also linear with a smaller slope. The turbulence intensity profiles are shown in Figure 5.1-14. The i_x values are generally higher near the surface with a maximum value of 12.8 percent at site L'. Above 5 cm the turbulence is low and ranges from 2.9 to 6.1 percent.

The variation of Fr with height is shown in Figure 5.1-15. The Fr values are generally higher near the ground and are nearly constant above 5 cm. The range of Fr values above 5 cm is 1.6

to 3.8. Based on Fr_T of 4.6, this case would be classed as Pasquill E. However, the dispersion pattern near the ground may be affected by the irregular flow field and care should be exercised when evaluating the concentration measurements.

6 ANALYSIS OF PLUME DISPERSION PATTERNS

6.1 Wind Tunnel Results

The photographic data provides qualitative information concerning the plume transport over Badger and Garfield Peaks. Figures 6.1-1 through 6.1-5 show the plume visualizations with and without the terrain for the two release heights studied. As can be seen the more dense portion of the plume remains above ground level for all cases studied, suggesting that plume impaction on elevated terrain does not occur. More detailed visual information can be obtained by viewing the motion picture of each test studied.

Quantitative information on the plume characteristics was obtained by analyzing the concentration data. The analysis will discuss these key factors: 1) horizontal and vertical dispersion rates (σ_y and σ_z), 2) height of maximum (Z_{max}) and mean (\bar{Z}) concentration above ground level, and 3) maximum centerline (K_H) and maximum ground-level (K_g) concentration. These parameters were calculated for all tests and are tabulated in Table 6.1. Each factor will be discussed in more detail.

• Horizontal and Vertical Dispersion Rates

The horizontal dispersion coefficient (σ_y) was computed using the measured concentration data at the 10.5 cm height (samples 10,11,12, 13,21,14,15,16,17) and the vertical coefficient (σ_z) was computed using samples 5,12,19,26,21,22,23, and 24. The computed values (model and prototype) are enumerated in Table 6.1. Values were computed even when the tracer gas sampling rake was not positioned directly in the center of the plume. The values which may be most effected by rake positioning are indicated in the table.

Since the spread of a plume versus distance is a direct indication of stability, the σ_y and σ_z values obtained in the wind tunnel have been scaled to prototype dimensions and plotted in comparison with the Pasquill-Gifford Diffusion Curves (PGDC) for the atmosphere. Figure 6.1-6 shows a plot of the vertical spread (σ_z) for the cases with an Fr of 2.2 or less in comparison with PGDC. The σ_z values for the terrain cases (325 and 349° wind directions) are between the Pasquill-Gifford (P-G), D and E lines at the intermediate location (G or G') and fall on the E line at the far distance (L or M'). For the no-terrain case the data at G' falls along the P-G D line whereas at L' the data falls between D and E stability. If σ_z alone were used as a stability indicator the P-G category would be between D and E for the cases with an Fr of 2.2 or less.

Figure 6.1-7 shows the σ_z data for the no-terrain case with $Fr = 2.7$ and the 349° wind direction with $Fr = 3.9$. For these cases it is evident that the vertical spread is characteristic of a neutral (D stability) atmosphere. Thus the σ_z values correlate directly with Fr . As Fr increases the vertical dispersion becomes greater.

The σ_y values for the cases with $Fr \leq 2.2$ are shown in Figure 6.1-8. The terrain case data are close to E stability at the intermediate location (G or G') and F stability at the far distance (L or M'). For the flat terrain cases the data fall on or below the P-G F line. An overall classification for these cases based on the horizontal dispersion is between a P-G category E and F.

The 349° wind direction case with $Fr = 3.9$ is shown in Figure 6.1-9. The horizontal spread follows the P-G E line. The flat terrain case with $Fr = 2.7$ is also shown in Figure 6.1-9. The P-G category based

on σ_y appears to be an F at the far distance (L) and is between E and F at the intermediate location (G).

In summary it appears that the horizontal dispersion coefficients observed in the wind tunnel are indicative of a stable atmosphere for all Fr cases. The σ_y values seem to be weakly dependent on Fr and correlate well with a P-G category between E and F for locations G and F at location L. The vertical dispersion coefficients are generally one P-G category less stable than the horizontal coefficients. For the cases with $Fr = 3.9$ and 2.7 the vertical coefficients followed the P-G neutral (D) line whereas for the cases with $Fr \leq 2.2$ the spread was close to the P-G E line.

A question that may be raised here is why the vertical spread is one stability category higher than the horizontal spread. As discussed in Pasquill (1974) the PGDC for σ_z were based on a surface roughness of 3 to 10 cm. At Colstrip the roughness is at least 1 m and possibly 10 m. Pasquill (1974) presents a curve (reproduced in Figure 6.1-10) that shows the correction factor to multiply the σ_z for a 10 cm roughness by to obtain the σ_z representative of the roughness at a particular site. As can be seen from the curve, the σ_z for stable conditions (or any other stability for that matter) could be from 1.4 to 1.1 times higher than the standard σ_z values. In general, the factor decreases with downwind distance. This is reflected in the wind-tunnel results by the σ_z values clustering around D or D-E stability at G or G' and moving to E at M or M'.

- Height of Plume above Ground Level

From an analysis of the concentration data tabulated in Appendix A the center of mass above ground level and height of maximum concentration

was obtained. The center of mass \bar{Z} was found using the equations and procedures given in Section 4.4. Since a finite sampling grid was employed the probability of positioning the rake directly in the center of the plume was small. However, it is felt that the center of mass at one vertical location is indicative of the overall height of the plume. A second indicator is the height of the maximum observed concentration Z_{\max} . Figures 6.1-11 through 6.1-18 show the height of the maximum concentration and center of mass plotted on terrain cross sections in relation to the initial release height. The \bar{Z} and Z_{\max} values were both plotted to give a visual estimate on the range of the expected height for the plume centerline. These two values (\bar{Z} and Z_{\max}) differ the most when the rake was not positioned directly in the center of the plume or when the maximum value was close to ground level.

For estimating concentrations on elevated terrain an important parameter is the plume height above ground level. Since \bar{Z} and Z_{\max} are both indicators of plume height (h), hereafter h will be set equal to $\frac{\bar{Z} + Z_{\max}}{2}$. Table 6.2 summarizes the ratio of the plume height to the initial release height for location G (or G') and L (or L'). This table should be referred to in the ensuing discussions.

Figure 6.1-11 shows the plume rise range ($\bar{Z} + Z_{\max}$) for the case with $Fr = 1.5$, a 349° wind direction and 7.6 cm (381 m in prototype) and 9.5 cm (476 m in prototype) release heights. The case corresponds to a P-G E stability and may be on the borderline of being an F stability. At point G' the ratio of the plume height to release height ($\frac{h}{H}$) is 0.74 and 0.84 for $H = 7.6$ and 9.5 cm, respectively. It is apparent that the plume has lost altitude relative to ground level due to the rising terrain and converging streamlines which are

characteristic of flow over hills. The ratios $\frac{h}{H}$ at L' are 0.47 and 0.65 for the 7.6 and 9.5 cm release heights.

The plume rise range for $Fr = 3.9$, a 349° wind direction (toward Badger Peak) and the two release heights is shown in Figure 6.1-12. This case is close to being classed as a P-G D (neutral) or slightly stable (D-E). At point G' the plume height relative to ground level is about equal to the initial release height ($\frac{h}{H} = 1.09$ and 0.92 for the 7.6 and 9.5 cm release heights, respectively). At point L the plumes pass close to the ground ($\frac{h}{H} = 0.36$ and 0.5 for $H = 7.6$ and 9.5 cm, respectively). This is due to the increase in vertical spreading associated with neutral or slightly stable conditions; more of the plumes reach the ground thus lowering the center of mass and the maximum centerline concentration. In fact at L the maximum value recorded was at ground level for the 7.6 cm release. The actual maximum was probably above ground level but not recorded due to the finite sampling grid.

The plume rise range for the 325° wind direction, an $Fr = 2.0$ and a 7.5 and 9.6 cm release height is shown in Figure 6.1-13. This case corresponds most closely to a P-G E. The plume heights above ground level at location G are close to the initial release elevation with $(\frac{h}{H}) = 0.97$ and 0.86 for the 7.6 and 9.5 cm release heights. The plume height relative to ground level decreases slightly at L with $\frac{h}{H} = 0.71$ and 0.82 for the high and low release height, respectively.

The plume rise results from the flat terrain case with $Fr = 2.2$ are shown in Figure 6.1-14. A slight increase in the height relative to the initial value was obtained for the test with $\frac{h}{H} = 1.09$ and 1.21 at G and 1.28 and 1.11 at L for the 7.6 and 9.5 cm release heights.

This is due in part to the center of mass (\bar{Z}) being consistently higher than the maximum concentration (giving an h larger than H). Some of the plume irregularities for this case are due to the inconsistencies observed in the flow field as discussed in Section 5.

Figure 6.1-14 shows the flat terrain results for $Fr = 2.7$. It is apparent from the figure that \bar{Z} and Z_{max} differed significantly from one another. This is due to the observed occurrence of parcels of the plume being broken off due to large-scale eddies giving the plume a nonsymmetric appearance. These eddies sometimes gave higher values of concentration either above or below the main body of the plume. Hence, the center of mass was either above or below the maximum concentration depending on whether the puffs occurred above or below the plume. The plume rise ratios for this test were 1.36 and 1.40 at location G' and 1.11 and 1.61 at location L' for the 7.6 and 9.5 cm release height, respectively. Again the irregularity in the dispersion results are explained by the flow field as discussed in Section 5.

- Maximum Ground-Level and Aerial Concentrations

Table 6.1 gives the maximum aerial and ground-level concentrations observed during the wind-tunnel tests. These data have been analyzed to obtain information on 1) the ratio of maximum to maximum ground-level concentration, 2) the ratio of maximum ground-level concentration with and without the terrain present, and 3) the ratio of computed (Gaussian model) and observed (wind tunnel) maximum centerline concentrations.

Ratio of Maximum to Maximum Ground-level Concentration

A parameter of importance for assessing concentrations at ground level is the ratio of maximum (K_H) to maximum ground-level (K_g) concentration at a given downwind location. For elevated terrain situations

this ratio (K_H/K_g) approaches 1 as the plume centerline approaches the ground. If the ratio is greater than 1 the implication is that the plume center is elevated above the terrain. At sufficient downwind distance, the ratio approaches 1 simply because the plume becomes uniformly mixed throughout the mixing layer. In general the ratio approaches 1 faster as the atmospheric stability goes from stable to unstable.

Table 6.3 summarizes the ratio of K_H/K_g for the data collected in the wind-tunnel tests. Also indicated in the table are the associated Froude number, Richardson number, and downwind distance. Some general trends can be deduced by referring to the table.

First the ratio K_H/K_g decreases as downwind distance increases for a given release height. This is the expected trend since more effluent reaches the ground as σ_z and downwind distance increase. Second, the ratio increases at a fixed distance as the release height increases. This again is the expected trend since less effluent reaches the ground at a given distance when the plume height is increased. In general the ratios are less when the terrain is present for a similar case (nearly equal Froude number) than when the terrain is absent. This implies the terrain enhances vertical mixing such that higher concentrations are observed at locations such as G (or G'). Also the plume center approaches the ground thereby increasing the ratio.

Another factor that should be considered in assessing the ratios is that the ground-level samplers on the model are some height above the ground (due to the sampling probe diameter or due to the probe being slightly elevated). The sampling probe diameter was approximately 1.6 mm which means the sampling height was approximately 0.8 mm above ground level. In some cases the probe recording the maximum concentration was elevated as high as 3 mm. Table 6.1 gives the height above

ground level of all maximum values. To estimate whether this factor would significantly reduced the measured values--that is, if a ground level sample were measured what would the value be--consider the following equations derived from Turner (1968):

$$K_g = \frac{H^2}{2\pi\sigma_y\sigma_z} \left\{ \exp\left[-\frac{1}{2}\left(\frac{z_g+h}{\sigma_z}\right)^2\right] + \exp\left[-\frac{1}{2}\left(\frac{z_g-h}{\sigma_z}\right)^2\right] \right\} \quad 6.1$$

$$K_o = \frac{H^2}{\pi\sigma_y\sigma_z} \exp\left[-\frac{1}{2}\left(\frac{h}{\sigma_z}\right)^2\right] \quad 6.2$$

where

K_g = the predicted value at sample height (z_g)

K_o = the predicted value at $z = 0$.

The ratio

$$\frac{K_o}{K_g} = \frac{2 \exp\left[-\frac{1}{2}\left(\frac{h}{\sigma_z}\right)^2\right]}{\exp\left[-\frac{1}{2}\left(\frac{z_g+h}{\sigma_z}\right)^2\right] + \exp\left[-\frac{1}{2}\left(\frac{z_g-h}{\sigma_z}\right)^2\right]} \quad 6.3$$

then gives the estimated correction factor that the measured data should be multiplied by. Table 6.4 gives calculated values for K_o/K_g for various σ_z , z_g , and h . As can be seen for $z = 0.079$ the error for the range of h and σ_z considered is negligible (all ratios close to 1.00). For $z = 0.3$ cm the error becomes significant only for large h and small σ_z . For these cases the values at the ground will be small anyhow. Based on this discussion no correction due to ground-level probe alignment was made.

Ratio of Maximum Ground-level Concentration (dimensionless) with and without Terrain

Table 6.5 summarizes the ratio of maximum observed ground-level concentration with and without the terrain present. The ratio $[K_g]_w / [K_g]_{wo}$ is computed using terrain case results (349 or 325°

wind direction) and the no-terrain case results that have the most similar Froude numbers. The table shows that the ground-level concentrations are higher with the terrain present for all except one case. An explanation for this anomaly is that both cases (with and without terrain) have maximum ground-level concentrations close to the background values in the wind tunnel. Hence both values can have a large error due to fluctuations in the background concentration. The remaining data show the expected trend of higher concentration when the terrain is present. When planning the program it was intended to use this data to predict the maximum value expected when the terrain is present. Since flatland diffusion model results are fairly accurate the prediction at L or L' was to be modified using the ratios in Table 6.5. However, since the stability conditions were not exactly the same (which to obtain in the wind tunnel would have required an unreasonable time and a better approach was developed as described below) and flow irregularities were observed for the flat terrain cases, this data will not be used to estimate concentrations on Badger or Garfield Peaks. Instead the ratio K_H/K_g as discussed earlier will be used in the manner described in Section 6.2

Observed and Predicted Maximum Concentrations

In order to assess whether the dispersion in the wind tunnel is similar to that in the atmosphere, a comparison of the maximum predicted and observed concentrations was made. The prime assumption here is that the Gaussian model for flat terrain will give representative estimates of maximum concentrations that can be expected in the atmosphere. A comparison of the wind-tunnel results with the predicted maximum concentration was made since the maximum centerline value (K_H) should be

relatively insensitive to the shape of plume. Ground-level values on the other hand would be more sensitive to the plume shape and proximity to the ground.

The equation for predicting the maximum concentration is

$$K_H = \frac{H^2}{2\pi\sigma_y\sigma_z} \left[1 + \left\{ \exp -2 \left(\frac{h}{\sigma_z} \right)^2 \right\} \right] \quad 6.4$$

where H is the release height and h the plume height above ground level (assumed equal to H). Since the σ_y and σ_z dispersion rates did not follow the same stability category in the wind tunnel, σ_y and σ_z were classified independently according to where the observed data fell on the PGDC. The data were classified by the location of the σ_y and σ_z values at G (or G') in relation to the PGDC. Table 6.6 shows the ratio of observed and computed centerline concentration and the associated P-G classification for σ_y and σ_z . As can be seen from the table at location G or G' , the ratio is between 0.77 and 1.13 for all cases where the maximum value was most likely observed. At L or L' the ratio ranges from 1.09 to 2.02 for all cases where the maximum was observed. The reason the ratio increased at L or L' is because the plume lost altitude with respect to ground level ($H < h$) and the reflection term in equation 6.1 becomes significant.

In summary the comparison between observed and computed concentrations is favorable suggesting the results in the wind tunnel give similar results to those that can be expected in the atmosphere.

6.2 Modification of Numerical Model

The numerical model used to estimate ground-level concentrations on Garfield and Badger Peaks is referred to as the Valley Model (Burt,

1977). This model makes use of the following equation from Turner (1968) integrated over a 22.5° sector.¹

$$\chi(x, y, z, h) = \frac{Q}{2\pi\sigma_y\sigma_z u} \left[\exp -\frac{1}{2} \left(\frac{y}{\sigma_y} \right)^2 \right] \left[\exp \left\{ -\frac{1}{2} \left(\frac{z-h}{\sigma_z} \right)^2 \right\} + \exp \left\{ \frac{1}{2} \left(\frac{z+h}{\sigma_z} \right)^2 \right\} \right] \quad 6.5$$

If a dimensionless concentration is defined as

$$K(x, y, z, h) = \frac{\chi(x, y, z, h) u H^2}{Q}$$

then equation 5.1 reduced to the following for $y = 0$ and $z = 0$:

$$K_o = K(x, 0, 0, h) = \frac{H^2}{\pi\sigma_y\sigma_z} \exp \left[-\frac{1}{2} \left(\frac{h}{\sigma_z} \right)^2 \right]. \quad 6.6$$

For $y = 0$ and $z = h$ the following equation results

$$K_H = K(x, 0, h, h) = \frac{H^2}{2\pi\sigma_y\sigma_z} \left[1 + \exp \left\{ -2 \left(\frac{h}{\sigma_z} \right)^2 \right\} \right]. \quad 6.7$$

The ratio of K_H to K_o is the same as the ratio of x_H (centerline concentration) to x_o (ground-level concentration) and represents the dilution between the plume centerline and ground level. In equation form

$$\frac{K_H}{K_o} = \frac{1 + \left\{ \exp -2 \left(\frac{h}{\sigma_z} \right)^2 \right\}}{2 \exp \left[-\frac{1}{2} \left(\frac{h}{\sigma_z} \right)^2 \right]} \quad 6.8$$

For plume impaction (i.e., $h = 0$) the ratio is equal to 1 and when the plume is slightly elevated (i.e., $h = \sigma_z/\sqrt{2}$) the ratio is less than 1 indicating that the ground-level concentration is larger than the

¹The integrated equation will not be used here since the only difference in the equation is a constant which would drop out in the final analysis.

centerline value. The latter case occurs due to the reflection term $(\exp -\frac{1}{2}(\frac{z+h}{\sigma_z})^2)$ in equation 6.1. When h is sufficiently large with respect to σ_z the ratio (K_H/K_o) quickly approaches infinity.

Using equation 6.8, the ratio of K_H/K_o versus H and σ_z can be computed and will give the same ratios as if using the Valley Model. To correct the ratio due to improper assumptions for flow over rough terrain the results of the wind-tunnel test were used. Although the source characteristics were not simulated in the experiment the flow field and atmospheric stability were. As discussed in section 6.1 the plume geometry was similar to what is expected for corresponding full-scale conditions. Since K_H/K_o is only a function of H/σ_z (that is if a normal distribution is assumed) and H/σ_z (or H/σ_y) in model and prototype are assumed equal, then

$$\left(\frac{K_H}{K_o}\right)_m = \left(\frac{K_H}{K_o}\right)_p .$$

The Valley Model was used to calculate the expected 1-hour average ground-level concentrations under conditions similar to those modeled in the wind tunnel (see Appendix C for computer listings). The estimated concentrations (x_v) were corrected based on the wind-tunnel results.

The following equation was used to correct the Valley Model results:

$$x_c = \frac{x_v * \left(\frac{K_H}{K_o}\right)_p}{\left(\frac{K_H}{K_g}\right)_m} \quad 6.9$$

where

x_c = the corrected concentration

x_v = the Valley Model prediction

$\left(\frac{K_H}{K_o}\right)_p$ = the centerline dilution computed from equation 6.8

$\left(\frac{K_H}{K_g}\right)_m^{1)}$ = the centerline dilution ratio observed in the wind tunnel for a similar stability and plume height

Table 6.7 gives the Valley Model 1-hour average concentration values computed using actual meteorological data at CPP for E stability. Also in the table are the corrected concentrations based on the results of the wind-tunnel tests. Two effective plume altitudes (381 and 476 m) were simulated in the wind tunnel; hence, to estimate the centerline dilution

$\left[\left(\frac{K_H}{K_g}\right)_m\right]$ for intermediate altitudes a linear interpolation was used. The

following two linear equations were developed--one for Badger and one for Garfield Peak--using the K_H/K_g values in Table 6.3:

- Garfield Peak:

$$\left(\frac{K_H}{K_g}\right)_m = 0.992H - 374.2 \quad 6.10$$

- Badger Peak:

$$\left(\frac{K_H}{K_g}\right)_m = 0.0383H - 12.90. \quad 6.11$$

The corrected concentration was then obtained by computing 1) $\left(\frac{K_H}{K_g}\right)_m$ from equation 6.10 or 6.11 as appropriate, 2) $\left(\frac{K_H}{K_o}\right)_p$ from equation 6.8, and 3) x_c from equation 6.9.

¹⁾ K_o and K_g are assumed equal for wind-tunnel observations.

The maximum Valley Model prediction is $44.93 \mu\text{g}/\text{m}^3$ for Badger Peak on 7/26/75 at 2400. After applying the appropriate corrections the maximum concentration becomes $12.5 \mu\text{g}/\text{m}^3$ for Badger Peak on 5/18/76 at 0600. The corrected values for the Garfield Peak predictions are all less than $5.0 \mu\text{g}/\text{m}^3$.

Table 6.8 gives the Valley Model computed concentrations using hypothetical meteorological data and corrected concentrations based on the wind-tunnel results for neutral stratification. Only one test (Badger Peak) was run in the wind tunnel with neutral stratification but as the results in Table 6.8 show even the Valley Model estimates are less than $5 \mu\text{g}/\text{m}^3$. This table is presented to show that even though the centerline dilution (K_H/K_g) is close to 1.0 (implies plume impaction) the resulting concentrations are low because high winds are required under neutral stratification to obtain plume rise values of 381 and 476 m.

REFERENCES

- Briggs, G. A., "Plume Rise Predictions," presented in Lectures on Air Pollution and Environmental Impact Analysis, sponsored by American Meteorological Society, September 29-October 3, 1975, Boston, MA.
- Burt, E., "Valley Model User's Guide," (EPA-450/2-77-018), Environmental Protection Agency, Research Triangle Park, NC, September 1977.
- Businger, J. A., "The Atmospheric Boundary Layer," Chapter 6 in Remote Sensing of the Troposphere, edited by V. E. Derr, U.S. Department of Commerce, National Oceanic and Atmospheric Administration, 1972.
- Cermak, J. E., "Applications of Fluid Mechanis to Wind Engineering," presented at Winter Annual Meeting of ASME, New York, November 17-21, 1974.
- Cermak, J. E., "Wind Tunnel for the Study of Turbulence in the Atmospheric Surface Layer," Fluid Dynamics and Diffusion Laboratory, Technical Report CER58-JEC42, Colorado State University, Fort Collins, Colorado, 1958.
- Csanady, G. T., Turbulent Diffusion in the Environment, D. Reidel Publishing Company, Doudrecht, Holland, 1973.
- Golder, D., "Relations among Stability Parameters in the Surface Layer," Boundary Layer Meteorology, Vol. 3, pp. 47-52, 1972.
- Hino, Mikio, "Maximum Ground-Level Concentration and Sampling Time," Atmospheric Environment, Vol. 2, Pergamon Press, pp. 149-165, 1968.
- Hinze, O. J., Turbulence, 2nd Edition, McGraw-Hill, Inc., 1975.
- Hoult, D. P. and J. Weil, "Turbulent Plume in a Laminar Cross Flow," Atmospheric Environment, 6:513-531, 1972.
- Kline, S. J. and F. A. McClintock, "Describing Uncertainties in Single-Sample Experiments," Mechanical Engineering, Vol. 75, pp. 3-8, 1953.
- McNair, H. M. and E. Bonelli, Basic Gas Chromatography, Consolidated Printers, Berkeley, CA, 1968.
- Ludwig, G. R. and G. T. Skinner, "Wind Tunnel Study of the Dispersion of Sulfur Dioxide in Southern Allegheny County, Pennsylvania," Colsan Corporation Report, Buffalo, New York, prepared for U.S. Environmental Protection Agency, Region III, Philadelphia, Pennsylvania, December 1976.
- Pasquill, F., Atmospheric Diffusion, 2nd Edition, John Wiley and Sons, New York, 1974.

Plate, E. J. and J. E. Cermak, "Micro-meteorological Wind Tunnel Facility," Fluid Dynamics and Diffusion Laboratory, Technical Report CER63EJP-JEC9, Colorado State University, Fort Collins, Colorado, 1963.

Schlichting, H., Boundary Layer Theory, McGraw-Hill, Inc., New York, 1968.

Slade, D. H., Meteorology and Atomic Energy, U.S. AEC, July 1968.

Snyder, W. H., "Similarity Criteria for the Application of Fluid Models to the Study of Air Pollution Meteorology," Boundary Layer Meteorology, Vol. 3, pp. 113-134, 1972.

Sutton, O. G., Micrometeorology, McGraw-Hill, Inc., New York, 1953.

Taylor, G. I., "Diffusion by Continuous Movements," Proceedings, London Meteorological Society, Vol. 20, pp. 196-211, 1921.

Touma, J. S., "Dependence of the Wind Profile Power Law on Stability for Various Locations," Journal of Air Pollution Control Ass'n., Vol. 27, No. 9, 1977.

Turner, P. B., Workbook of Atmospheric Dispersion Estimates, U.S. Department of Health, Education and Welfare, Public Health Service Publ. No. 999, Cincinnati, Ohio, AP-26, 88 p., 1969.

Whaley, H., "Derivation of Plume Dispersion Parameters from Measured 3-D Data," Atmospheric Environment, Vol. 8, 1974.

TABLES

Table 4.1 Summary of Model Parameters for Wind Tunnel Tests

<u>Parameter</u>	
1) Release Probe Diameter - D (cm)	1.42
2) Release Height - H (cm)	7.6 and 9.5
3) Volume Flow Rate - V (cm^3/s)	18.5 to 38.0
4) Gas Mixture (%)	
. Nitrogen	90.8
. Ethane	9.2
5) Ambient Velocity at H - u_H (m/s)	0.32 to 0.81
6) Wind Directions	325, 349 & Flat Terrain
7) Tower Top Froude Number - Fr_T at Site A	1.8 to 6.5

Table 4.2 Summary of Prototype Parameters for Colstrip Power Plant

<u>Parameter</u>	
1) Stack Height - h_s (m)	210.9
2) Stack Diameter - D (m)	11.0
3) Exit Velocity - u_s (m/s)	30.3
4) Exit Temperature - T_s ($^{\circ}\text{K}$)	361
5) Base Elevation of Stack (m, MSL)	989.9
6) Elevation of Badger Peak (m, MSL)	1348.2
7) Elevation of Garfield Peak (m, MSL)	1315.9
8) Effective Plume Altitude for E Stability - H (m, AGL)	381, 476

Table 4.3 Summary of Wind-Tunnel Tests

Run#	Terrain	Wind Direction	Fr		Ri		Release Model (cm)	Height H Prototype (m)	Release Model Volume Flow (cc/s)	Model Velocity at H (m/s)
			@ 10 cm	@ 1.9 cm	@ 10 cm	@ ~1.9 cm				
3	IN	325	2.0	3.3	0.49	0.15	7.6	381	18.5	0.38
4							9.5	476	18.5	0.40
5	IN	349	1.5	1.9	0.75	0.20	7.6	381	32.9	0.32
6							9.5	476	32.9	0.34
7			3.9	6.5	0.12	0.11	7.6	381	38.0	0.71
8							9.5	476	38.0	0.81
9	OUT	N/A	2.7	4.6	0.16	0.11	7.6	381	27.8	0.58
10							9.5	476	27.8	0.64
11			2.2	1.8	0.27	0.25	7.6	381	27.8	0.49
12							9.5	476	27.8	0.57

Table 4.4 Sampling Grid Coordinates for:

a) Flat terrain runs at site L' with $Fr_T = 4.6$

<u>Location#</u>	<u>Y(cm)</u>	<u>Z(cm)</u>
1	-47.0	0
2	-31.8	
3	-16.5	
4	-8.9	
5	0	
6	6.4	
7	14.0	
8	29.2	
9	44.4	0
10	-47.0	14.6
11	-31.8	
12	-16.5	
13	-8.9	
14	6.4	
15	14.0	
16	29.2	
17	44.4	14.6
18	0	6.6
19		9.2
20		11.7
21		14.9
22		19.3
23		24.4
24	0	29.5

b) Flat terrain runs at site G' for $Fr_T = 1.8$ and 4.6
and at site L' with $Fr_T = 1.8$

<u>Location#</u>	<u>Y(cm)</u>	<u>Z(cm)</u>
1	-47.0	0
2	-31.8	
3	-16.5	
4	-8.9	
5	0	
6	6.4	
7	14.0	
8	29.2	
9	44.4	0
10	-47.0	10.5
11	-31.8	
12	-16.5	
13	-8.9	
14	6.4	
15	14.0	
16	29.2	
17	44.4	10.5
18	0	2.5
19		5.1
20		7.6
21		10.8
22		15.2
23		20.3
24	0	25.4

Table 4.4 (continued)

c) 325° wind direction runs at site L with $Fr_T = 3.3$

<u>Location#</u>	<u>Y(cm)</u>	<u>Z(cm)</u>
1	-47.0	-3.2
2	-31.8	-3.2
3	-16.5	-1.6
4	-8.9	-1.0
5	0	0
6	6.4	0.6
7	14.0	0
8	29.2	0.3
9	44.4	-1.6
10	-47.0	10.5
11	-31.8	
12	-16.5	
13	-8.9	
14	6.4	
15	14.0	
16	29.2	
17	44.4	10.5
18	0	2.5
19		5.1
20		7.6
21		10.8
22		15.2
23		20.3
24	0	25.4

d) 325° wind direction runs at site G with $Fr_T = 3.3$

<u>Location#</u>	<u>Y(cm)</u>	<u>Z(cm)</u>
1	-47.0	0.3
2	-31.8	
3	-16.5	
4	-8.9	
5	0	0.3
6	6.4	0.6
7	14.0	1.3
8	29.2	1.6
9	44.4	1.6
10	-47.0	10.8
11	-31.8	
12	-16.5	
13	-8.9	
14	6.4	
15	14.0	
16	29.2	
17	44.4	10.8
18	0	2.8
19		5.4
20		7.9
21		11.1
22		15.6
23		20.6
24	0	25.7

Table 4.4 (continued)

e) 349° wind direction runs at site M' with $Fr_T = 1.9$ and 6.5

<u>Location#</u>	<u>Y(cm)</u>	<u>Z(cm)</u>
1	-47.0	0.2
2	-31.8	0.2
3	-16.5	0.5
4	-8.9	0.8
5	0	0.0
6	6.4	1.5
7	14.0	1.5
8	29.2	3.4
9	44.4	2.4
10	-47.0	11.0
11	-31.8	
12	-16.5	
13	-8.9	
14	6.4	
15	14.0	
16	29.2	
17	44.4	11.0
18	0	3.0
19		5.6
20		8.1
21		11.3
22		15.7
23		20.8
24	0	25.9

f) 349° wind direction runs at site G' with $Fr_T = 1.9$ and 6.5

<u>Location#</u>	<u>Y(cm)</u>	<u>Z(cm)</u>
1	-47.0	0.5
2	-31.8	0.2
3	-16.5	1.5
4	-8.9	1.5
5	0	0.5
6	6.4	0.8
7	14.0	1.5
8	29.2	0.8
9	44.4	1.5
10	-47.0	11.0
11	-31.8	
12	-16.5	
13	-8.9	
14	6.4	
15	14.0	
16	29.2	
17	44.4	11.0
18	0	3.0
19		5.6
20		8.1
21		11.3
22		15.7
23		20.8
24	0	25.9

Table 5.1 EPA Stability Criteria for Colstrip Power Plant

Pasquill Category	Potential Temperature	Wind Speed Range (m/s)
	Lapse Rate $\Delta\theta/\Delta z$ ($^{\circ}\text{C}/100\text{m}$)	
D	$-0.1 < \frac{\Delta\theta}{\Delta z} < 1.0$	$0 \rightarrow ?$
E	$1 < \frac{\Delta\theta}{\Delta z} < 5$	$0 - 10$
F	$5 < \frac{\Delta\theta}{\Delta z}$	$0 - 6$

Table 5.2 Revised Stability Criteria Based on Froude Number for Colstrip Power Plant

Pasquill Category	$Fr_T^{1)}$ range
D	$\infty \rightarrow 5.86$
E	$5.86 \rightarrow 1.57$
F	$1.57 \rightarrow 0$

1)

$$Fr_T = \sqrt{\frac{u_T}{\frac{g}{T} \frac{\Delta\theta}{\Delta z}}} z_T \quad \text{where } u_T \text{ is wind speed at top of tower}$$

$$(z_T = 93.3\text{m})$$

Table 5.3 Example of Power Law Exponent Variations with Stability from a) Touma, 1977 and b) Sutton, 1953

a) <u>Touma, 1977</u>								
Stability Class	Missouri ^a 1973-74	Missouri ^a 1974-75	Kansas ^a 1973-74	Kansas ^a 1974-75	Iowa ^a 1973-74	Texas ^a 1973-74	Michigan ^a 1975-76	Missouri ^b 1973-74
A	0.103	0.099	0.124	0.091	0.104	0.120	0.109	0.111
B	0.079	0.092	0.145	0.103	0.101	0.123	0.085	0.119
C	0.082	0.080	0.152	0.122	0.114	0.128	0.078	0.104
D	0.115	0.144 ^c	0.199	0.172	0.188	0.174	0.116	0.136
E	0.271	0.273	0.341	0.282	0.313	0.331	0.261	0.272
F	0.423	0.385	0.480	0.412	0.466	0.562	0.425	0.242
G	0.504	0.417	0.506	0.452	0.444	0.624	0.516	0.447
Terrain	Rolling	Rolling	Rolling	Rolling	Rolling	Rolling	Hilly	Rolling

^aStability class based on a ΔT of 10 to 60 m.

^bStability class based on a ΔT of 10 to 90 m.

63

b) Sutton, 1953

$\Delta T = T_{400} - T_5$, ($^{\circ}$ F)			n
0 to 2			0.32
2 to 4			0.44
4 to 6			0.59
6 to 8			0.63
8 to 10			0.62
10 to 12			0.77

Table 5.4 Velocity Profiles for 325° Wind Direction and $Fr_T = 3.3$

<u>Location A</u>						
Z (cm)	u (m/s)	i _x (percent)	T (°K)	Fr	Ri	z _m
0.62	0.089	5.73	288.5			
1.51	0.160	4.09	291.0	3.49	0.12	0.92
1.96	0.229	4.06	293.5	3.30	0.11	1.61
2.58	0.269	4.51	295.0	3.12	0.19	2.26
5.10	0.354	5.10	298.0	2.46	0.59	5.70
10.19	0.414	5.58	300.5	1.99	0.33	14.68
20.35	0.657	7.21	305.5	1.86	0.23	29.33
40.67	0.954	2.48	309.0	1.81		
<u>Location B</u>						
0.64	0.173	4.82	291.5			
1.29	0.245	7.35	294.0	5.29	0.10	0.93
1.93	0.301	6.51	295.0	5.18	0.70	1.59
2.57	0.332	3.51	297.0	4.19	0.44	2.23
5.08	0.432	5.00	300.0	3.38	0.25	3.68
10.16	0.511	4.61	302.0	2.64	0.53	7.33
20.35	0.586	4.09	305.0	1.92	1.75	14.67
40.67	0.836	1.78	309.0	1.92	0.42	29.35
<u>Location C</u>						
0.64	0.168	5.94	291.5			
1.28	0.233	7.25	294.0	5.03	0.13	0.92
1.90	0.307	4.86	296.0	4.68	0.08	1.57
2.54	0.344	5.57	297.0	4.50	0.15	2.20
5.07	0.369	7.55	299.5	2.97	3.33	3.66
10.16	0.398	6.82	302.5	2.01	5.91	7.32
20.34	0.621	9.26	306.0	1.96	0.23	14.67
40.68	0.969	1.73	309.5	1.97	0.19	29.34
<u>Location D</u>						
0.63	0.129	5.16	290.0			
1.26	0.179	4.99	291.5	5.01	0.13	0.91
1.91	0.207	4.24	293.0	3.86	0.42	1.56
2.53	0.242	4.84	294.3	3.47	0.22	2.21
5.09	0.328	4.24	298.0	2.64	0.42	3.66
10.16	0.509	5.77	303.0	2.36	0.25	7.34
20.28	0.763	7.09	307.0	2.23	0.20	14.64
40.66	1.015	2.25	310.3	1.94	0.34	29.30
<u>Location H</u>						
0.63	--	--	289.3			
1.28	0.159	5.92	290.7	4.60	--	--
1.90	0.204	4.05	291.7	4.25	0.10	1.57
2.55	0.251	4.19	293.0	3.86	0.15	2.21
5.08	0.392	3.85	298.0	3.02	0.20	3.64
10.16	0.461	2.07	301.5	2.20	1.22	7.33
20.34	0.578	3.98	304.3	1.79	0.67	14.67
40.68	0.950	2.45	308.7	1.85	0.21	29.34

Table 5.4 Velocity Profiles for 325° Wind Direction and $Fr_T = 3.3$
(continued)

Location I

Z (cm)	v (m/s)	i _x (percent)	T (°K)	Fr	Ri	z _m
0.64	0.081	6.79	289.3		0.00	0.92
1.28	0.109	6.35	289.3	6.76	0.17	1.58
1.92	0.148	6.48	290.5	3.87	0.08	2.23
2.55	0.198	5.31	291.5	3.69	0.14	3.67
5.07	0.367	3.47	296.3	3.08	0.71	7.32
10.16	0.474	3.46	301.2	2.26	0.57	14.66
20.32	0.606	4.01	304.2	1.87	0.22	29.32
40.66	0.981	2.51	309.0	1.89		

Location J

0.64	0.083	6.84	288.5		0.17	0.93
1.30	0.115	5.80	289.3	4.36	0.20	1.59
1.92	0.142	6.01	290.0	3.71	0.16	2.22
2.55	0.182	6.31	291.2	3.27	0.16	3.66
5.07	0.310	6.18	294.3	2.91	0.35	7.32
10.16	0.483	3.92	300.5	2.32	0.50	14.67
20.34	0.645	2.94	304.5	1.94	0.26	29.34
40.67	0.986	2.07	309.2	1.86		

Location L

0.64	0.190	4.42	293.0		0.14	0.92
1.28	0.229	4.02	294.0	7.83	0.13	1.58
1.92	0.270	4.64	295.0	6.16	0.08	2.22
2.55	0.329	4.37	296.3	5.38	0.16	3.68
5.11	0.480	4.61	300.3	4.04	0.94	7.35
10.17	0.542	4.28	302.5	2.94	0.48	14.67
20.34	0.685	2.64	305.5	2.34	0.26	29.34
40.68	1.003	1.11	309.5	2.13		

Location M

0.63	0.132	5.67	293.5		0.35	0.92
1.28	0.157	4.17	294.5	5.42	2.31	1.60
1.92	0.164	4.02	295.0	4.32	0.23	2.25
2.55	0.198	2.74	296.3	3.52	0.25	3.68
5.08	0.268	2.51	297.8	2.95	0.46	7.28
10.17	0.384	1.83	301.5	2.27	0.42	14.68
20.37	0.537	2.29	304.5	1.95	0.26	29.37
40.69	0.863	1.60	308.8	1.90		

Location N

0.64	0.085	6.97	291.0		0.70	0.92
1.27	0.104	5.76	292.2	3.24	1.57	1.84
2.57	0.131	4.87	294.5	2.07	5.32	3.69
5.09	0.150	6.64	296.8	1.41	0.62	7.34
10.17	0.246	3.52	300.2	1.35	0.29	14.66
20.31	0.459	6.35	304.2	1.52	0.13	29.31
40.64	0.872	2.84	307.5	1.85		

Location O

0.62	0.146	8.21	288.5		1.89	1.37
2.58	0.181	6.18	292.0	2.86	0.45	3.70
5.10	0.234	4.81	293.5	2.37	0.43	7.34
10.16	0.359	2.90	297.5	1.99	0.48	14.66
20.33	0.549	2.83	302.7	1.75	0.87	29.33
40.65	0.758	1.68	308.5	1.45		

Table 5.5 Summary of Similarity Theory Analysis of Velocity Profiles for the 325° Wind Direction and an Fr at 10 cm (Location A) of 2.0

Location	z_o (cm)	$1/L(m^{-1})$	u^* (cm/s)	Re_{z_o}	\hat{e} (cm/s)	n
A	0.243	2.8	3.6	5.7	1.9	0.54
B	0.133	1.0	4.3	3.7	2.1	0.36
C	0.246	1.2	4.9	7.9	6.2	0.39
D	0.370	1.9	4.9	11.9	3.4	0.51
H	0.481	1.2	5.4	17.0	3.9	0.49
I	0.540	1.8	5.0	17.7	3.4	0.62
J	0.512	2.3	4.4	14.7	2.5	0.62
L	0.176	1.6	4.7	5.4	2.8	0.41
M	0.068	6.4	1.9	0.8	1.1	0.47
N	22.204	-17.7	-1.1	-	1.1	0.59
O	0.252	2.4	3.1	5.1	3.8	0.44
Average	0.300	2.3	4.2	9.0	3.1	0.49

Table 5.6 Velocity Profiles for 349° Wind Direction and $Fr_T = 1.9$

<u>Location A</u>						
Z (cm)	u (m/s)	i _x (percent)	T (°K)	Fr	Ri	z _m
0.64	0.050	7.69	284.6		0.28	1.16
1.90	0.153	7.76	291.6	1.85	0.13	2.20
2.54	0.218	4.75	294.1	2.09	0.67	3.67
5.09	0.288	6.36	298.0	1.78	0.88	7.34
10.18	0.343	5.64	299.6	1.47	0.61	14.68
20.34	0.497	6.79	304.0	1.35	0.28	29.32
40.61	0.820	2.08	308.5	1.44		
<u>Location B</u>						
0.63	0.208	4.50	292.5		0.37	0.88
1.20	0.240	4.82	294.5	5.84	0.10	1.50
1.84	0.297	3.73	296.0	5.20	0.28	2.17
2.53	0.332	2.87	297.5	4.44	0.09	3.63
5.02	0.407	3.54	299.5	3.53	1.47	7.28
10.13	0.470	2.75	301.7	2.60	0.49	14.63
20.30	0.549	5.46	304.2	1.93	0.33	29.29
40.62	0.845	2.48	308.7	1.81		
<u>Location D</u>						
0.63	-	-	284.6		-	-
1.27	0.101	4.15	288.5	1.73	0.18	1.54
1.85	0.148	2.64	290.5	1.96	0.62	2.15
2.47	0.174	3.67	292.5	1.55	0.77	3.59
5.01	0.236	3.37	296.0	1.59	0.41	7.26
10.10	0.385	5.02	301.5	1.56	0.33	14.60
20.27	0.584	5.84	305.5	1.53	0.63	29.28
40.62	0.765	3.61	308.7	1.33		
<u>Location G</u>						
0.65	0.132	6.97	291.0		0.07	0.95
1.32	0.219	5.90	293.5	4.69	0.07	0.95
1.32	0.219	5.90	293.5	4.69	0.11	1.59
1.90	0.277	2.98	295.5	4.20	0.24	2.17
2.46	0.308	2.54	296.75	3.85	0.61	3.64
5.15	0.371	3.08	299.5	2.88	0.45	7.33
10.06	0.444	3.29	301.0	2.35	0.72	14.62
20.58	0.552	3.22	303.5	1.87	0.25	29.33
40.59	0.893	3.00	308.0	1.85		
<u>Location H</u>						
0.63	0.073	15.11	289.5		0.67	0.86
1.13	0.084	14.16	290.0	4.04	0.24	1.52
1.99	0.127	18.82	291.5	2.87	0.39	2.23
2.49	0.148	11.86	292.5	2.55	0.21	3.64
5.09	0.267	11.24	296.0	2.37	0.19	7.31
10.10	0.483	2.22	301.5	2.33	0.35	14.61
20.30	0.645	2.95	304.25	2.02	0.35	29.28
40.58	0.916	1.43	308.25	1.82		
<u>Location I</u>						
0.63	0.099	10.71	288.5		0.28	0.94
1.33	0.128	15.58	289.5	4.37	-	1.58
1.86	0.128	7.85	291.5	2.40	0.10	2.16
2.48	0.160	8.60	292.0	2.55	0.14	3.64
5.11	0.339	4.66	297.0	2.63	0.34	7.32
10.09	0.477	2.40	301.0	2.26	0.58	14.58
20.25	0.596	3.29	303.5	1.85	0.31	29.38
40.90	0.923	7.94	308.5	1.77		

Table 5.6 Velocity Profiles for 349° Wind Direction and $Fr_T = 1.9$
(continued)

<u>Location J</u>						
<u>z</u> (cm)	<u>u</u> (m/s)	<u>i_x</u> (percent)	T (°K)	Fr	Ri	<u>z_m</u>
0.62	0.083	5.78	287.5		0.06	0.85
1.14	0.158	12.40	289.5	3.83	0.99	1.47
1.85	0.226	17.35	291.25	5.10	0.12	2.19
2.56	0.284	14.17	293.0	3.59	0.06	3.65
5.01	0.546	4.25	298.5	3.76	0.50	7.25
10.08	0.646	3.25	301.5	2.88	0.55	14.83
20.87	0.774	3.22	304.0	2.257	0.20	29.67
40.65	1.150	1.21	308.5	2.125		
<u>Location K</u>						
0.64	0.194	4.57	291.0		0.05	0.89
1.20	0.277	4.86	293.0	6.67	0.10	1.49
1.83	0.333	3.88	294.5	5.79	-	-
2.46	0.335	3.76	295.5	4.737	0.32	3.61
5.08	0.425	3.23	298.5	3.53	0.34	7.30
10.10	0.551	2.75	301.75	2.814	0.35	14.65
20.40	0.733	2.30	305.2	2.34	0.32	29.41
40.74	1.011	1.70	309.0	2.05		
<u>Location L</u>						
0.63	0.208	6.34	291.75		0.24	0.91
1.26	0.247	6.18	293.5	6.43	0.10	1.54
1.86	0.300	6.18	295.0	5.43	0.14	2.17
2.51	0.328	6.15	295.5	5.06	0.09	3.62
5.02	0.521	3.64	299.5	4.29	0.24	7.26
10.09	0.677	1.22	303.0	3.59	1.17	14.60
20.28	0.761	0.89	305.5	2.48	0.37	29.28
40.61	1.027	1.16	309.5	2.10		
<u>Location M</u>						
0.65	0.215	3.83	291.5		0.16	0.94
1.30	0.268	1.32	293.5	6.42	0.29	1.56
1.86	0.299	4.79	295.0	5.12	0.19	2.16
2.48	0.322	4.91	295.5	4.81	0.22	3.60
5.02	0.446	1.11	299.5	3.61	1.55	7.27
10.11	0.498	0.97	302.0	2.57	0.58	14.64
20.36	0.645	0.46	304.5	2.15	0.26	29.32
40.59	0.958	2.35	308.5	2.00		

Table 5.7 Summary of Similarity Theory Analysis of Velocity Profiles
for the 349° Wind Direction and an Fr at 10 cm (Location A)
of 1.5

Location	z_o (cm)	$1/L(m^{-1})$	u^* (cm/s)	Re_{z_o}	ϵ (cm/s)	n
A	0.40	2.4	3.4	8.9	2.7	0.64
B	0.08	1.6	3.4	1.8	3.7	0.32
D	0.73	1.0	5.1	24.3	2.3	0.58
G	0.18	1.6	4.0	4.7	3.6	0.42
H	0.70	1.4	5.4	27.7	4.0	0.67
I	0.57	1.4	5.1	19.0	4.1	0.60
J	0.55	0.6	8.1	29.1	4.9	0.63
K	0.08	2.5	3.7	1.9	1.1	0.38
L	0.27	0.6	6.6	11.7	3.8	0.41
M	0.05	2.7	3.2	1.1	2.0	0.35
Average	0.36	1.6	4.8	13.0	3.2	0.50

1) The value for viscosity was taken to be $0.153 \text{ cm}^2 \text{s}^{-1}$.

Table 5.8 Velocity Profiles for 349° Wind Direction and $Fr_T = 6.5$

<u>Location A</u>						
Z (cm)	U (m/s)	i _x (percent)	T (°K)	Fr	Ri	Z _m
0.64	0.287	8.31	296.5		0.07	0.89
1.20	0.358	6.63	298.5	8.70	0.14	1.54
1.93	0.423	7.66	301.0	6.48	0.08	2.20
2.49	0.472	9.11	302.0	6.08	0.21	3.63
5.08	0.573	9.31	304.5	4.65	0.12	7.34
10.19	0.801	5.91	310.5	3.88		
<u>Location G</u>						
0.64	0.369	13.44	299.5		0.06	0.93
1.30	0.430	12.36	300.5	14.87	0.06	1.55
1.83	0.485	11.35	301.5	11.32	0.32	2.17
2.54	0.512	9.85	302.5	8.89	0.21	3.66
5.06	0.635	5.61	306.5	5.54	0.21	7.36
10.28	0.822	5.57	311.0	4.09	0.24	14.83
20.55	1.080	7.44	316.0	3.24	0.18	29.54
40.84	1.689	1.10	326.5	2.85		
<u>Location II</u>						
0.65	0.479	8.53	300.5		0.09	0.92
1.26	0.551	7.75	302.75	12.63	1.82	1.55
1.89	0.565	7.91	304.5	9.25	0.07	2.19
2.53	0.627	8.27	305.75	8.25	0.08	3.66
5.09	0.824	3.93	309.5	6.34	1.03	7.39
10.30	0.893	4.92	312.5	4.35	0.19	14.82
20.50	1.132	6.72	316.0	3.50	0.15	29.55
40.94	1.728	1.67	324.5	3.09		
<u>Location I</u>						
0.66	0.160	9.50	298.0		0.02	1.02
1.50	0.310	13.74	300.0	7.40	0.18	1.69
1.90	0.343	10.96	301.5	5.94	0.03	2.17
2.47	0.442	9.77	303.25	5.82	0.06	3.63
5.10	0.730	5.12	309.5	4.95	2.68	7.04
9.41	0.769	2.22	312.5	3.54	0.26	14.26
20.54	1.000	3.38	316.5	2.83	0.18	29.52
40.79	1.433	1.93	322.0	2.55		
<u>Location J</u>						
0.64	0.198	14.94	295.5		0.14	0.92
1.27	0.237	15.74	296.5	8.14	0.16	1.56
1.90	0.288	13.02	298.5	5.41	0.05	2.17
2.47	0.376	12.22	300.5	5.08	0.07	3.61
5.06	0.661	6.11	307.5	4.40	0.21	7.43
10.44	0.882	2.48	313.5	3.47	0.36	14.84
20.34	1.043	2.49	316.5	2.78	0.26	29.35
40.70	1.415	1.69	322.24	2.39		
<u>Location K</u>						
0.64	0.400	11.33	300.5		0.02	0.93
1.30	0.550	10.09	302.75	12.71	0.12	1.59
1.93	0.604	6.92	304.5	9.87	0.16	2.22
2.54	0.654	6.10	306.5	8.06	0.06	3.66
5.08	0.888	4.70	310.5	6.50	0.28	7.38
10.29	1.055	2.14	315.25	4.65	0.34	14.72
20.26	1.198	2.37	317.5	3.57	0.37	29.06
40.49	1.486	1.24	322.5	2.78		

Table 5.8 Velocity Profiles for 349° Wind Direction and $Fr_T = 6.5$
(continued)

<u>Location L</u>						
Z (cm)	u (m/s)	i _x (percent)	T ("K)	Fr	Ri	z _m
0.64	0.419	10.77	301.5		0.06	0.92
1.28	0.494	9.27	303.0	14.00	0.11	1.58
1.92	0.551	6.94	304.75	10.02	0.04	2.22
2.56	0.651	8.51	306.5	8.78	0.08	3.69
5.10	0.891	3.77	312.0	6.37	0.72	7.37
10.22	0.969	1.97	314.75	4.52	0.33	14.80
20.57	1.132	1.99	317.5	3.45	0.24	29.49
40.67	1.507	0.36	323.0	2.85		
<u>Location M</u>						
0.64	0.349	7.91	299.25		0.03	0.95
1.34	0.481	5.22	301.5	11.08	1.21	1.60
1.90	0.496	3.75	303.0	8.39	0.04	2.20
2.54	0.579	4.14	304.5	7.61	0.12	3.68
5.12	0.777	2.74	310.0	5.46	0.66	7.41
10.30	0.863	2.99	313.0	3.93	0.20	14.78
20.41	1.113	3.48	317.0	3.23	0.23	29.47
40.88	1.517	1.11	323.0	2.72		

Table 5.9 Summary of Similarity Theory Analysis of Velocity Profiles
for the 349° Wind Direction and an Fr at 10 cm (Location A)
of 3.9

Location	z_0 (cm)	$1/L(m^{-1})$	u^* (cm/s)	$Re_{z_0}^{1)}$	\hat{e} (cm/s)	n
A	0.56	-0.58	15.4	56.4	14.7	0.40
G	0.01	6.9	3.0	0.2	1.6	0.37
H	0.25	2.9	5.1	8.3	5.2	0.31
I	0.41	0.7	9.5	25.5	5.3	0.52
J	0.47	0.6	10.1	31.0	5.8	0.52
K	0.12	0.4	8.9	6.7	2.6	0.31
L	0.11	0.7	8.2	5.9	4.7	0.31
M	0.08	1.7	6.4	3.4	2.8	0.34
Average	0.25	1.7	8.3	17.2	5.3	0.39

¹⁾The value for viscosity was taken to be $0.153 \text{ cm}^2 \text{s}^{-1}$.

Table 5.10 Flat Terrain Velocity Profiles for $Fr_T = 1.8$

<u>Location A'</u>	<u>Z (cm)</u>	<u>u (m/s)</u>	<u>ix (percent)</u>	<u>T (°K)</u>	<u>Fr</u>	<u>Ri</u>	<u>z_m</u>
	0.61	0.034	15.43	292.9		0.28	0.89
	1.24	0.077	10.45	295.4	1.71	0.28	1.55
	1.91	0.127	8.18	298.6	1.75	0.23	2.18
	2.51	0.182	6.25	301.9	1.84	0.13	3.63
	5.05	0.379	5.46	307.5	2.30	0.20	7.29
	10.13	0.591	4.98	314.1	2.18	0.38	14.63
	20.32	0.775	4.56	318.2	1.88	0.61	29.34
	40.63	0.961	3.84	321.6	1.57		
<u>Location C'</u>							
	0.64	0.083	9.29	292.8		0.18	0.89
	1.22	0.138	6.74	295.5	2.89	0.08	1.52
	1.85	0.240	5.16	297.7	3.00	0.10	2.16
	2.51	0.330	4.53	303.3	3.07	0.33	3.12
	3.84	0.405	3.95	307.6	2.72	0.13	4.45
	5.11	0.465	5.38	308.8	2.67	0.20	6.27
	7.62	0.556	5.37	311.0	2.52		
	10.16	0.602	6.20	312.7	2.28	0.64	8.84
	15.24	0.689	5.40	314.9	2.05	0.46	12.52
	20.35	0.753	5.09	316.3	1.89	0.53	17.68
	27.97	0.842	4.44	318.4	1.74	0.64	23.95
	40.74	1.003	3.48	321.8	1.63	0.51	33.96
	61.04	1.213	3.18	327.5	1.48	0.79	50.22
	81.38	1.294	3.02	330.0	1.32		70.71
<u>Location I'</u>							
	0.64	0.061	12.39	293.0		0.13	0.91
	1.24	0.131	8.05	296.2	2.53	10.29	1.55
	1.91	0.157	7.02	297.9	2.02	0.08	2.21
	2.51	0.214	5.93	300.3	2.37	0.03	3.12
	3.84	0.288	4.63	304.4	2.21	0.18	4.42
	5.08	0.363	3.91	307.0	2.23	0.13	6.27
	7.62	0.527	5.32	311.3	2.38		
	10.16	0.618	4.93	313.4	2.32	0.43	12.55
	15.27	0.707	3.41	315.6	2.08	1.04	17.70
	20.37	0.756	3.68	317.2	1.87	0.30	23.98
	27.97	0.887	3.03	319.4	1.81	0.89	33.93
	40.63	0.991	3.00	321.9	1.61	0.51	50.57
	61.93	1.220	2.58	326.0	1.51	8.81	71.22
	81.38	1.266	2.87	329.2	1.31		
<u>Location L'</u>							
	0.64	0.016	22.98	289.5		18.11	0.89
	1.22	0.021	20.82	291.8	0.474	0.81	1.52
	1.91	0.043	13.52	293.5	0.695	0.76	2.18
	2.51	0.055	12.14	295.0	0.70	0.18	3.12
	3.84	0.143	8.64	298.1	1.23		
	5.08	0.239	5.83	302.0	1.55	0.18	4.42
	7.62	0.398	4.49	307.6	1.80	0.18	6.27
	10.19	0.577	4.97	311.7	2.06	0.10	8.84
	15.24	0.690	3.68	315.3	1.90	0.46	17.68
	20.37	0.771	3.86	317.2	1.78	0.30	23.95
	27.94	0.896	3.48	319.2	1.72	0.86	33.91
	40.63	1.006	3.04	321.9	1.54	0.48	50.55
	61.90	1.256	2.46	326.7	1.46	23.34	71.22
	81.43	1.281	2.51	329.2	1.26		

Table 5.11 Summary of Similarity Theory Analysis of Velocity Profiles for Flat Tunnel and an Fr at 10 cm (Location A) of 2.2

Location	z_o (cm)	$1/L(m^{-1})$	u^* (cm/s)	Re_{z_o}	ϵ (cm/s)	n
A	0.855	0.34	8.6	48.1	4.7	0.22
G	0.486	0.54	7.3	23.2	2.3	0.14
I	0.830	0.35	8.8	47.7	4.7	0.18
L	1.511	0.23	10.9	107.7	9.1	0.53
Average	0.92	0.37	8.9	56.7	5.2	0.27

Table 5.12 Flat Terrain Velocity Profiles for $Fr_T = 4.6$

<u>Location A'</u>						
<u>z</u> (cm)	<u>u</u> (m/s)	<u>ix</u> (percent)	T (°K)	Fr	Ri	Zm
0.69	0.154	6.52	296.8			
1.30	0.210	7.35	298.6	5.21	0.13	0.97
1.91	0.265	7.10	300.2	4.61	0.10	1.57
2.54	0.261	7.35	302.2	3.34	25.83	2.21
3.86	0.353	7.82	304.5	3.26	0.13	3.15
5.11	0.388	9.14	307.3	2.74	0.91	4.45
7.65	0.579	6.45	311.4	2.92	0.28	8.84
10.16	0.657	6.72	313.5	2.72	0.15	14.66
20.32	0.950	4.63	317.8	2.54	0.51	29.31
40.64	1.176	3.33	321.9	2.06		
<u>Location C'</u>						
0.61	0.170	4.77	298.2			
1.24	0.257	4.24	300.0	6.79	0.05	0.89
1.91	0.343	4.32	302.8	5.30	0.03	2.21
2.54	0.458	3.17	305.0	5.34	79.93	3.15
3.86	0.455	5.59	306.7	4.06	0.15	4.47
5.11	0.510	4.97	307.8	3.80	1.07	6.32
7.67	0.540	5.29	309.0	3.18	1.09	8.86
10.16	0.576	4.41	310.8	2.76	0.30	14.66
20.35	0.767	5.80	314.2	2.35	0.25	29.34
40.64	1.108	3.36	319.0	2.13		
<u>Location I'</u>						
0.66	0.047	9.87	294.0			
1.27	0.141	5.92	296.7	2.90	0.05	0.94
1.27	0.160	5.96	298.3	2.61	--	--
1.91	0.217	4.83	300.6	2.73	0.15	1.57
2.46	0.300	3.63	302.8	3.05	0.05	2.18
3.76	0.454	3.13	306.3	3.36	0.05	3.07
5.11	0.526	5.23	308.4	3.18	0.18	4.42
10.21	0.596	4.23	311.2	2.42	0.91	7.37
20.37	0.736	4.60	314.4	1.98	0.51	14.71
40.59	1.122	2.88	319.6	1.94	0.23	29.34
<u>Location L'</u>						
0.66	0.024	12.75	290.3			
1.27	0.034	11.45	291.8	0.932	1.65	1.57
1.93	0.050	12.49	293.7	0.866	3.48	2.21
2.54	0.058	11.44	294.8	0.808	0.15	3.68
5.11	0.214	6.12	299.3	1.62	0.13	7.37
10.21	0.597	4.02	309.8	2.27	0.36	14.68
20.29	0.800	3.45	314.3	1.99	0.66	29.29
40.61	0.956	2.98	316.8	1.61		

Table 5.13 Summary of Similarity Theory Analysis of Velocity Profiles for Flat Tunnel and an Fr at 10 cm (Location A) of 2.7

Location	z_o (cm)	$1/L(m^{-1})$	u^* (cm/s)	Re_{z_o}	ϵ (cm/s)	n
A	0.573	0.90	8.0	30.0	5.8	0.53
G	0.197	1.20	5.6	7.2	3.8	0.42
I	0.644	0.38	8.7	36.6	4.8	0.77
L	1.364	-0.11	11.9	106.1	11.6	1.09
Average	0.69	0.59	8.6	45.0	6.5	0.70

Table 6.1 Summary of Concentration Measurements

Description	Fr/Fr _T	Distance/Location (m)	Velocity @ Release Height (cm/s)			K _H	Model (cm)	z _{max} Prototype (m)	z̄			σ _y Prototype (m)	Model (cm)	σ _z Prototype (m)	
			H (cm)	K _H	Model (cm)				Prototype (m)	Model (cm)	Prototype (m)	z _g (cm)	K _g		
FLAT Terrain	2.2/1.8	2.45 / G'	7.6	0.49	0.500	7.6	380	9.0	450	0.079	0.018	7.3	364	3.1	152
			9.5	0.57	0.666	10.8	540	12.1	605	0.079	0.005	6.9	346	4.4	217
		5.49 / L'	7.6	0.49	0.323	10.5	525	9.06	303	0.079	0.070	8.8	440	3.9	195
			9.5	0.57	0.357	10.5	525	10.51	526	0.079	0.037	11.1	555	3.6	183
	2.7/4.6	2.45 / G'	7.6	0.58	0.325	10.5	525	13.2	660	0.079	0.007	7.3	364	4.2	208
			9.5	0.64	0.320	10.5	525	16.1	805	0.079	0.001	8.1	407	4.4	219 ¹
		5.48 / L'	7.6	0.58	0.131	6.6	330	10.3	516	0.079	0.059	11.4	570	6.2	312 ³
			9.5	0.64	0.159	14.6	730	15.9	796	0.079	0.015	11.3	565	7.1	354 ³
349° Wind Direction	1.5/1.9	2.45 / G'	7.6	0.32	0.498	5.6	280	5.7	284	0.079	0.172	12.1	603	2.4	121 ³
			9.5	0.34	0.442	8.1	405	7.8	392	0.500	0.025	10.0	502	2.4	119 ¹
		5.49 / M'	7.6	0.32	0.168	3.0	150	4.1	206	0.079	0.099	12.2	608	2.6	127 ^{1,3}
			9.5	0.34	0.539	5.6	280	6.7	332	0.079	0.101	14.9	745	2.8	140 ³
	3.9/6.5	2.45 / G'	7.6	0.71	0.198	8.1	405	8.4	420	0.079	0.046	11.4	572	3.3	163 ^{1,2}
			9.5	0.81	0.509	8.1	405	9.4	470	0.078	0.070	9.1	457	3.7	185 ¹
		5.49 / M'	7.6	0.71	0.143	0	0	5.4	270	0.079	0.143	18.2	907	3.5	173 ³
			9.5	0.81	0.234	5.6	280	5.3	265	0.079	0.159	18.5	926	3.5	173 ³
325° Wind Direction	2.0/3.3	2.24 / G	7.6	0.38	0.159	7.9	395	6.8	340	0.300	0.060	10.1	505	3.0	148 ¹
			9.5	0.40	0.918	7.9	395	8.7	435	0.300	0.009	6.8	340	2.0	97
	5.28 / L	7.6	0.38	0.435	5.1	255	5.7	287	0.079	0.116	10.5	523	2.7	134	
			9.5	0.40	0.588	7.6	380	8.0	398	0.079	0.006	10.1	505	2.6	128

¹High probability maximum value (K_H) was missed.

²High probability maximum ground level value (K_g) was missed.

³σ_y data questionable.

Table 6.2 Height of Plume (h)¹⁾ Relative to Release Height (H) at Locations G and L

Description	$Fr^2)$	H (cm)	$\frac{h}{H} @ G$	$\frac{h}{H} @ L$
FLAT Terrain	2.2	7.0	1.09	1.28
		9.5	1.21	1.11
	2.7	7.6	1.56	1.11
		9.5	1.46	1.61
349° Wind Direction	1.5	7.6	0.74	0.47
		9.5	0.84	0.65
	3.9	7.6	1.09	0.36
		9.5	0.92	0.57
325° Wind Direction	2.0	7.6	0.97	0.71
		9.5	0.87	0.82

1) $h = \frac{z_{max} + \bar{z}}{2}$ and is the plume height above ground level

2) Fr calculated at 10 cm height for location A

Table 6.3 Ratio of Maximum Aerial Concentration (K_H) to Maximum Ground-Level Concentration (K_g) and the Associated Model and Full-Scale Conditions

Description	Fr		Ri		Model (cm)	K_H Prototype (m)	Distance		$\frac{K_H}{K_g}$
	@ 10 cm	@ ~1.9 cm	@ 10 cm	@ ~1.9 cm			Model (cm)	Prototype (km)	
FLAT terrain	2.2	1.8	0.27	0.25	7.6	381	2.45	12.3	27.78
							5.49	27.5	4.61
					9.5	476	2.45	12.3	133.2
							5.49	27.5	9.65
	2.7	4.6	0.16	0.11	7.6	381	2.45	12.3	46.43
							5.49	27.5	2.18
					9.5	476	2.45	12.3	320.0
							5.49	27.5	10.60*
349° Wind Direction (Badger Peak)	1.5	1.9	0.75	0.20	7.6	381	2.45	12.3	2.89
							5.49	27.5	1.70*
					9.5	476	2.45	12.3	17.64*
							5.49	27.5	5.34
	3.9	6.5	0.12	0.11	7.6	381	2.45	12.3	1.36*
							5.49	27.5	1.00
					9.5	476	2.45	12.3	7.27
							5.49	27.5	1.47
325° Wind Direction (Garfield Peak)	2.0	3.3	0.49	0.15	7.6	381	2.24	11.2	2.65*
							5.28	26.4	3.75
	9.5				9.5	476	2.24	11.2	102.00
							5.28	26.4	98.00

*Observed K_H significantly different than maximum K_H .

Table 6.4 Predicted Correction Factor (K_o/K_g) for Ground-Level Measurements as a Function of σ_z , z_g and h

σ_z (cm)	z_g (cm)	h(cm)				
		0	2	4	6	8
2.0	0.079	1.0008	1.0000	0.9980	0.9940	0.9880
3.0	0.079	1.0004	1.0002	0.9997	0.9990	0.9990
4.0	0.079	1.0002	1.0002	1.0000	0.9998	0.9994
2.0	0.300	1.0113	1.0000	0.9675	0.9169	0.8531
3.0	0.300	1.0050	1.0023	0.9961	0.9852	0.9703
4.0	0.300	1.0028	1.0021	1.0000	0.9965	0.9916

Table 6.5 Ratio of Maximum Ground Level Concentrations (Dimensionless) with and without Terrain for Similar Stabilities (Froude Numbers)

Description	$(Fr_T)_w$	$(Fr_T)_{wo}$	H (cm)	$\frac{(K_o)_w}{G} / \frac{(K_o)_{wo}}{L}$
349° Wind Direction	1.9	1.8	7.6	9.56
			9.5	5.00
	6.5	4.6	7.6	20.86
			9.5	70.00
325° Wind Direction	3.3	1.8	7.6	3.33
			9.5	1.80

Table 6.6 Comparison of Maximum Observed Dimensionless Concentration with that Predicted Using the Gaussian Model

Description	Fr_T	σ_y	Pasquill Category	σ_z	H (cm)	$(K_H)_{\text{observed}} / (K_H)_{\text{calculated}}$
		G		L		
Flat terrain	1.8	F	D-E	σ_z	7.6	0.90
					9.5	0.77
	4.6	E	D	σ_z	7.6	1.12
					9.5	0.71*
349° Wind Direction	1.9	F	D-E	σ_z	7.6	0.90
					9.5	0.51*
	6.5	E	D	σ_z	7.6	0.69*
					9.5	1.13
325° Wind Direction	3.3	F	D-E	σ_z	7.6	0.24*
					9.5	0.90
						1.75

*Values for which maximum observed value $(K_H)_{\text{observed}}$ was more likely missed due to sampling grid spacing or location.

Table 6.7 Valley Model Computed Concentrations with Associated Model Input and the Corrected Concentration Based on Wind-Tunnel Results for E-Stability (Gas Temperature Equal 361°K and $\sigma_z = 125$ m)

Date	Hour	Stack Exit Wind Speed m/s	G=Garfield Point B=Badger Point	x_v $\mu\text{g}/\text{m}^3$	Effective Plume Height-H m	$\left(\frac{K_H}{K_g}\right)_m$	$\left(\frac{K_H}{K_o}\right)_p$	x_c $\mu\text{g}/\text{m}^3$ ¹⁾
5/16/75	0600	5.3	G	19.83	388	10.70	0.91	1.7
6/06/75	0600	5.8	G	18.83	380	3.75	0.93	4.7
7/26/75	2400	1.4	B	44.93	483	5.60	0.93	7.5
9/21/75	2200	4.8	B	24.65	394	2.21	0.96	10.8
9/23/75	0300	5.3	B	22.83	387	1.92	0.98	11.8
	0400	5.8	B	21.11	382	1.71	0.98	12.2
9/30/75	0700	1.9	G	26.38	474	96.0	1.07	0.5
3/04/76	0200	1.4	G	19.09	521	98.0	1.70	0.5
	0500	5.3	G	18.36	403	25.6	0.89	0.6
	0900	5.8	G	17.35	398	20.6	0.89	0.8
5/18/76	2100	5.3	B	22.89	385	1.81	0.98	12.5
8/21/76	0600	5.8	B	21.22	379	1.6	0.95	*
10/29/76	2000	5.3	B	22.64	390	2.0	0.91	11.0
	2100	5.8	B	21.02	305	1.9	0.98	*
4/01/77	2300	5.3	G	19.09	396	18.6	0.90	0.9
8/06/77	0100	1.0	G	21.40	532	98.0	1.95	0.4
0/05/77	0600	5.3	G	20.12	385	7.72	0.92	2.4
9/23/77	2100	5.3	B	22.71	389	2.0	0.91	10.8
12/15/77	1600	2.9	B	33.35	436	3.8	0.89	7.8

*plume height below range of wind-tunnel observation.

¹⁾For H values above 476 m the ratio $\left[\left(\frac{K_H}{K_g}\right)_m\right]$ for H = 476 m was used.

Table 6.8 Valley Model Computed Concentrations with Associated Model Inputs and the Corrected Concentration Based on Wind-Tunnel Results for D Stability (Gas Temperature Equals 361°K; $\sigma_z = 240\text{m}$)

Description	Receptor Height above Base - Z_r (m)	Effective Plume Height H - (m)	Plume Height above Receptor h (m)	Wind Speed @ 211 m (m/s)	X_v 1 hr Average ($\mu\text{g}/\text{m}^3$)	$\left(\frac{K_H}{K_o}\right)_p \left(\frac{K_H}{K_g}\right)_m$	X_c 1 hr Average ($\mu\text{g}/\text{m}^3$)
Hypothetical Data - Toward Badger Peak	359	476	117	9.7	0.74	0.91	1.47
	359	381	22	15.2	1.05	1.00	1.00
Hypothetical Data - Toward Garfield Peak	326	476	150	9.7	0.75	0.89	*
	326	381	55	15.2	1.05	0.98	*

*Not tested in wind tunnel.

FIGURES

0 1 2 3 4 5 6 7 km
SCALE

349° Wind
Direction North

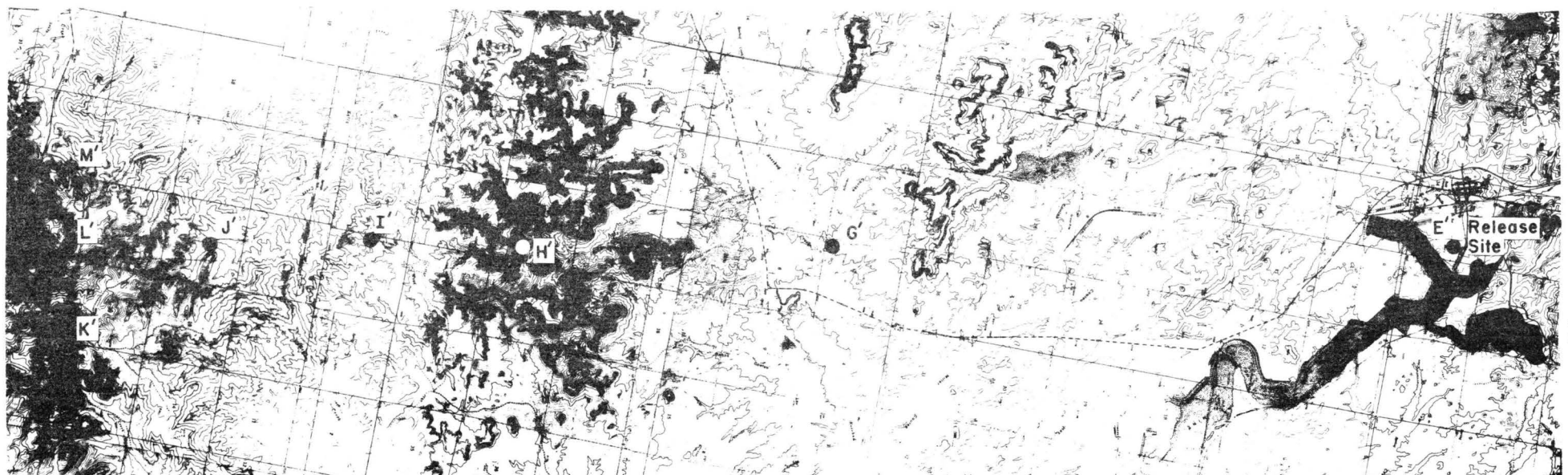


Figure 4.2-1 Topographic Map of the Area Modeled in the Wind Tunnel
for the 349° Wind Direction (Badger Peak)

0 1 2 3 4 5 6 7 km
SCALE

325° Wind Direction
← North →

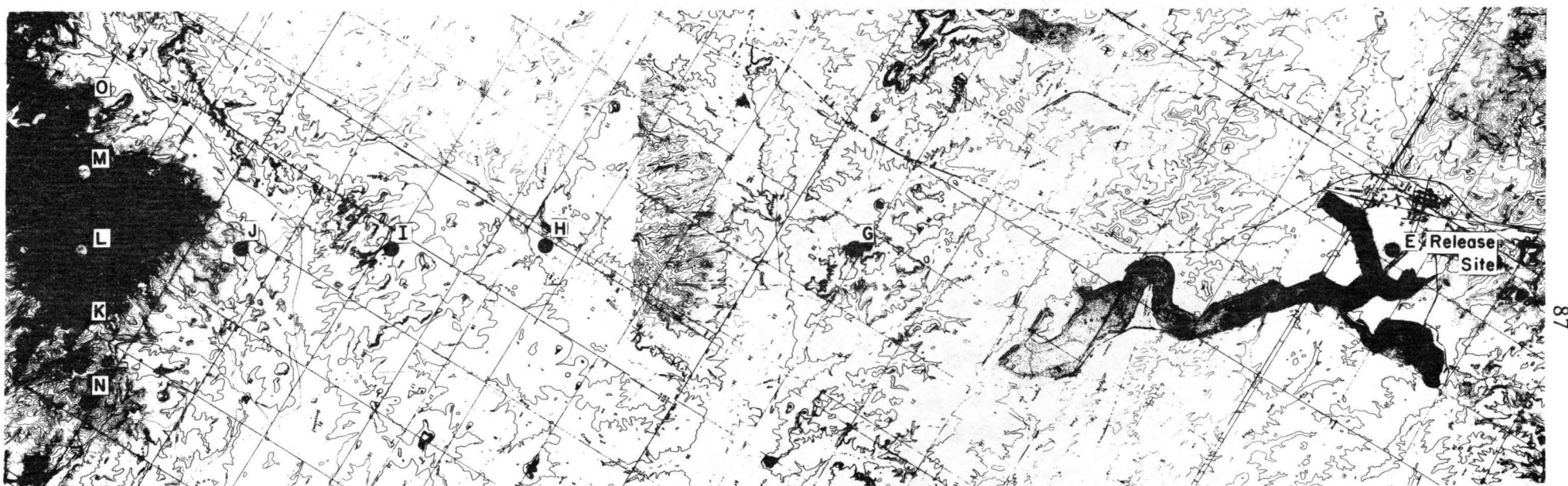


Figure 4.2-2 Topographic Map of the Area Modeled in the Wind Tunnel for the 325° Wind Direction (Garfield Peak)

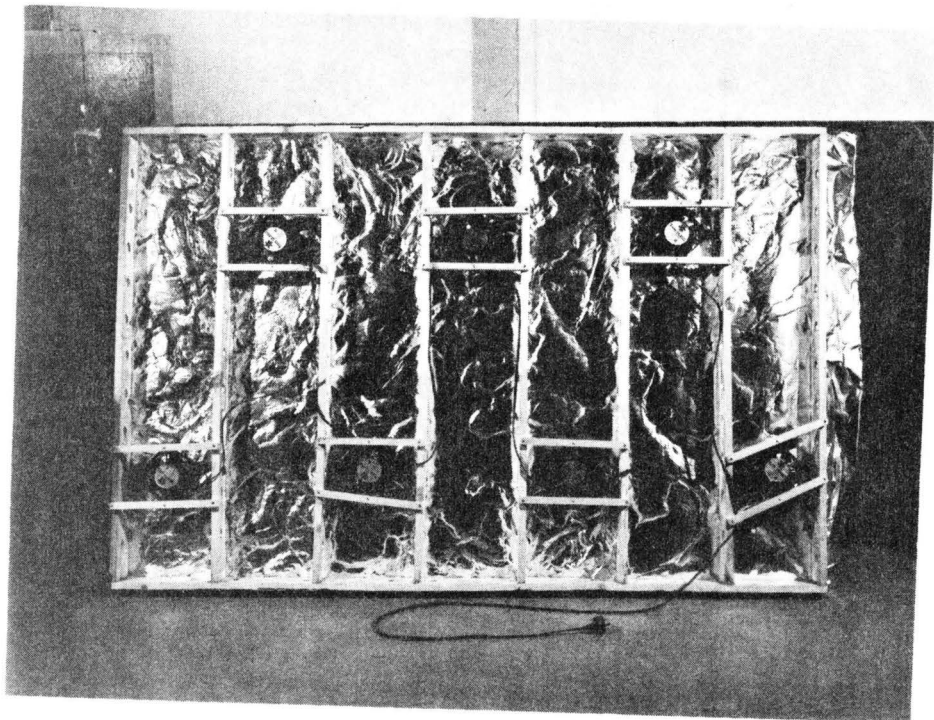


Figure 4.2-3 Picture of Wood Frame and Attached Fans
to which the Aluminum Sheets were Fixed
that Conform with the Topography

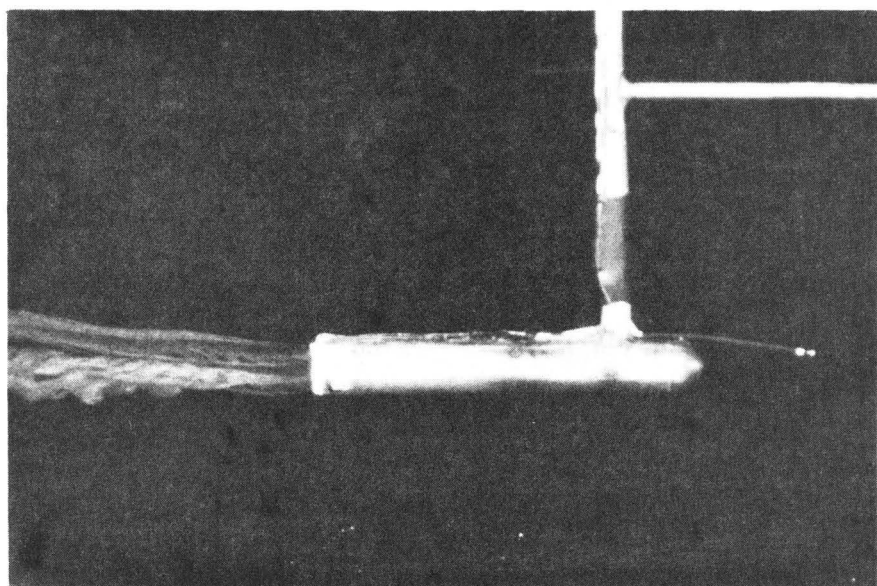


Figure 4.2-4 Picture of Probe from which Smoke and Trace Gas were Released

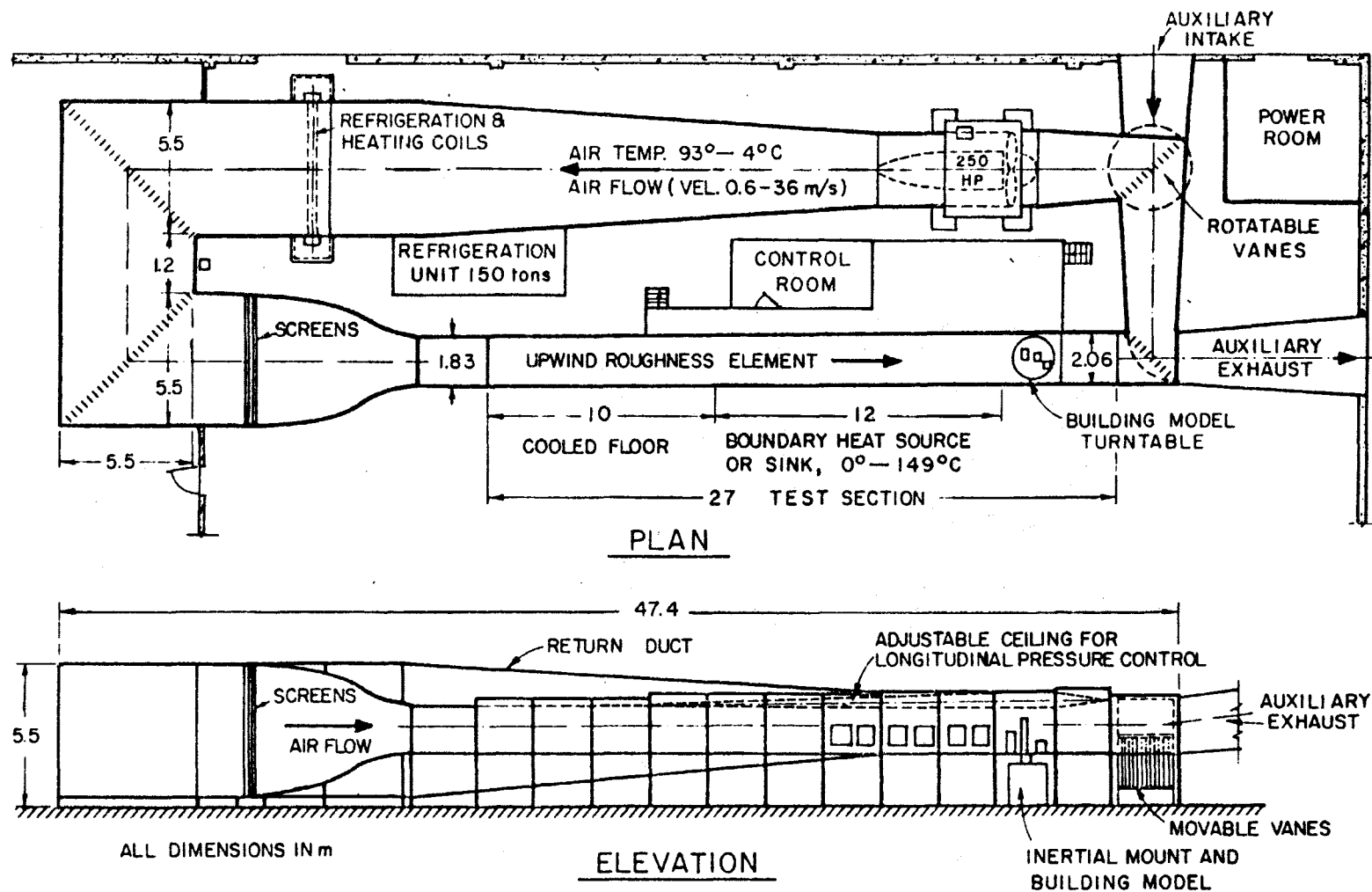


Figure 4.2-5 Meteorological Wind Tunnel. Fluid Dynamics and Diffusion Laboratory, Colorado State University

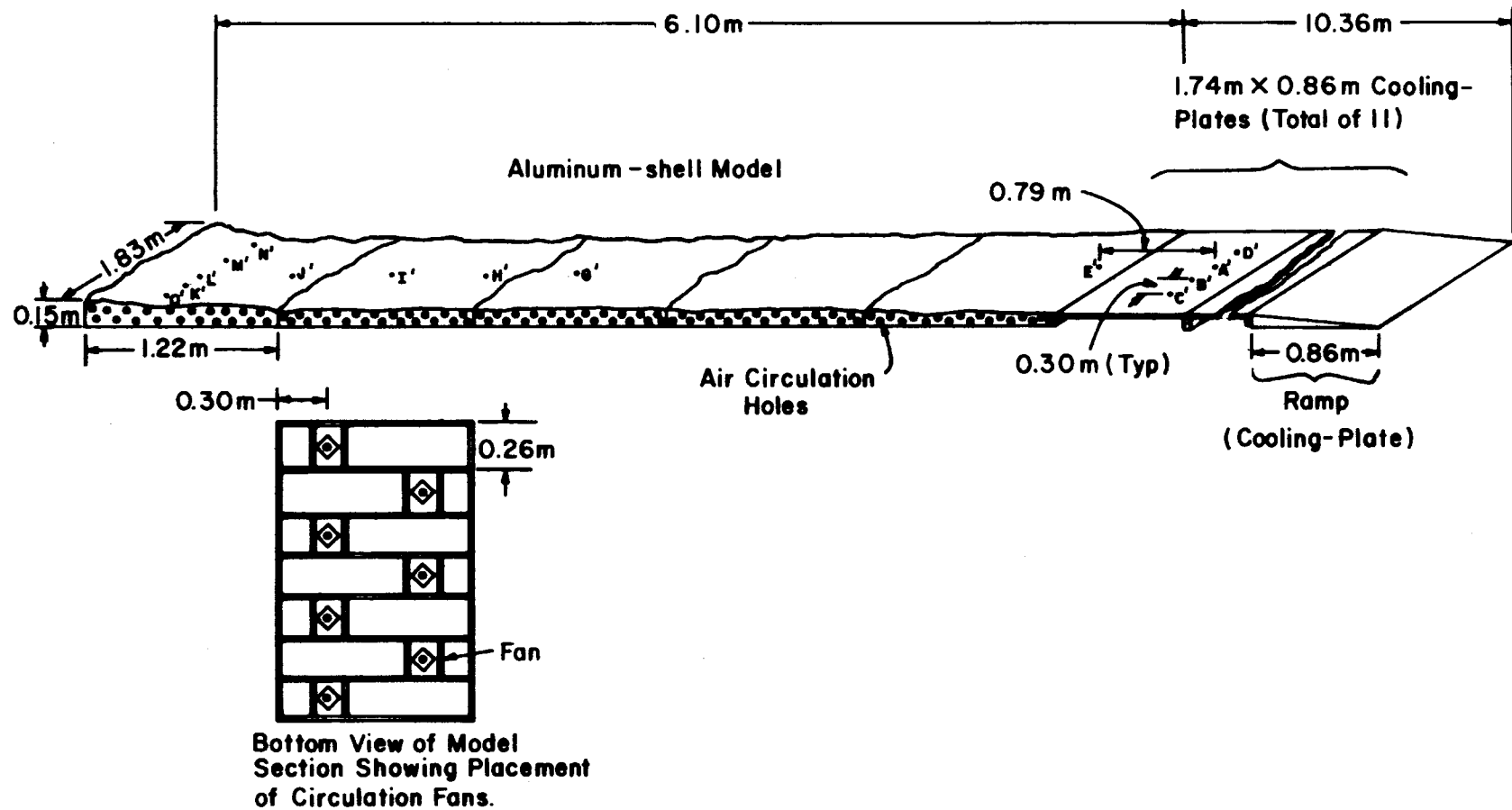


Figure 4.2-6 Three-Dimensional Sketch of Wind-Tunnel Configuration
for the Stable Boundary-Layer Tests

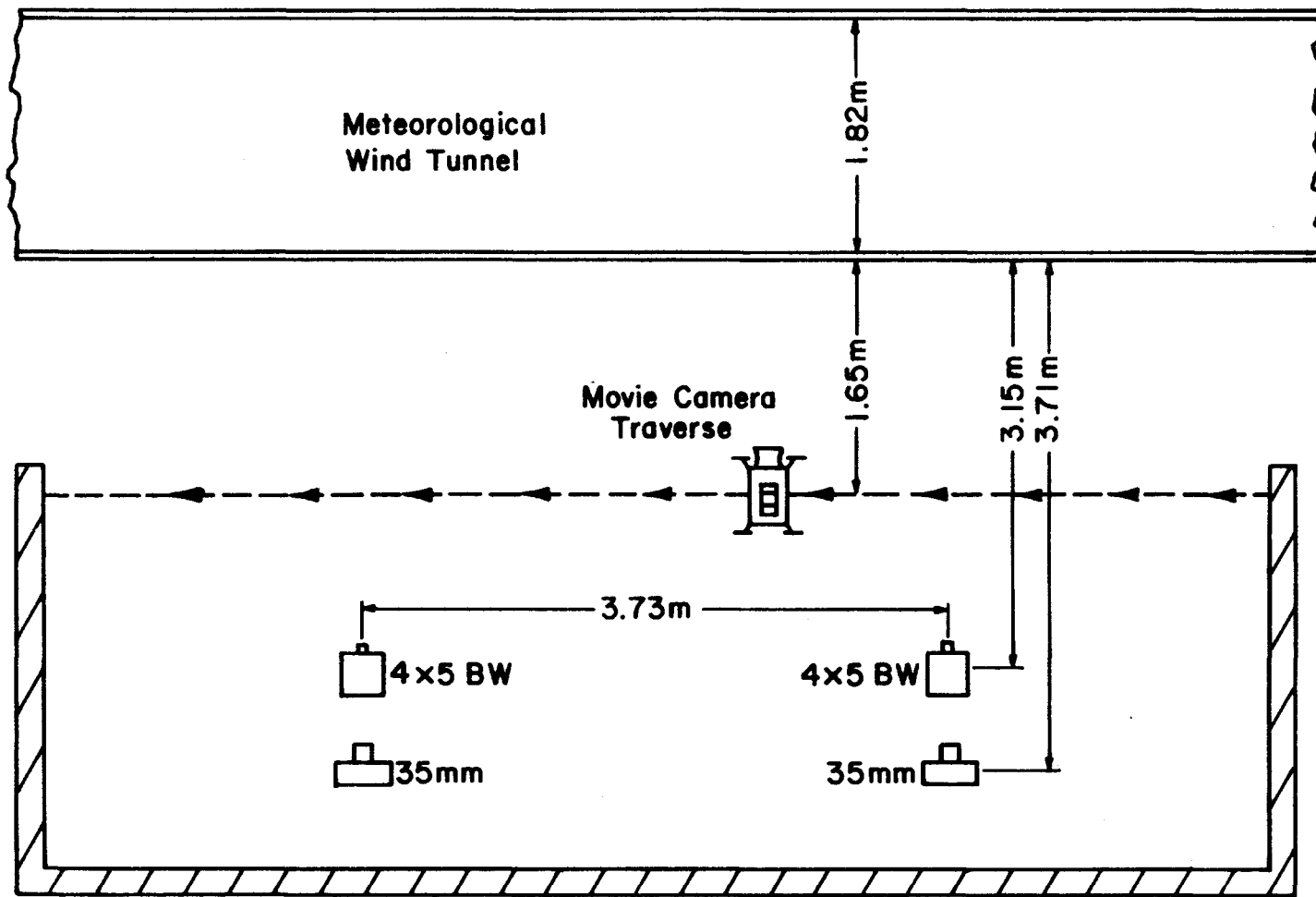


Figure 4.3-1 Camera Setup for the Stable Boundary-Layer Tests of Colstrip Power Plant

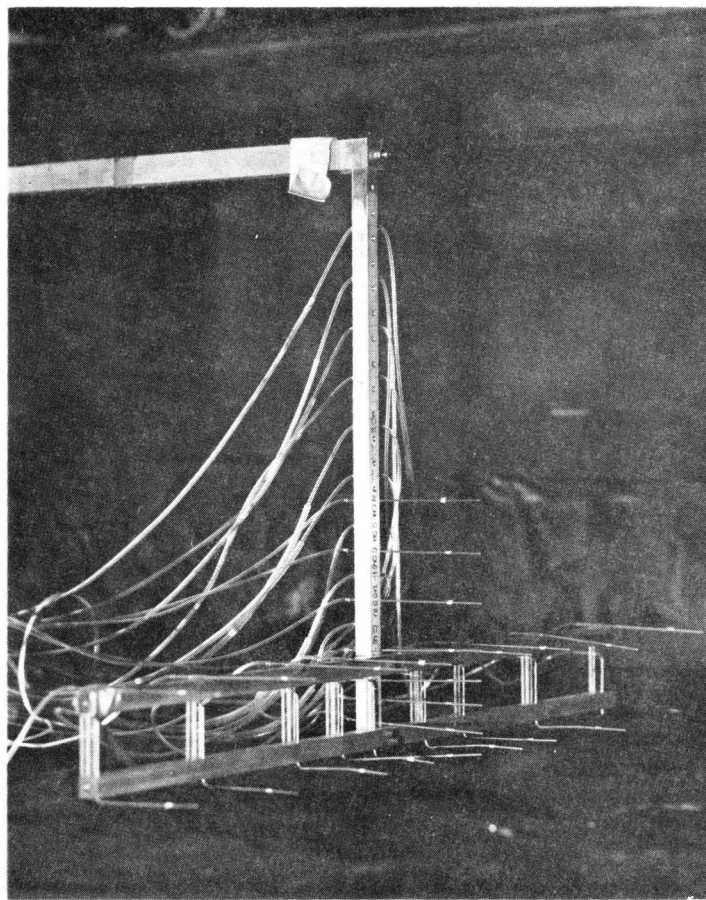


Figure 4.4-1 Photograph of Sampling Rake used to Withdraw Gas from the Wind Tunnel

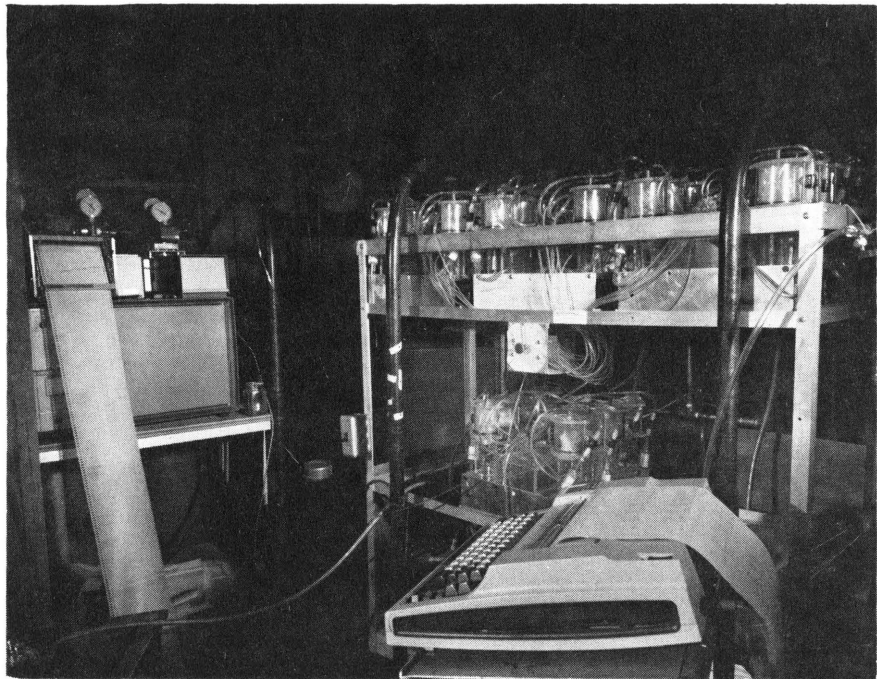


Figure 4.4-2 Photograph of Flame Ionization Gas Chromotograph and Gas Sampling System

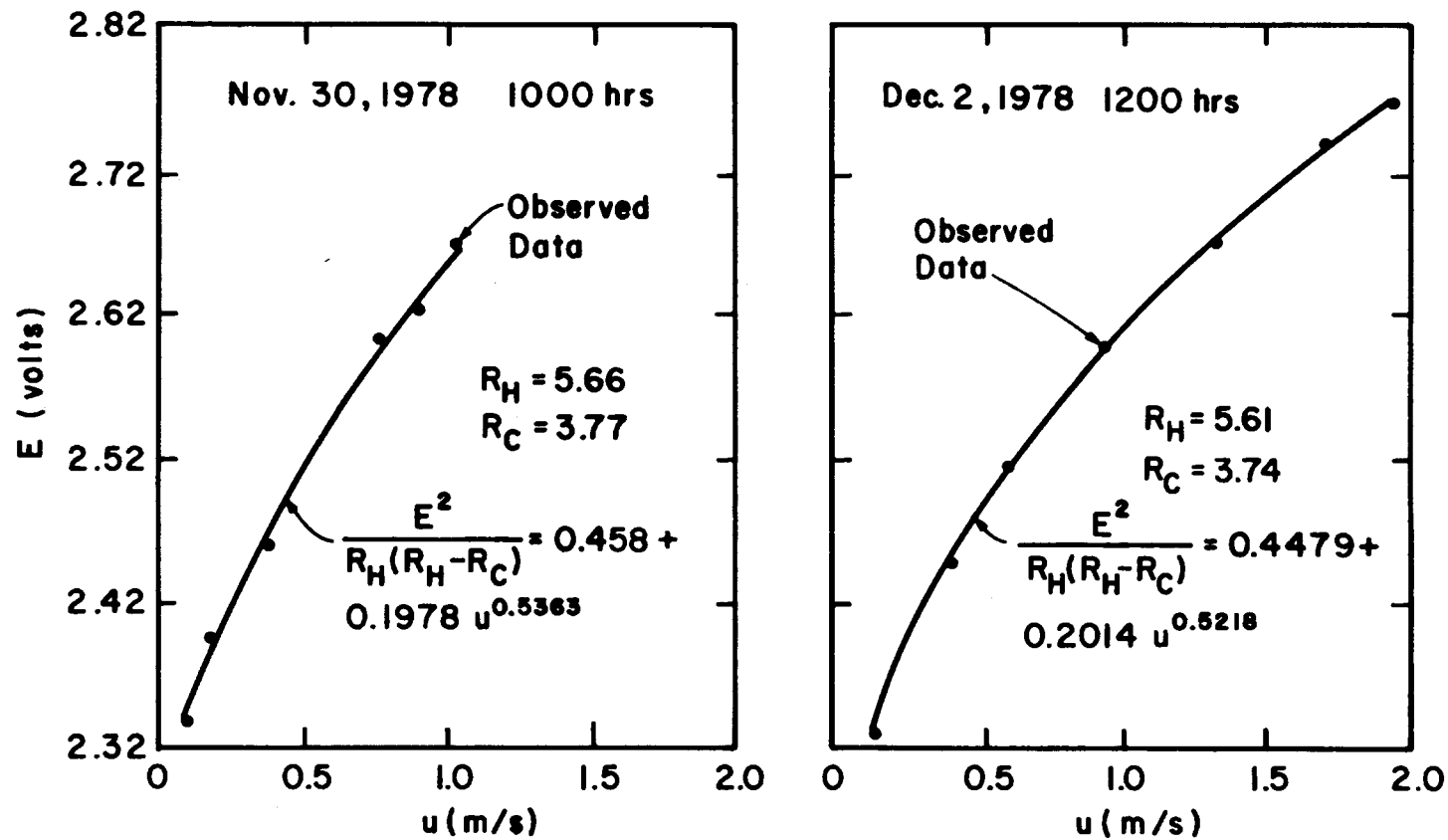


Figure 4.5-1 Typical Calibration Curves for Hot-Film Sensor (Matheson Linear Flow Meter was used as Calibration Standard)

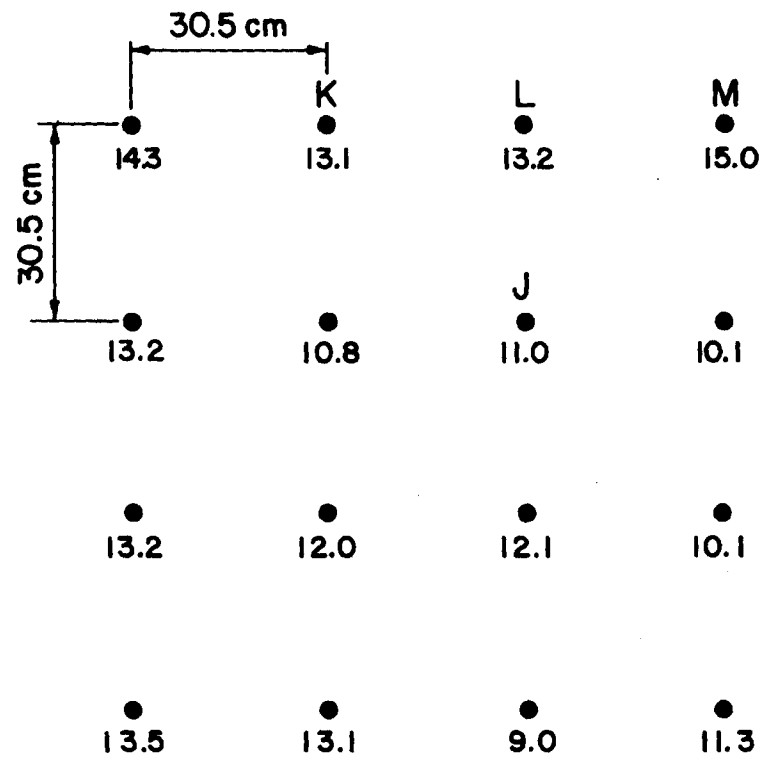


Figure 4.5-2 Values and Location of Surface Temperature ($^{\circ}\text{C}$) on the Aluminum Shell Model for Wind Tunnel Conditions Set During Runs 3 and 4

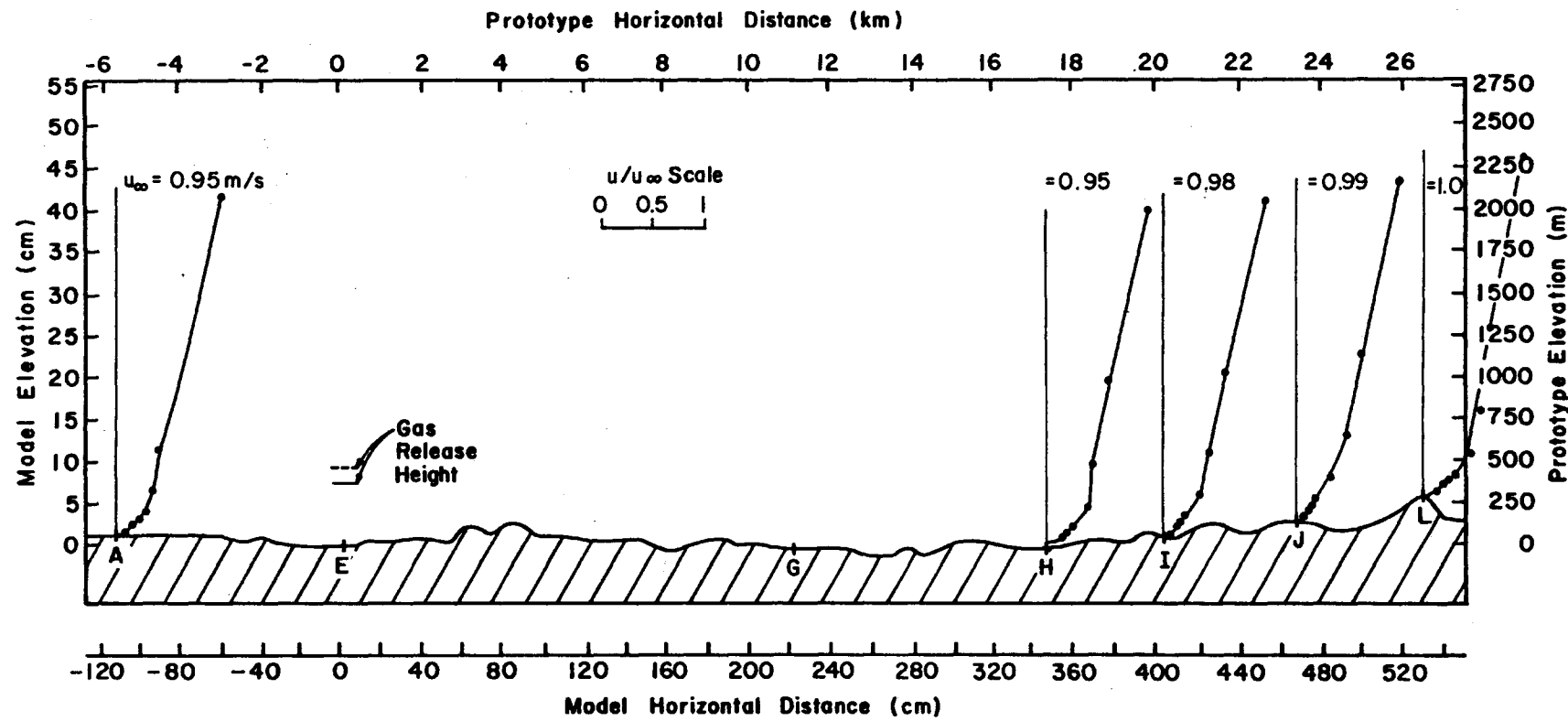


Figure 5.2-1 Dimensionless Velocity Profiles for the 325° Wind Direction (Garfield Peak) and a Fr_T of 3.3

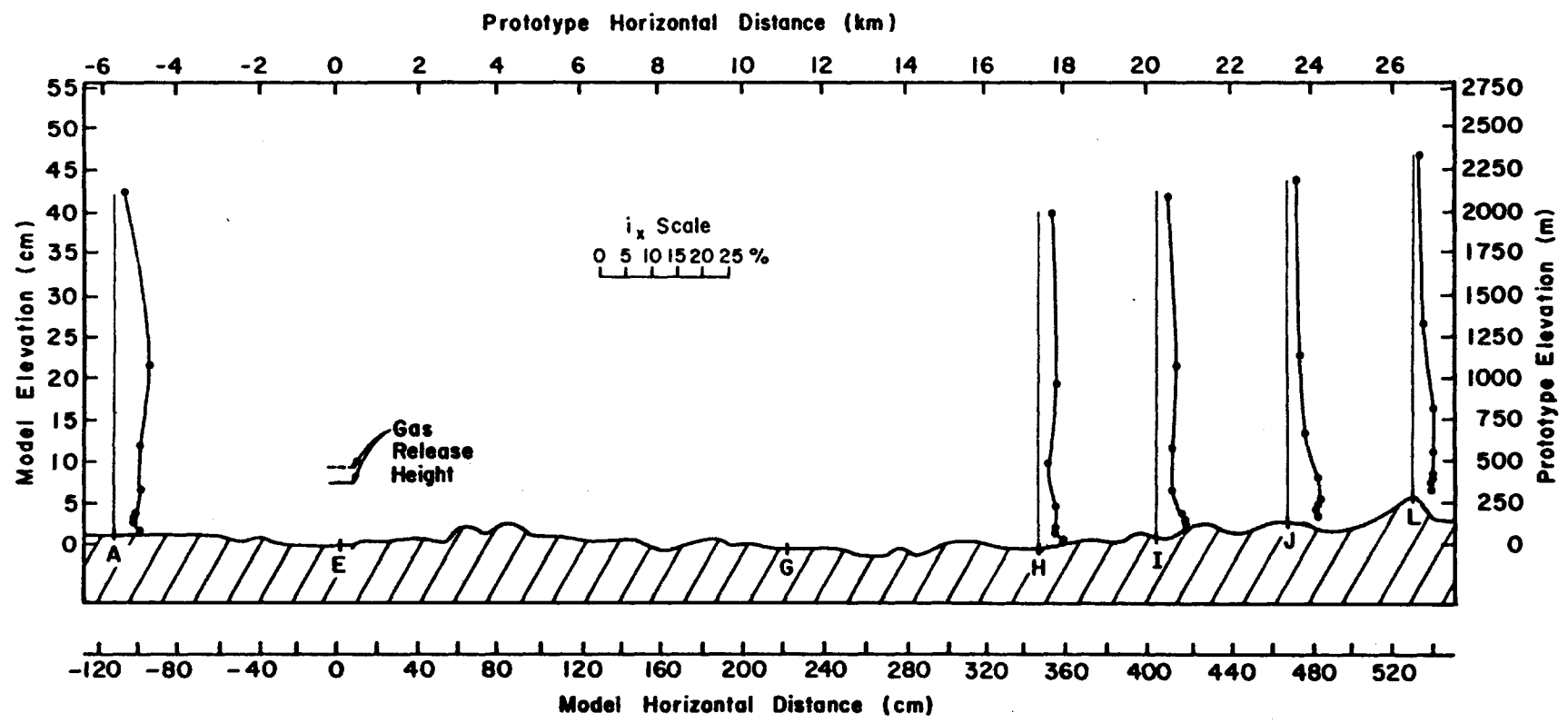


Figure 5.2-2 Vertical Profiles of Longitudinal Turbulence Intensity for the 325° Wind Direction (Garfield Peak) and Fr_T of 3.3

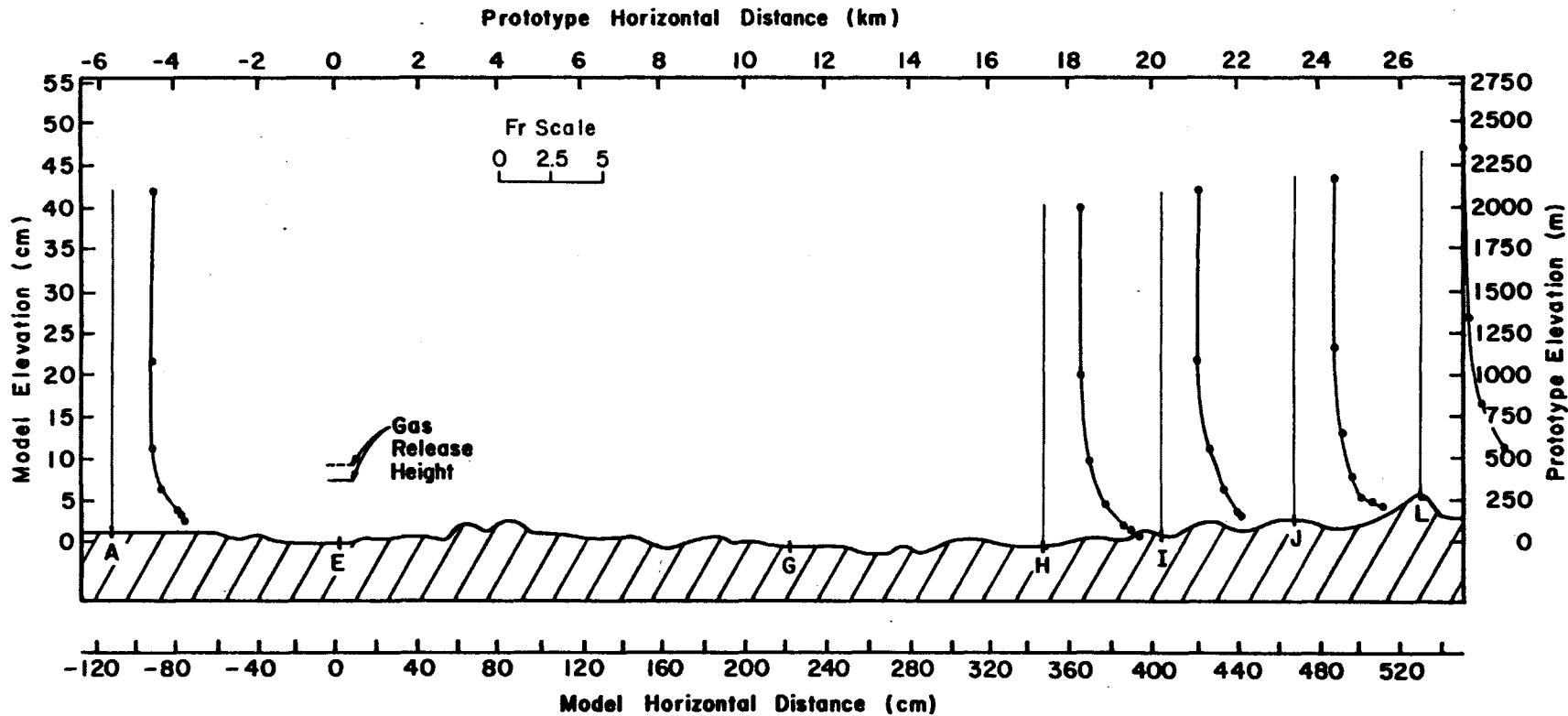


Figure 5.2-3 Vertical Profile of Froude Number for the 325° Wind Direction (Garfield Peak) and a Fr_T of 3.3

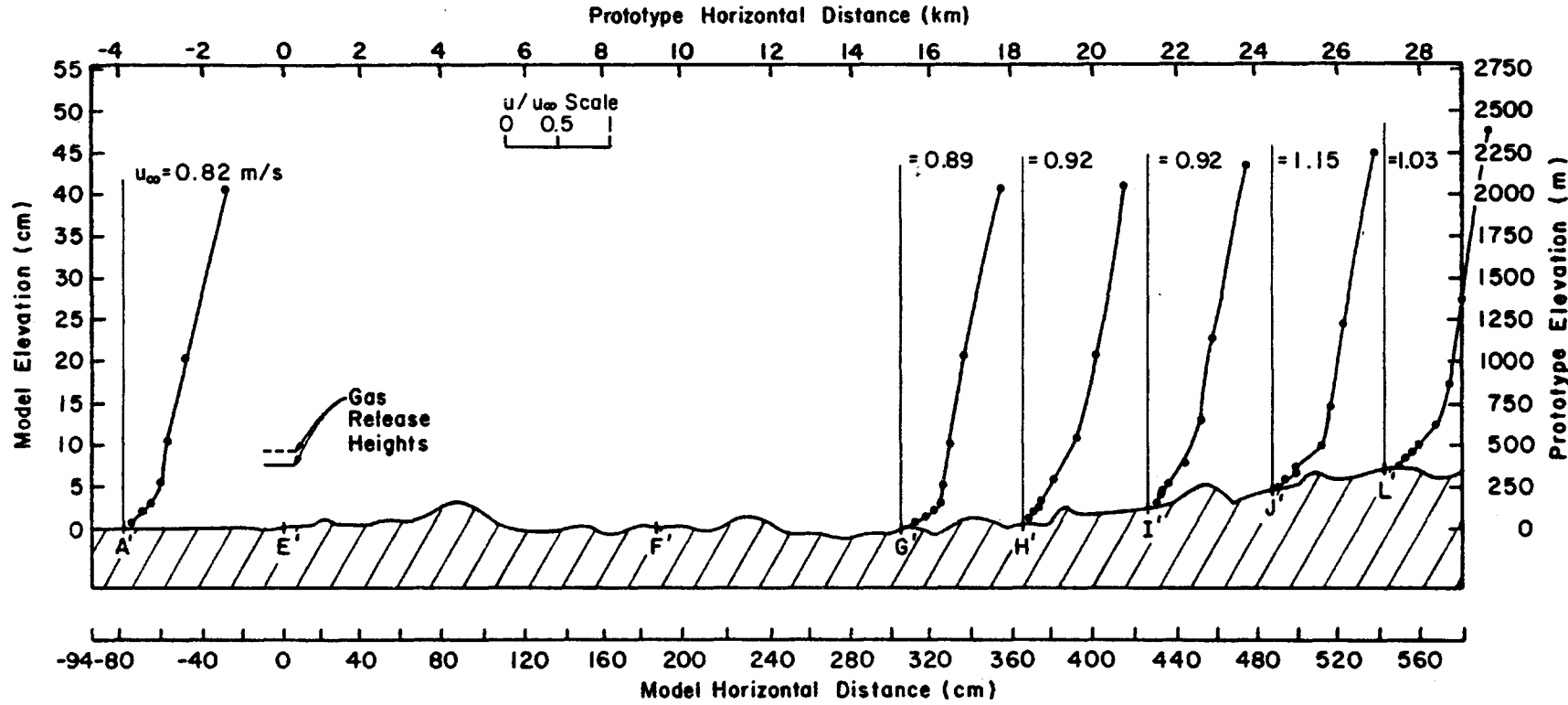


Figure 5.2-4 Dimensionless Velocity Profiles for the 349° Wind Direction (Badger Peak) and a Fr_T of 1.9

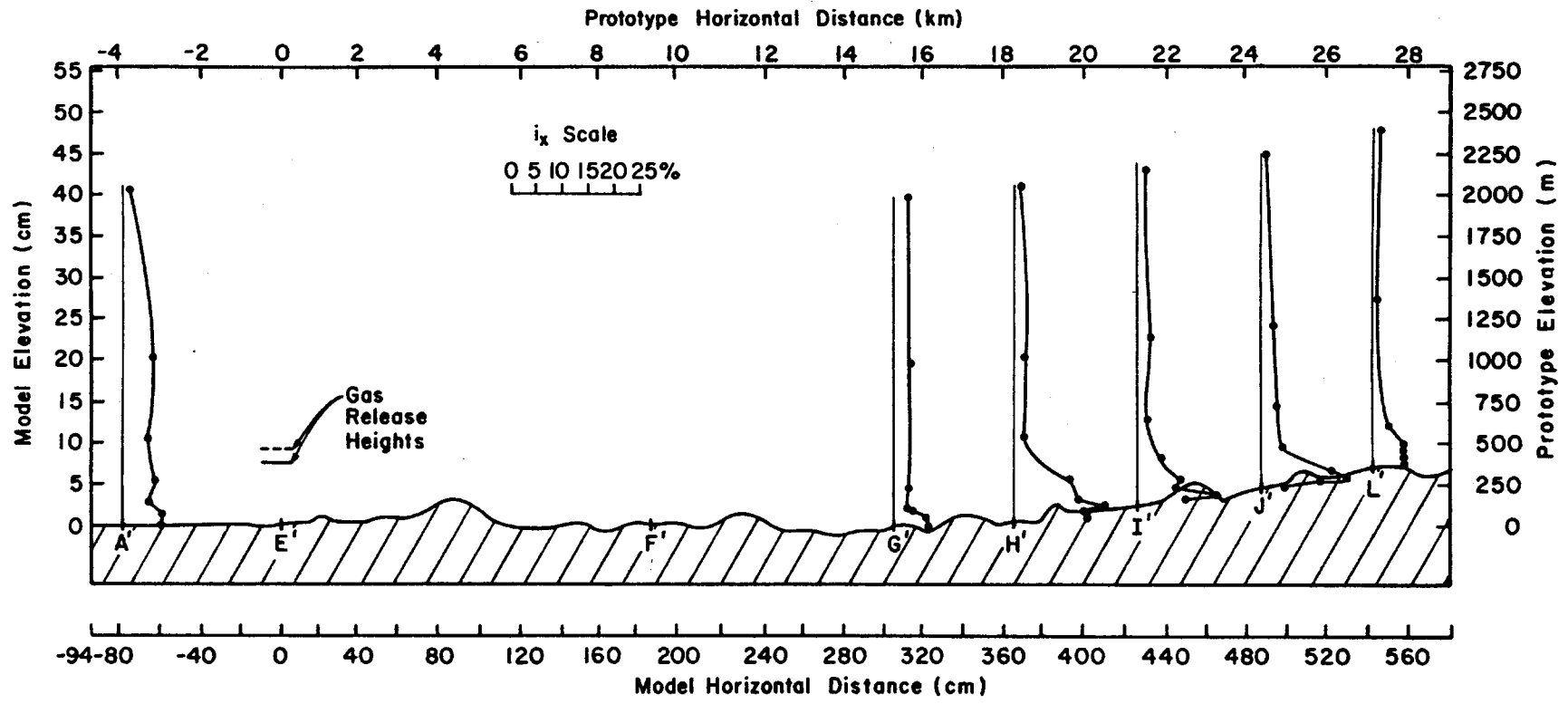


Figure 5.2-5 Vertical Profiles of Longitudinal Turbulence Intensity for the 349° Wind Direction (Badger Peak) and a Fr_T of 1.9

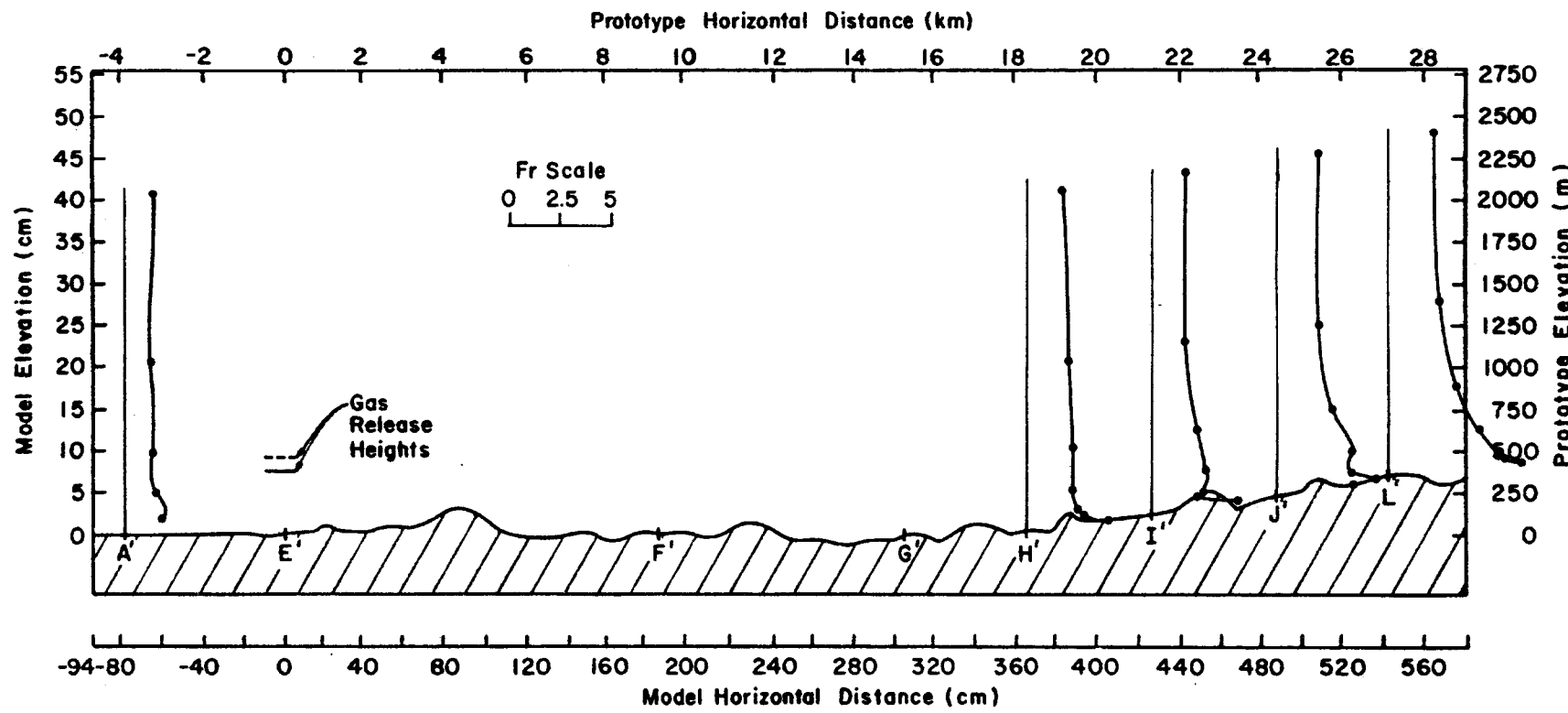


Figure 5.2-6 Vertical Profiles of Froude Number for the 349° Wind Direction (Badger Peak) and a Fr_T of 1.9

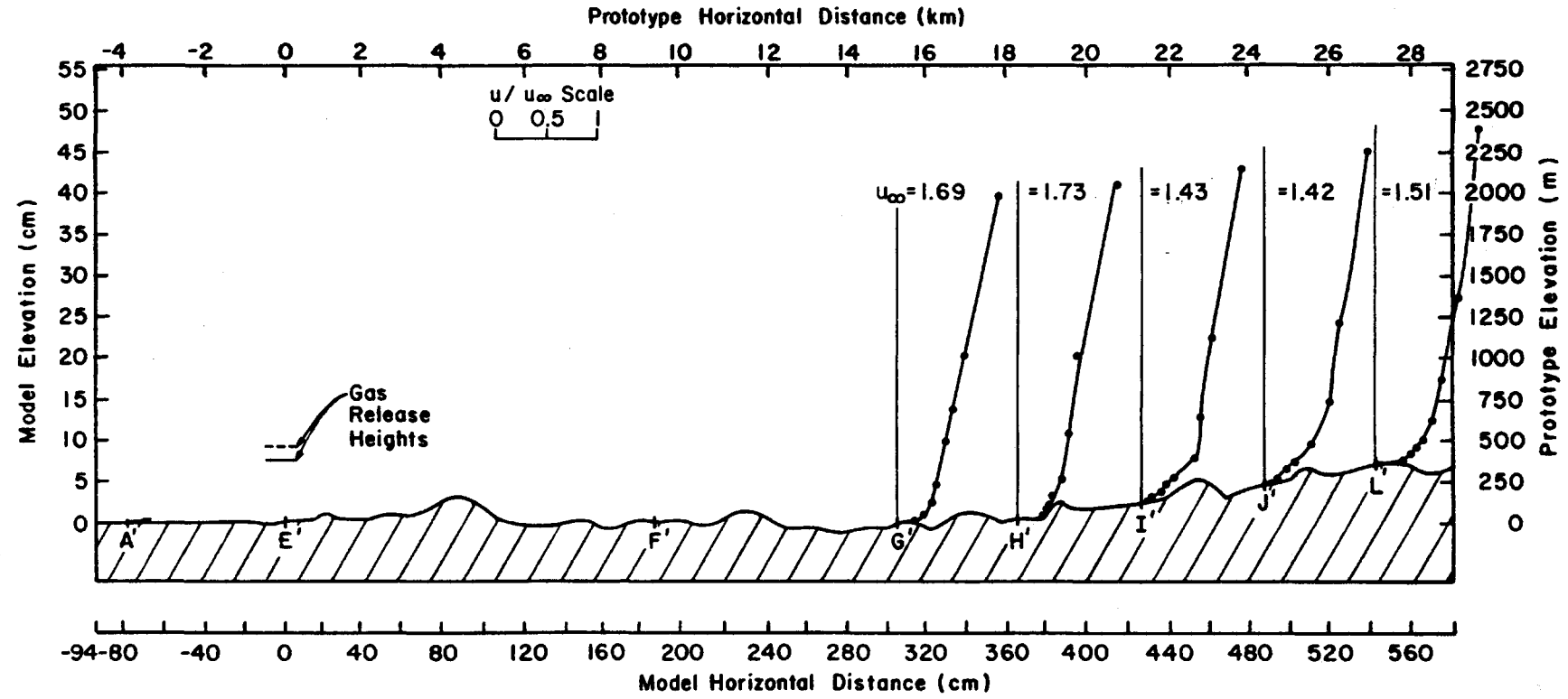


Figure 5.2-7 Dimensionless Velocity Profile for the 349° Wind Direction (Badger Peak) and a Fr_T of 6.3

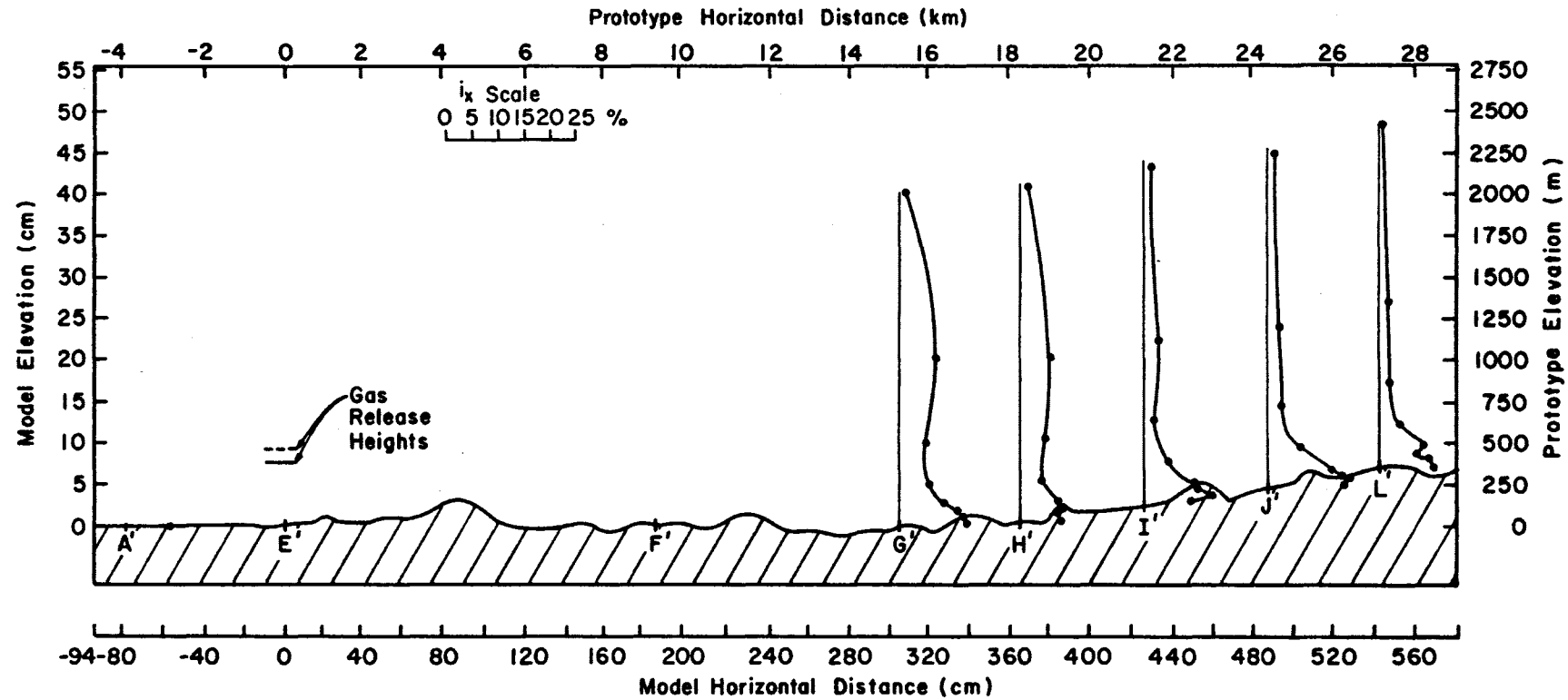


Figure 5.2-8 Vertical Profiles of Longitudinal Turbulence Intensity for the 349° Wind Direction (Badger Peak) and a Fr_T of 6.3

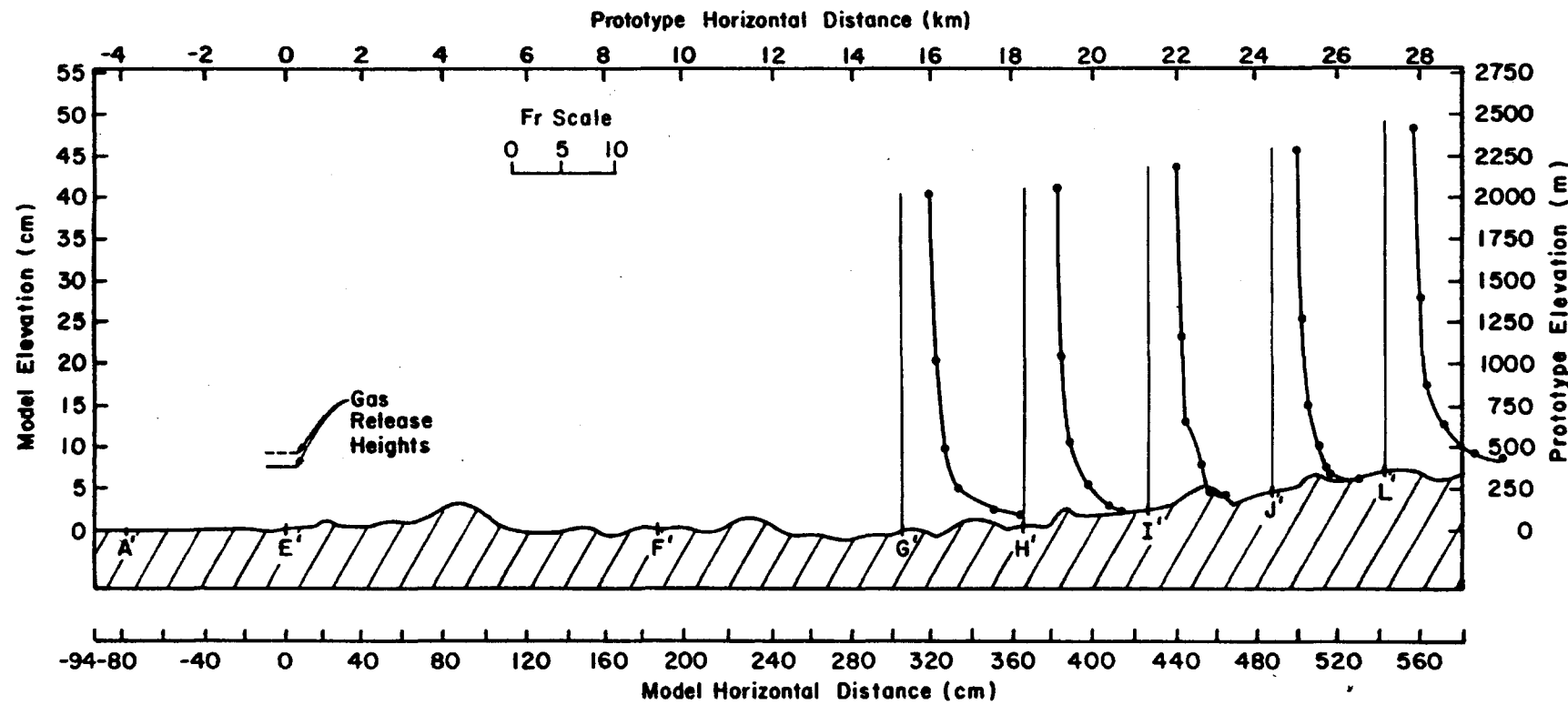


Figure 5.2-9 Vertical Profiles of Froude Number for the 349° Wind Direction (Badger Peak) and a Fr_T of 6.3

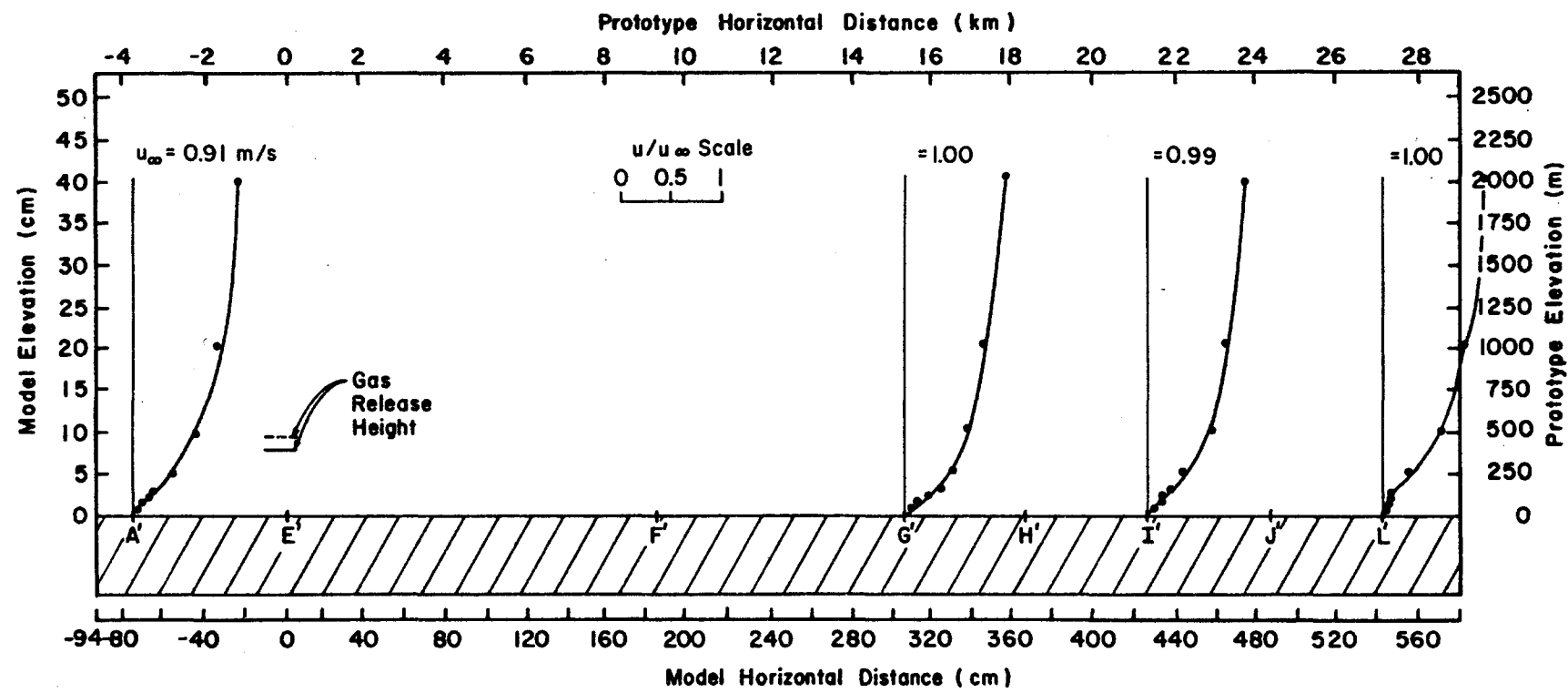


Figure 5.2-10 Dimensionless Velocity Profiles for the Flat Terrain Case and a Fr_T of 1.8

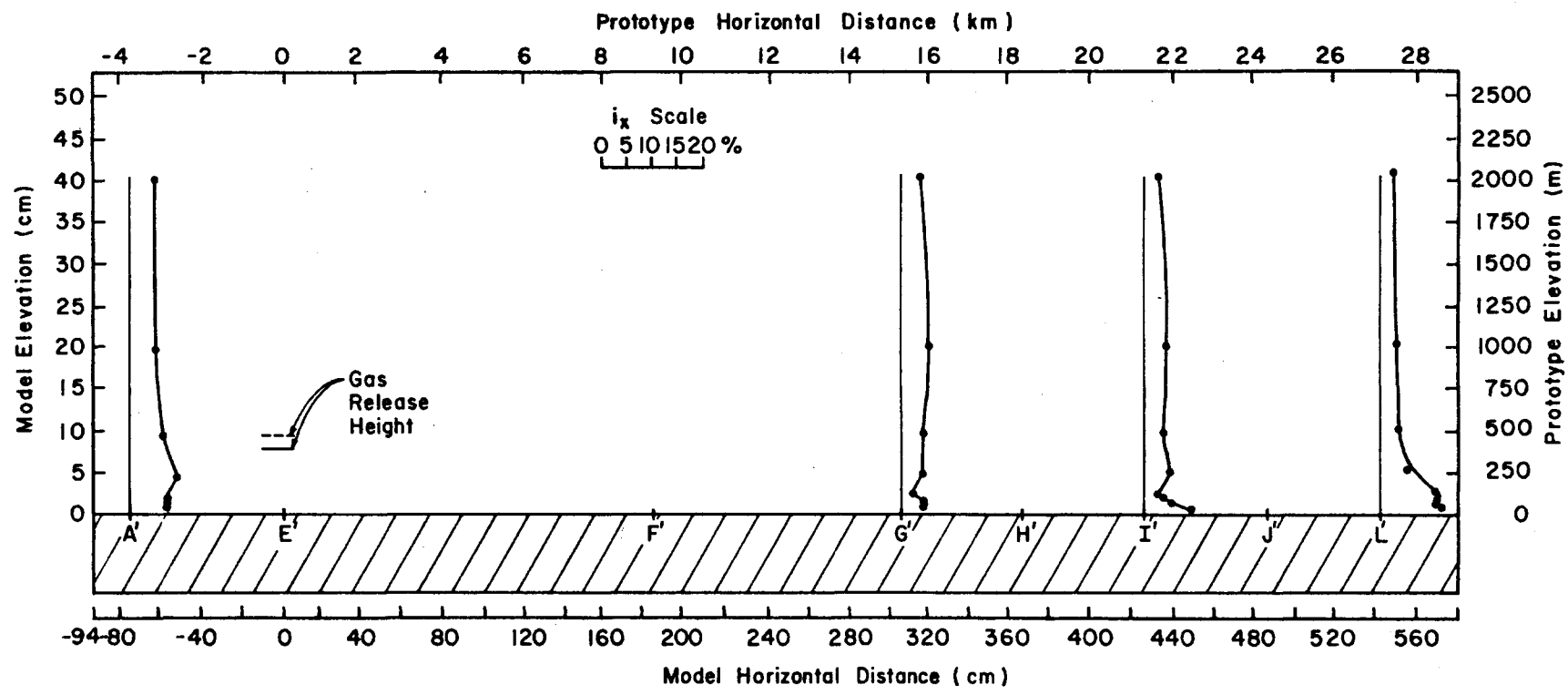


Figure 5.2-11 Vertical Profile of Longitudinal Turbulence Intensity for the Flat Terrain Case
 Fr_T of 1.8

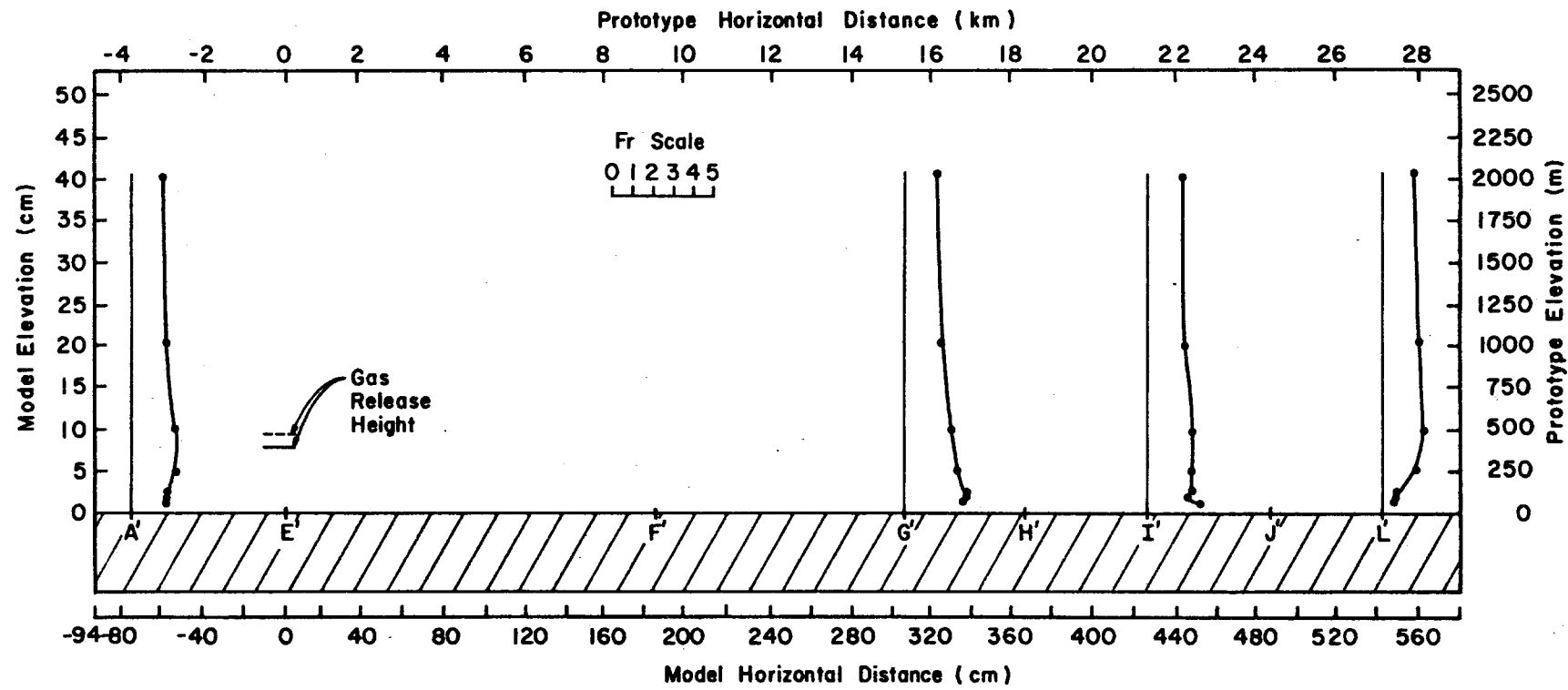


Figure 5.2-12 Vertical Profile of Froude Number for the Flat Terrain Case and a Fr_T of 1.8

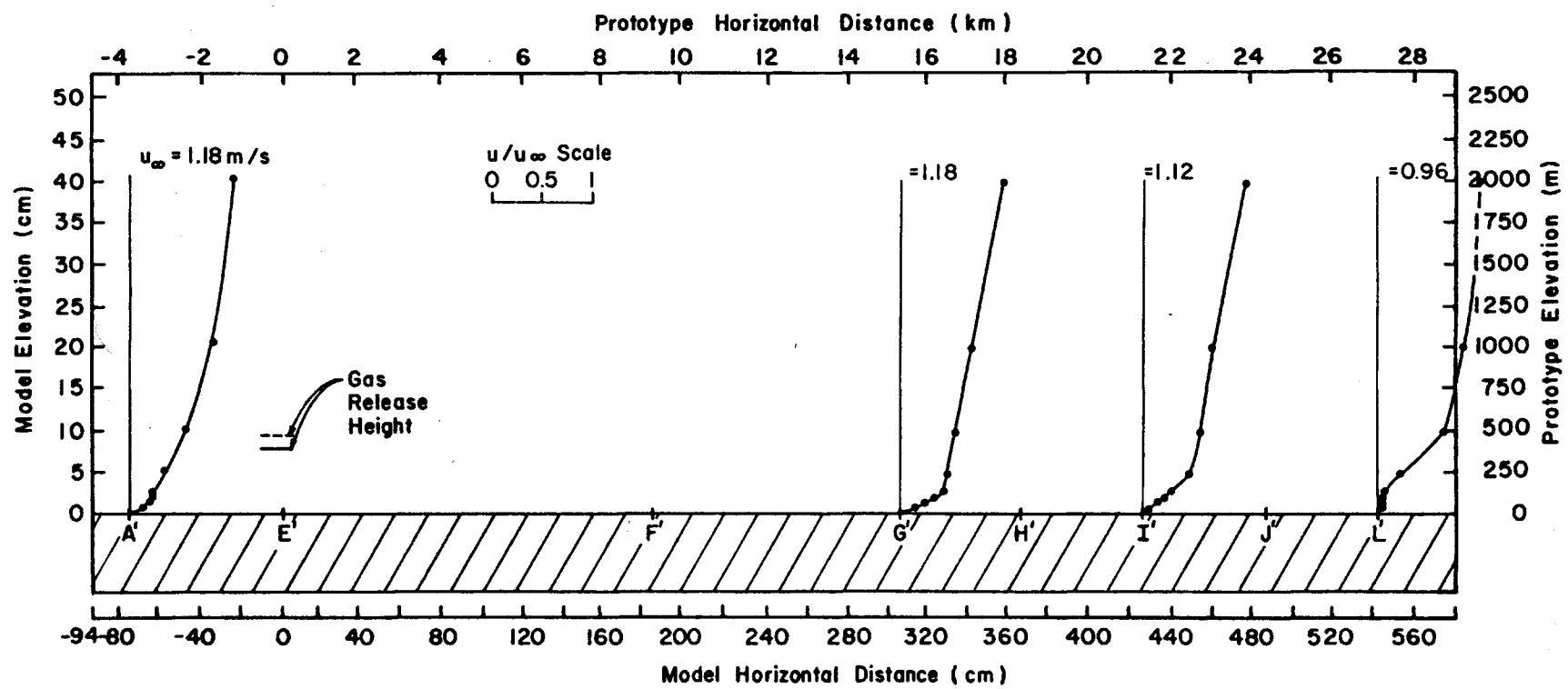


Figure 5.2-13 Dimensionless Velocity Profiles for the Flat Terrain Case and a Fr_T of 4.6

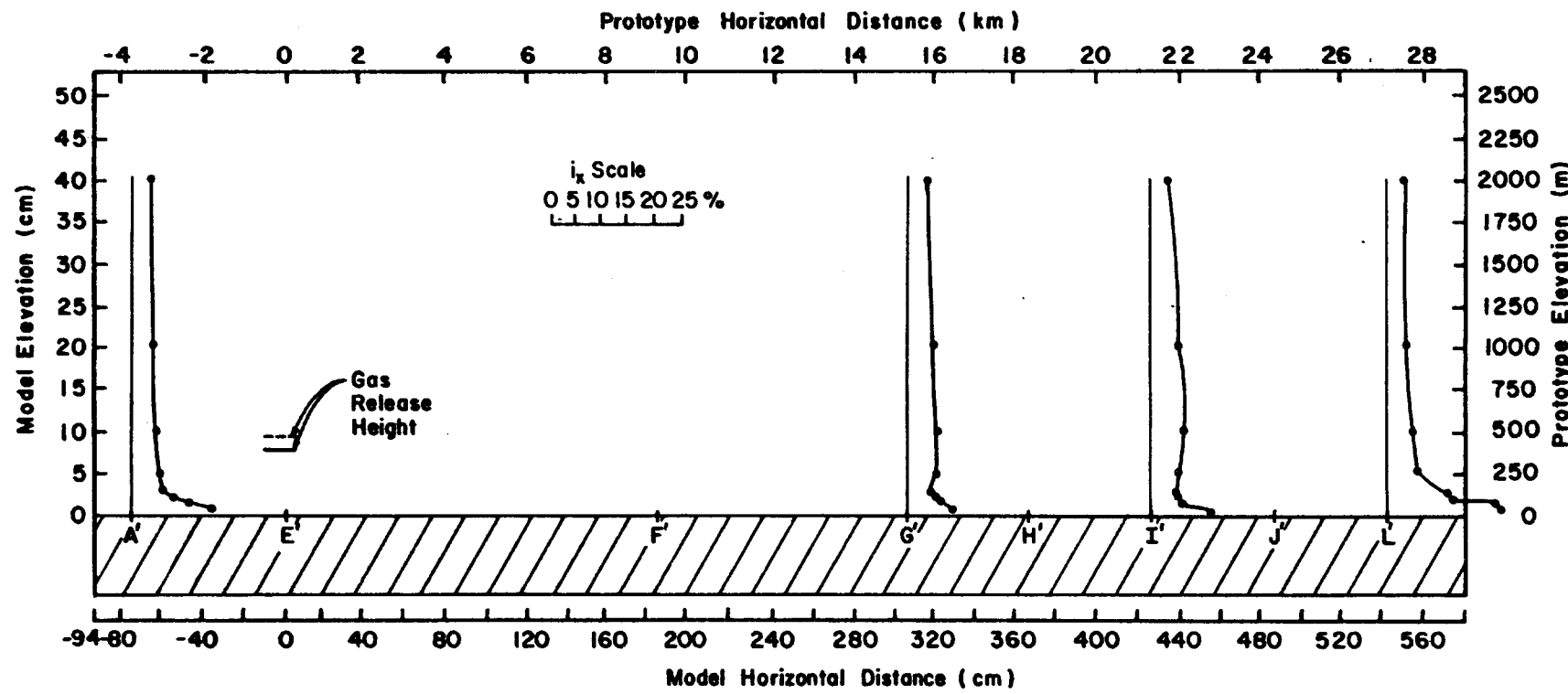


Figure 5.2-14 Vertical Profiles of Longitudinal Turbulence Intensity for the Flat Terrain Case and a Fr_T of 4.6

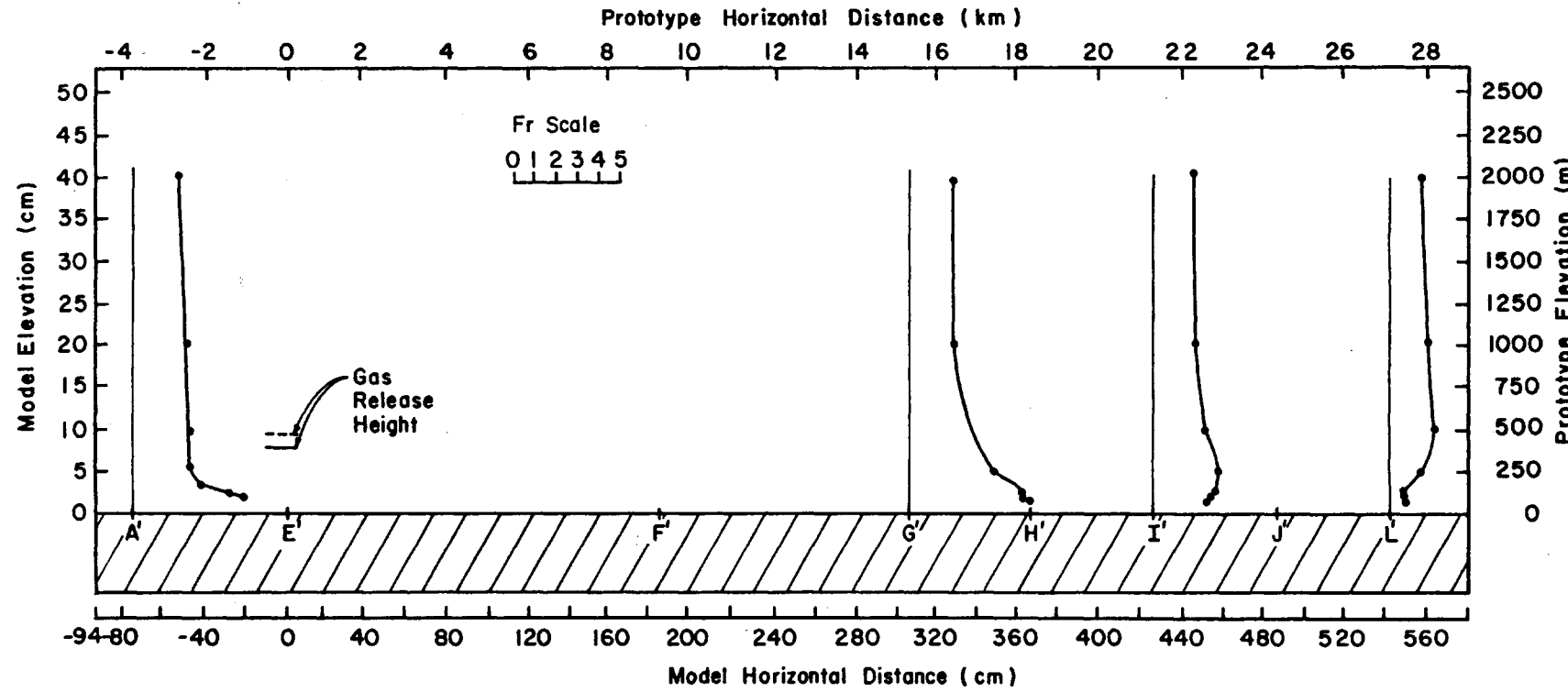


Figure 5.2-15 Vertical Profile of Froude Number for the Flat Terrain Case and a Fr_T of 4.6

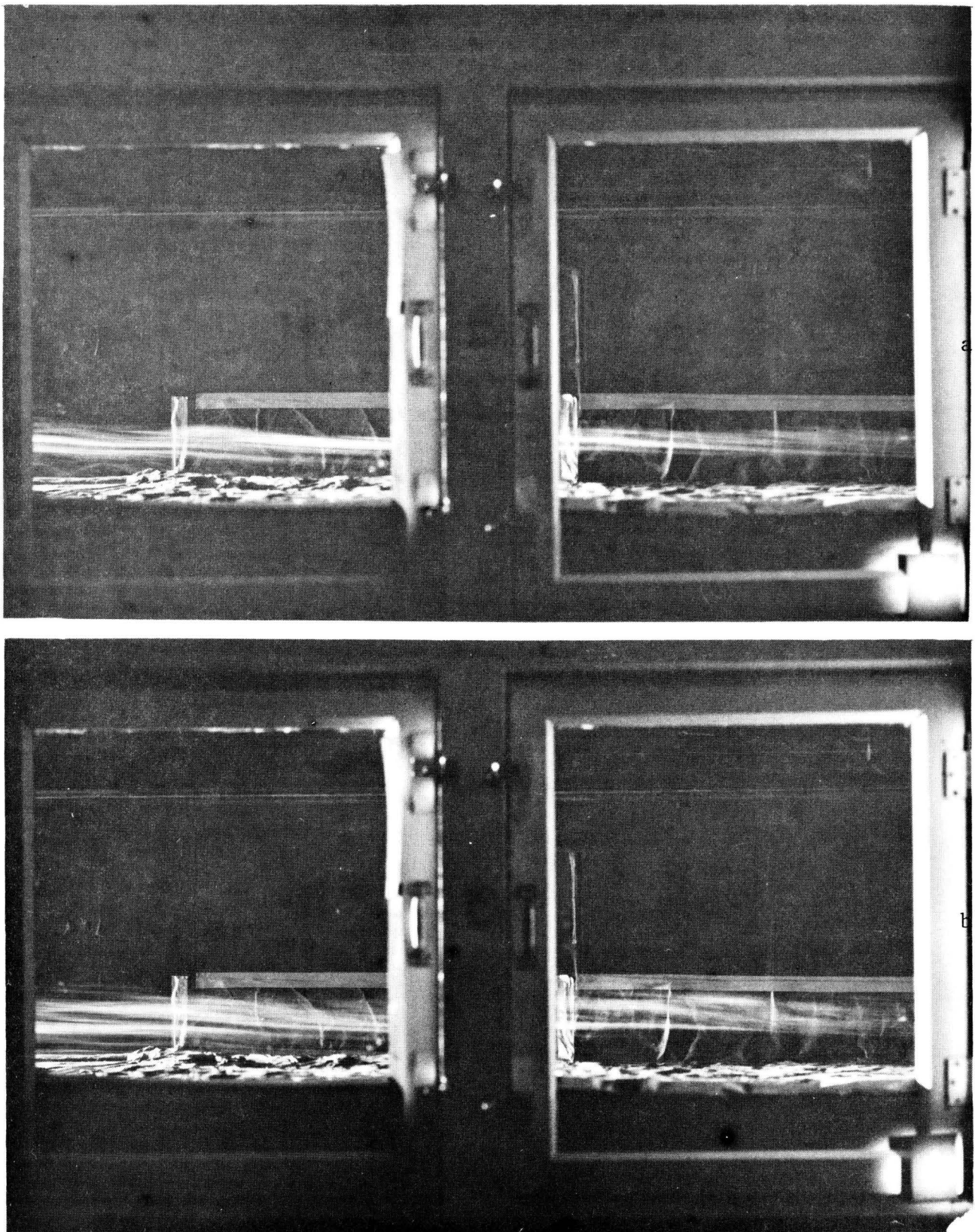
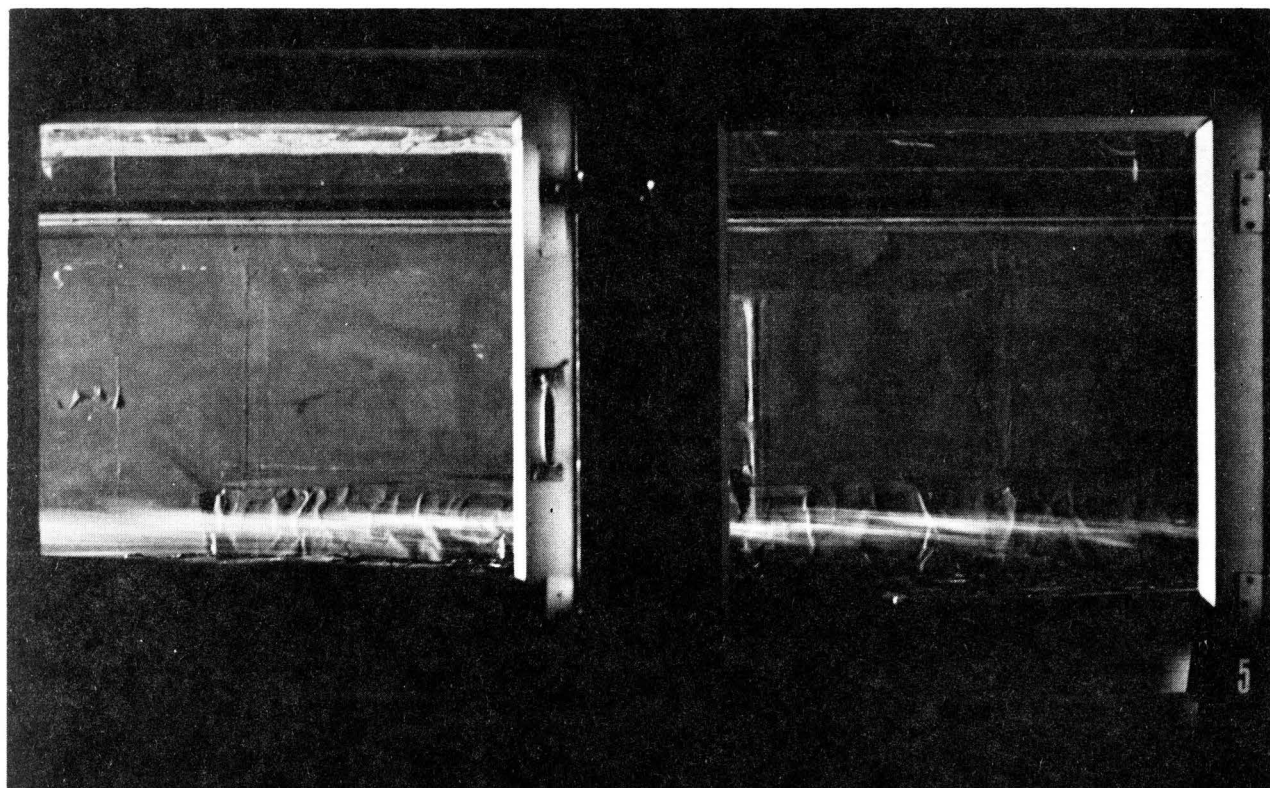
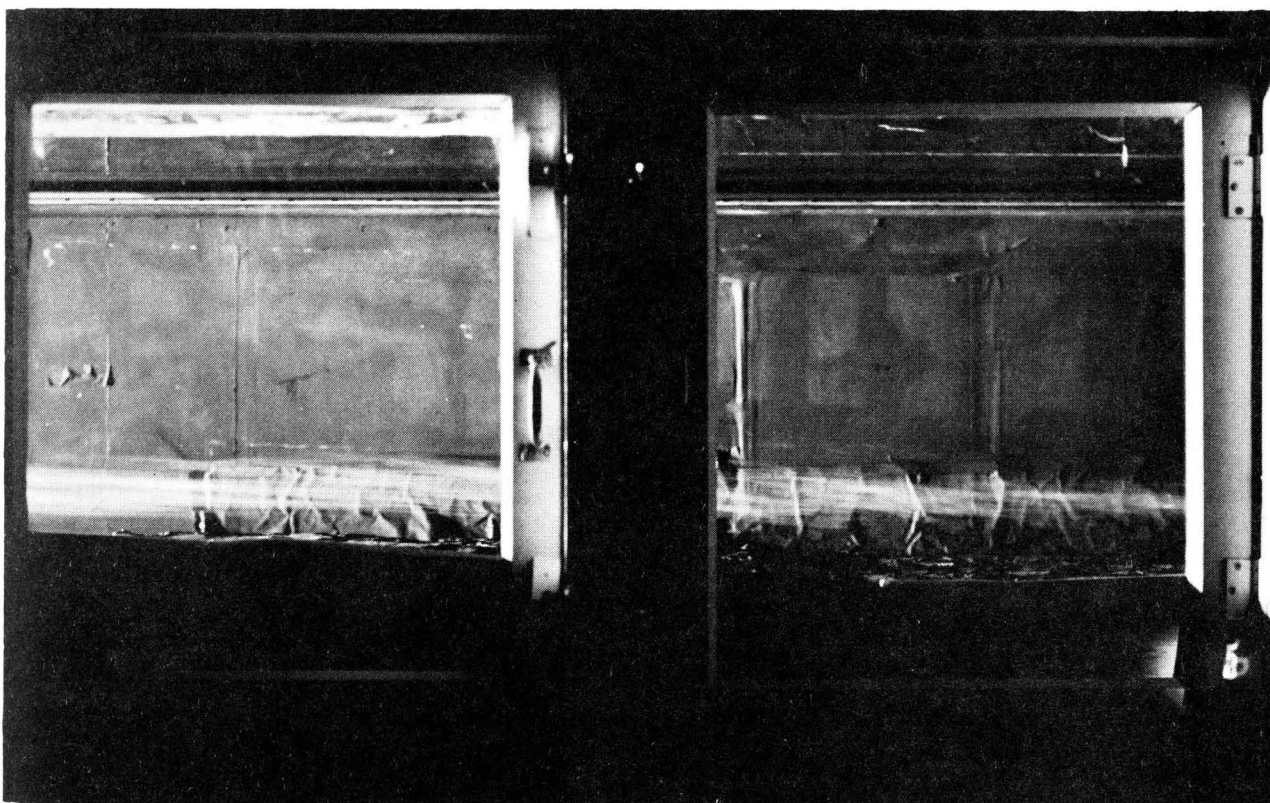


Figure 6.1-1 Plume Visualization for 325° Wind Direction (Badger Peak).
 $Fr_T = 3.3$ and a Release Height of a) 7.6 cm (381 m prototype),
b) 9.5 cm (476 m prototype)

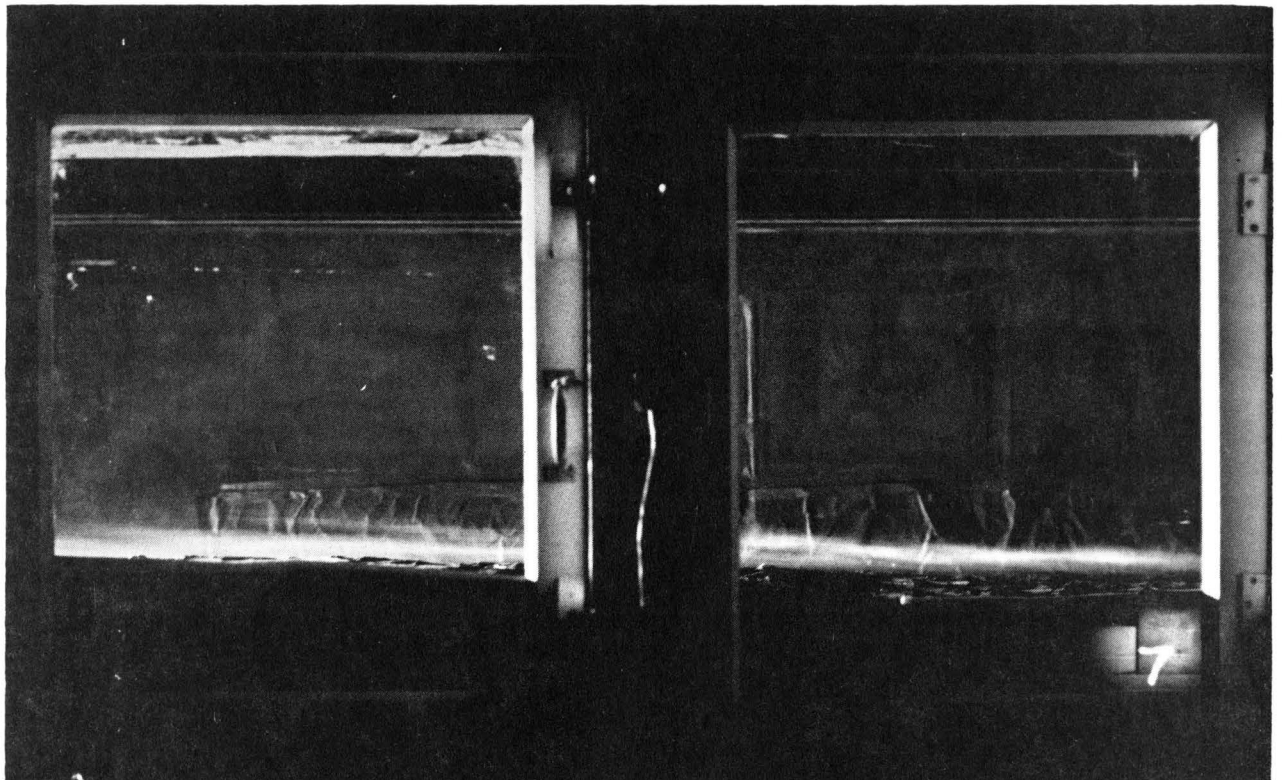


a

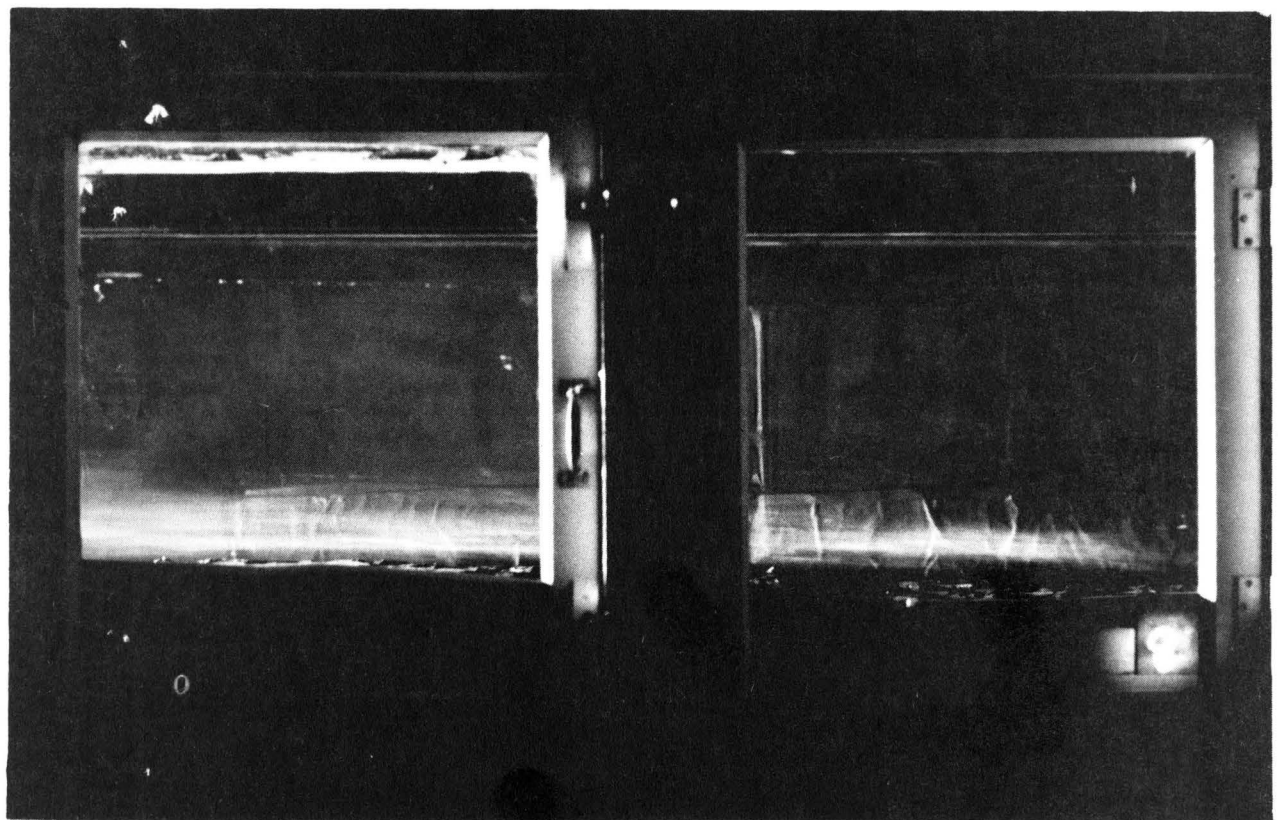


b

Figure 6.1-2 Plume Visualization for the 349° Wind Direction (Garfield Peak), $Fr_T = 1.9$ and a Release Height of a) 7.6 cm (381 m prototype), b) 9.5 cm (476 m prototype)



a



b

Figure 6.1-3 Plume Visualization for 349° Wind Direction (Badger Peak),
 $Fr_T = 6.5$ and a Release Height of a) 7.6 cm (381 m prototype),
b) 9.5 cm (476 m prototype)

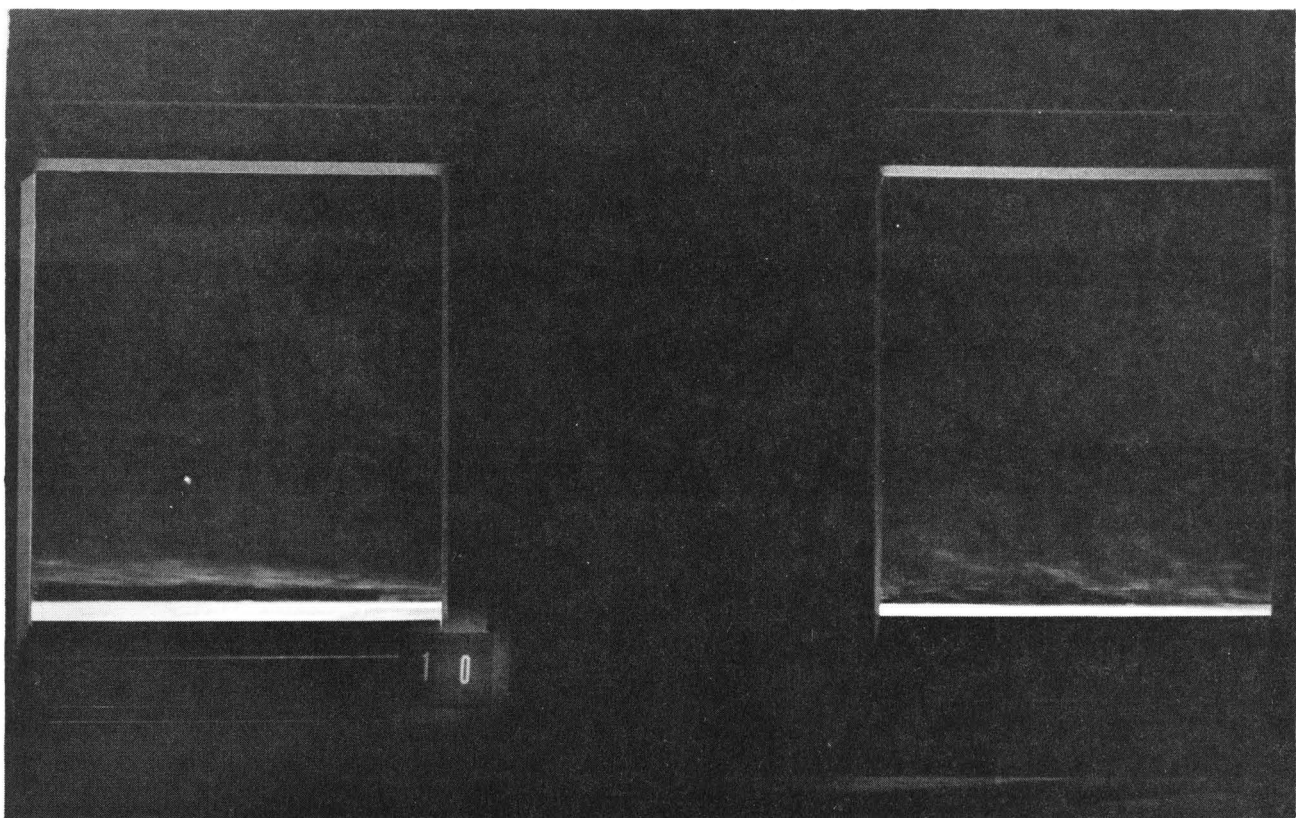
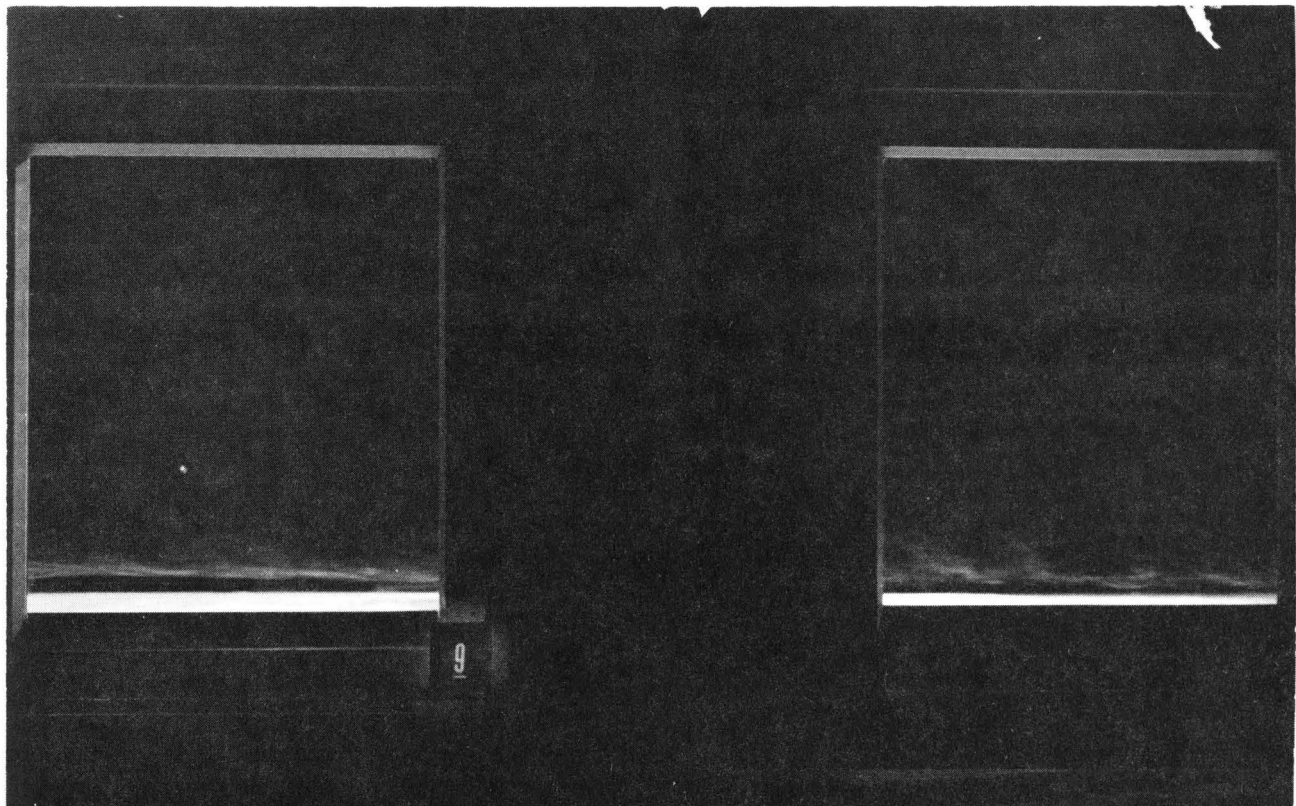


Figure 6.1-4 Plume Visualization for Flat Terrain, $Fr_T = 4.6$ and a Release Height of a) 7.6 cm (381 m prototype), b) 9.5 cm (476 m prototype)

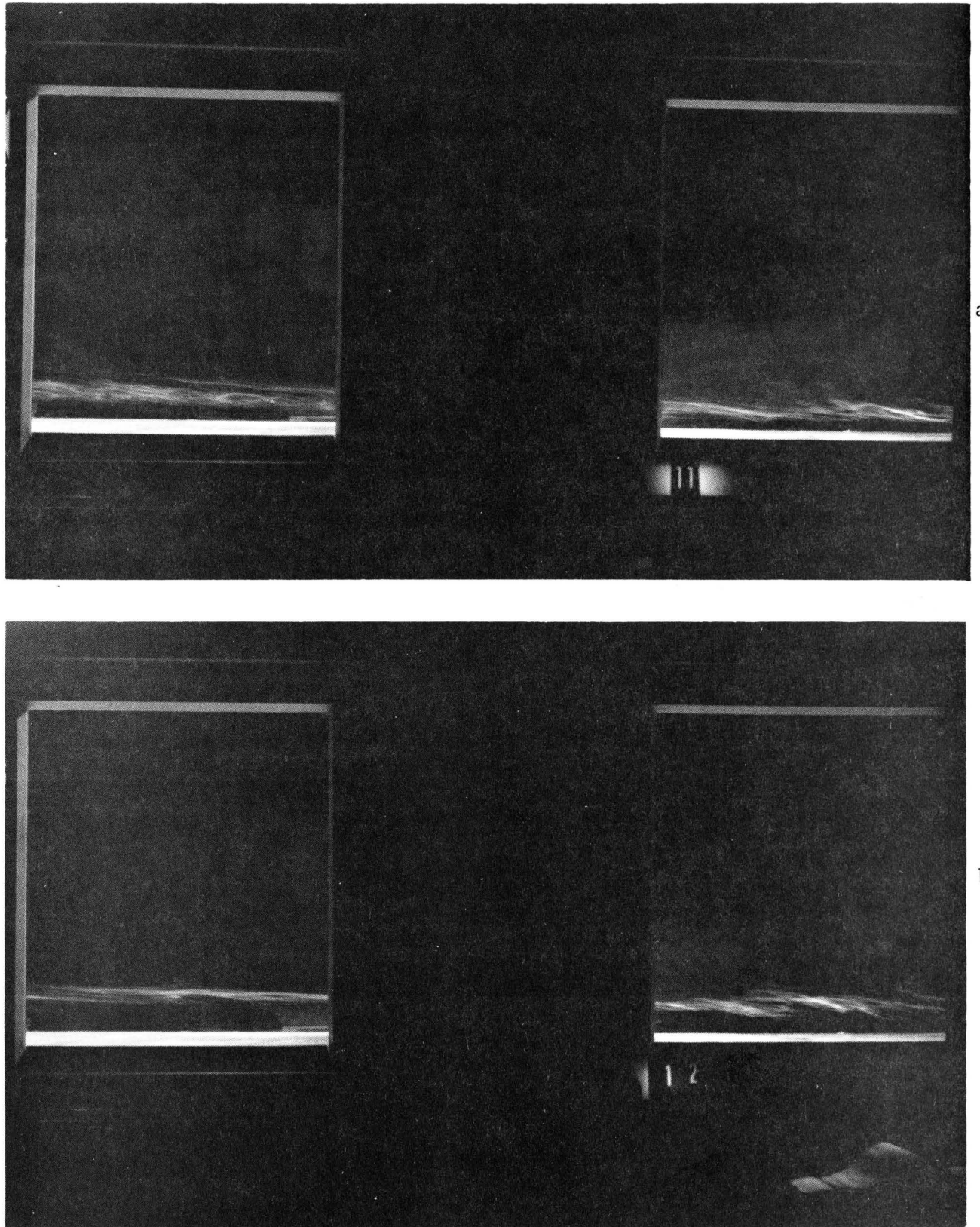


Figure 6.1-5 Plume Visualization for Flat Terrain, $Fr_T = 1.8$ and a Release Height of a) 7.6 cm (381 m prototype), b) 9.5 cm (476 m prototype)

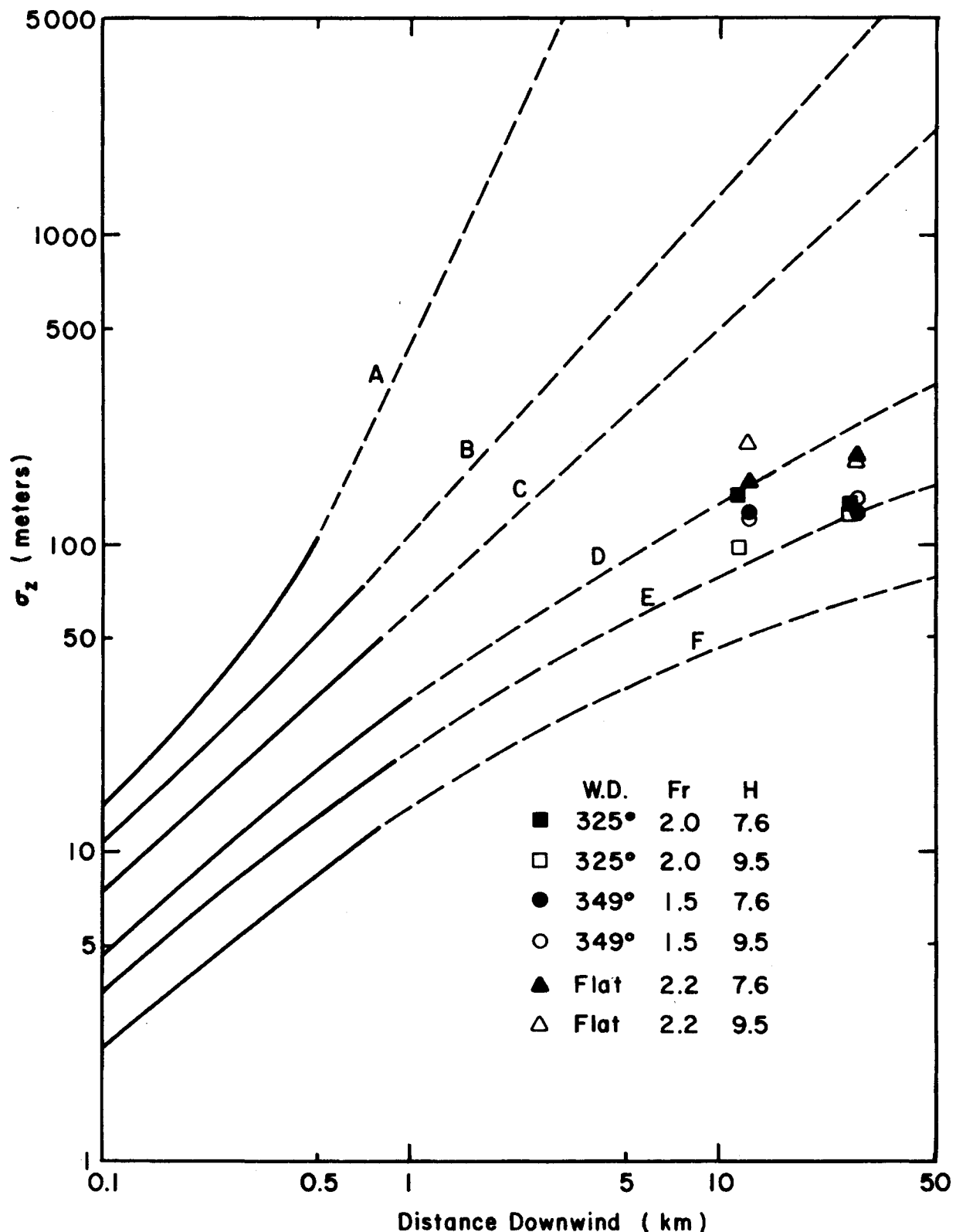


Figure 6.1-6 Plot of Observed σ_z Values in Comparison to the Pasquill-Gifford Curves for Low Fr Cases

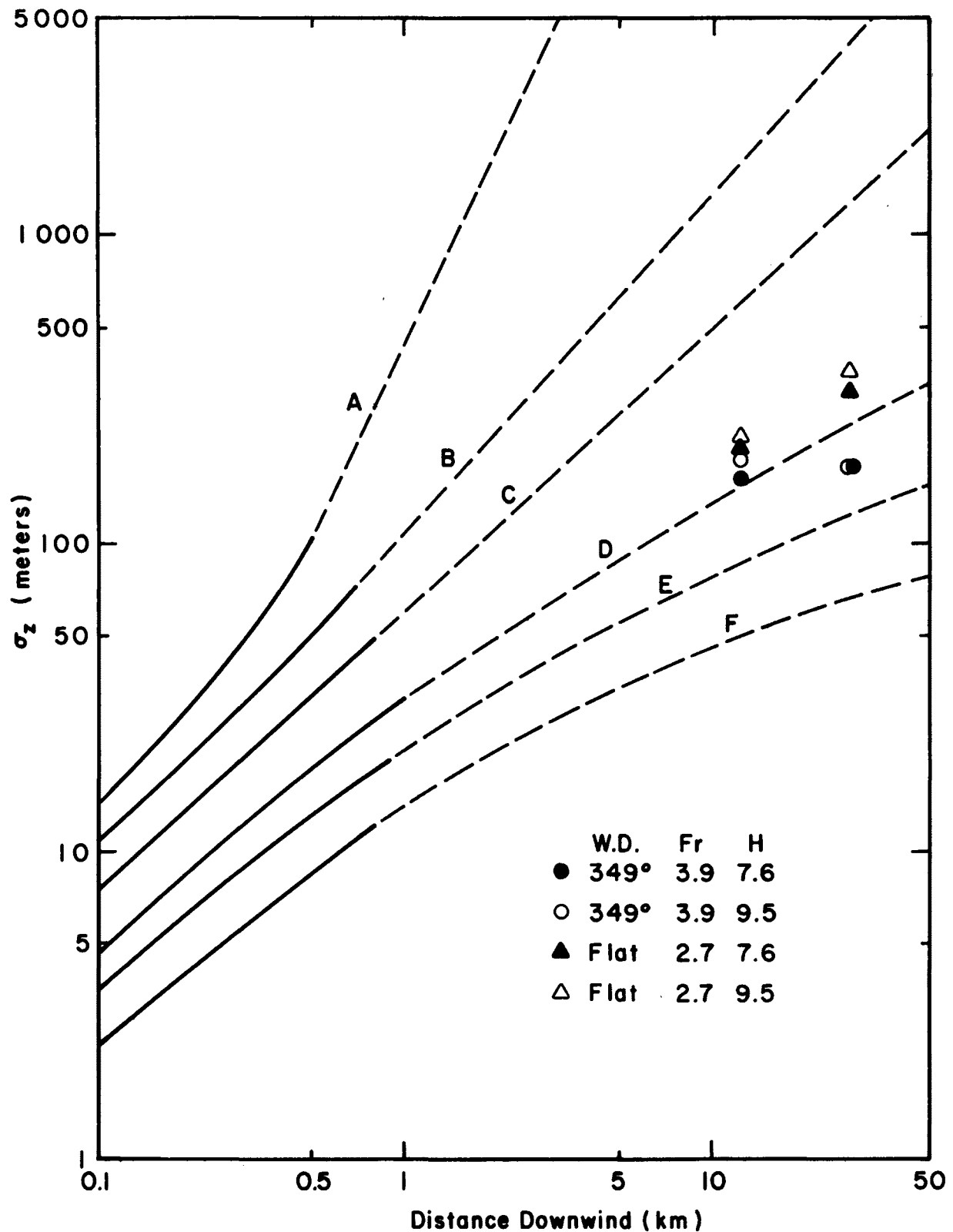


Figure 6.1-7 Plot of Observed σ_z Values in Comparison to Pasquill-Gifford Curves for High Fr Cases

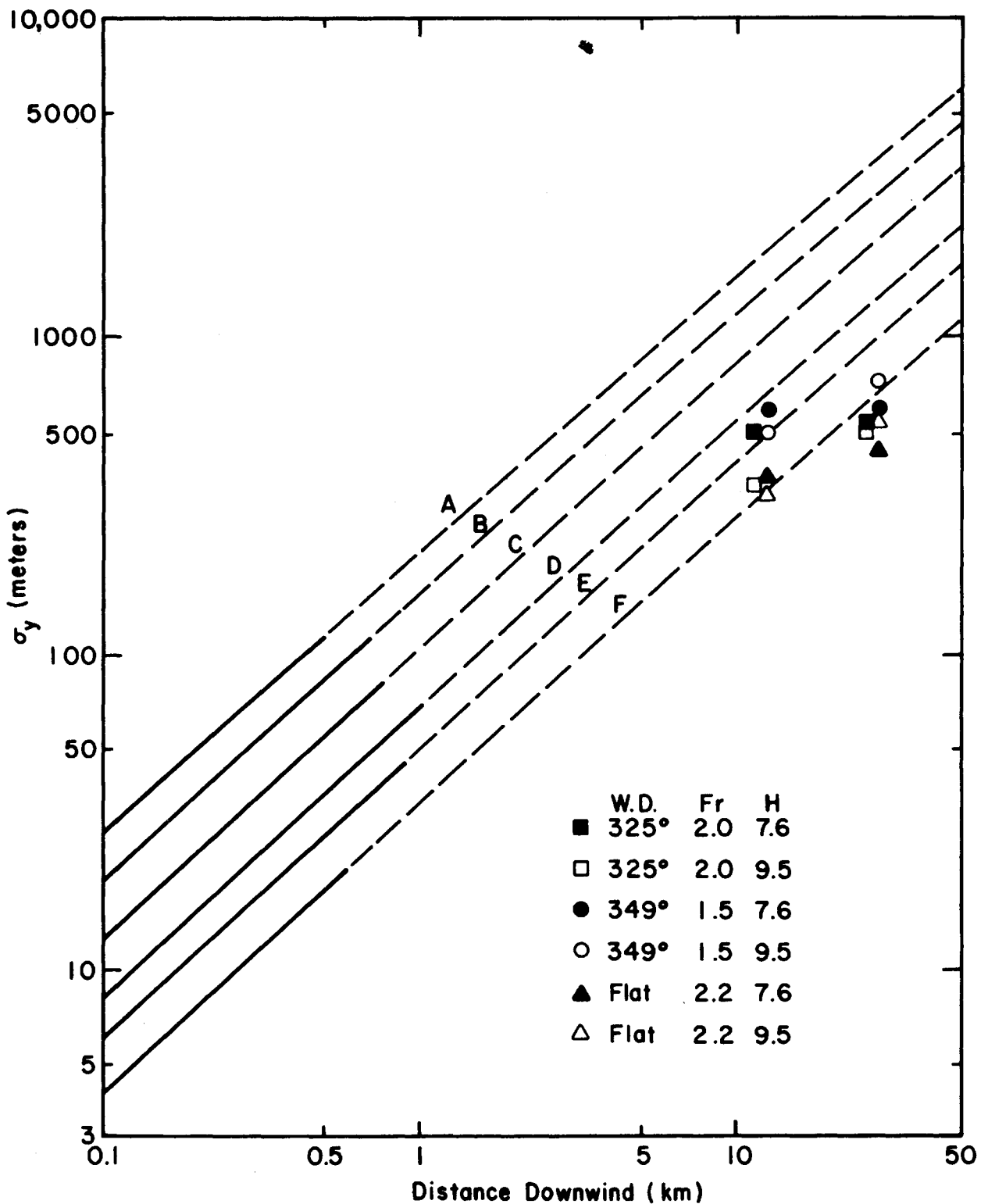


Figure 6.1-8 Plot of Observed σ_y Values in Comparison to Pasquill-Gifford Curves for Low Fr Cases

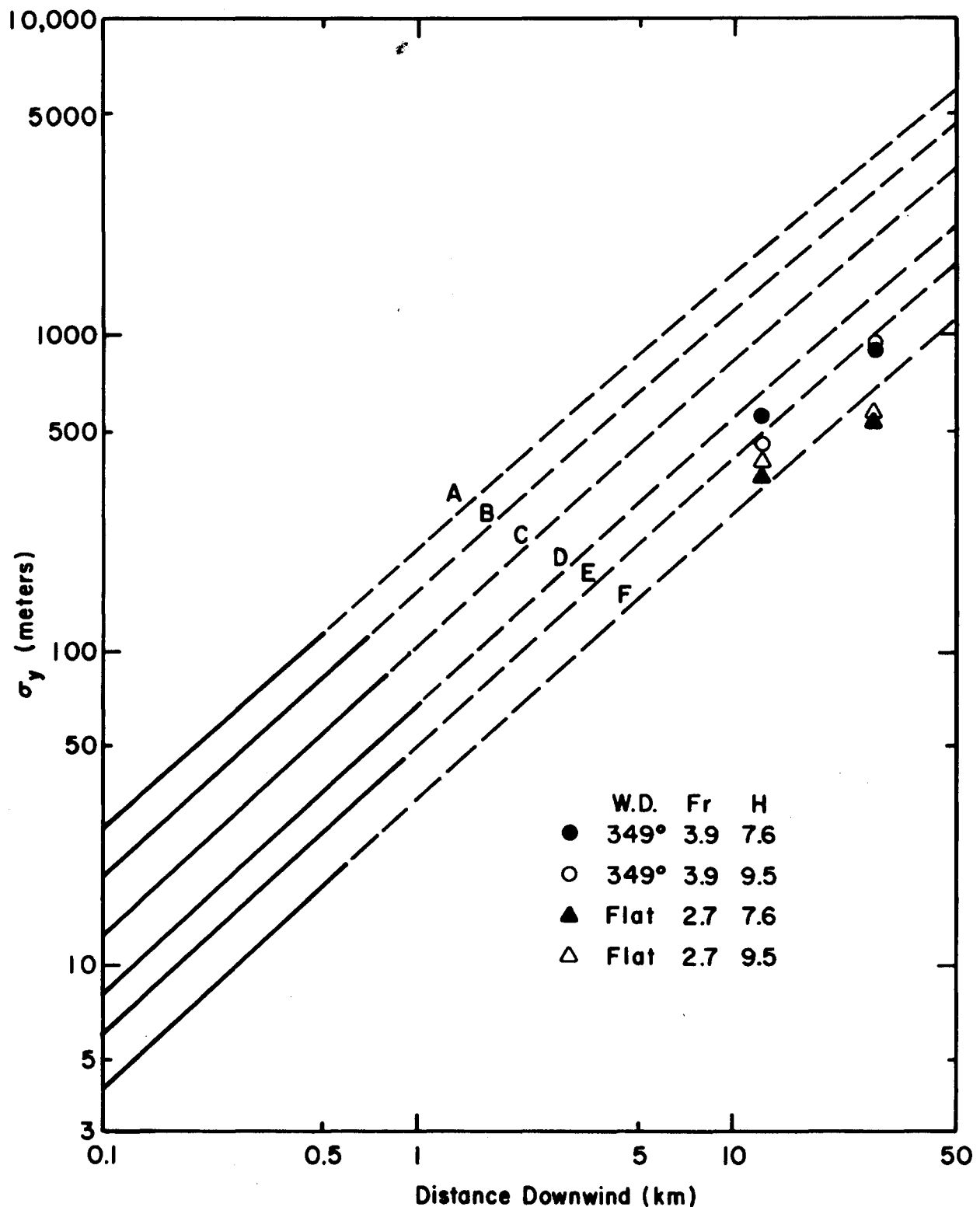


Figure 6.1-9 Plot of Observed σ_y Values in Comparison to Pasquill-Gifford Curves for High Fr Cases

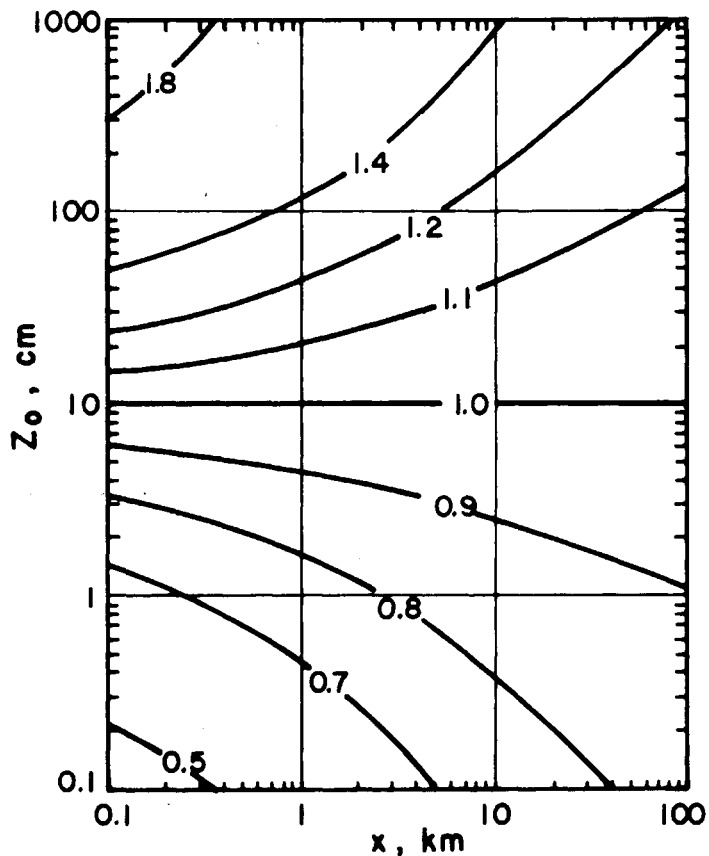


Figure 6.1-10 Isopleths of $\sigma_z(z_0)/\sigma_z(z_0) = 10 \text{ cm}$, Virtually Independent of Heat Flux based on Pasquill (1974)

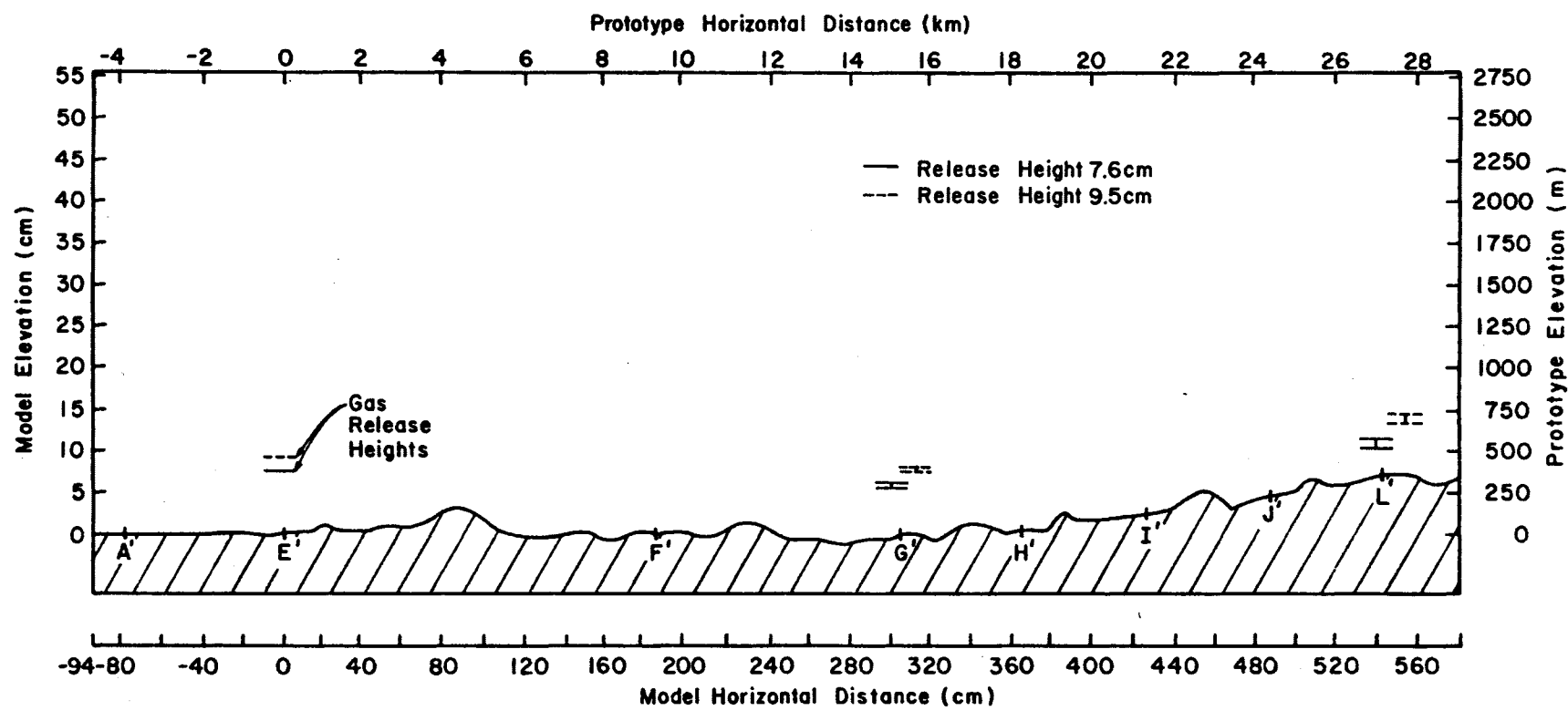


Figure 6.1-11 Plot of Plume Height Range ($Z_{\max} \rightarrow \bar{Z}$) versus Downwind Distance for the 349° Wind Direction and an Fr_T of 1.8

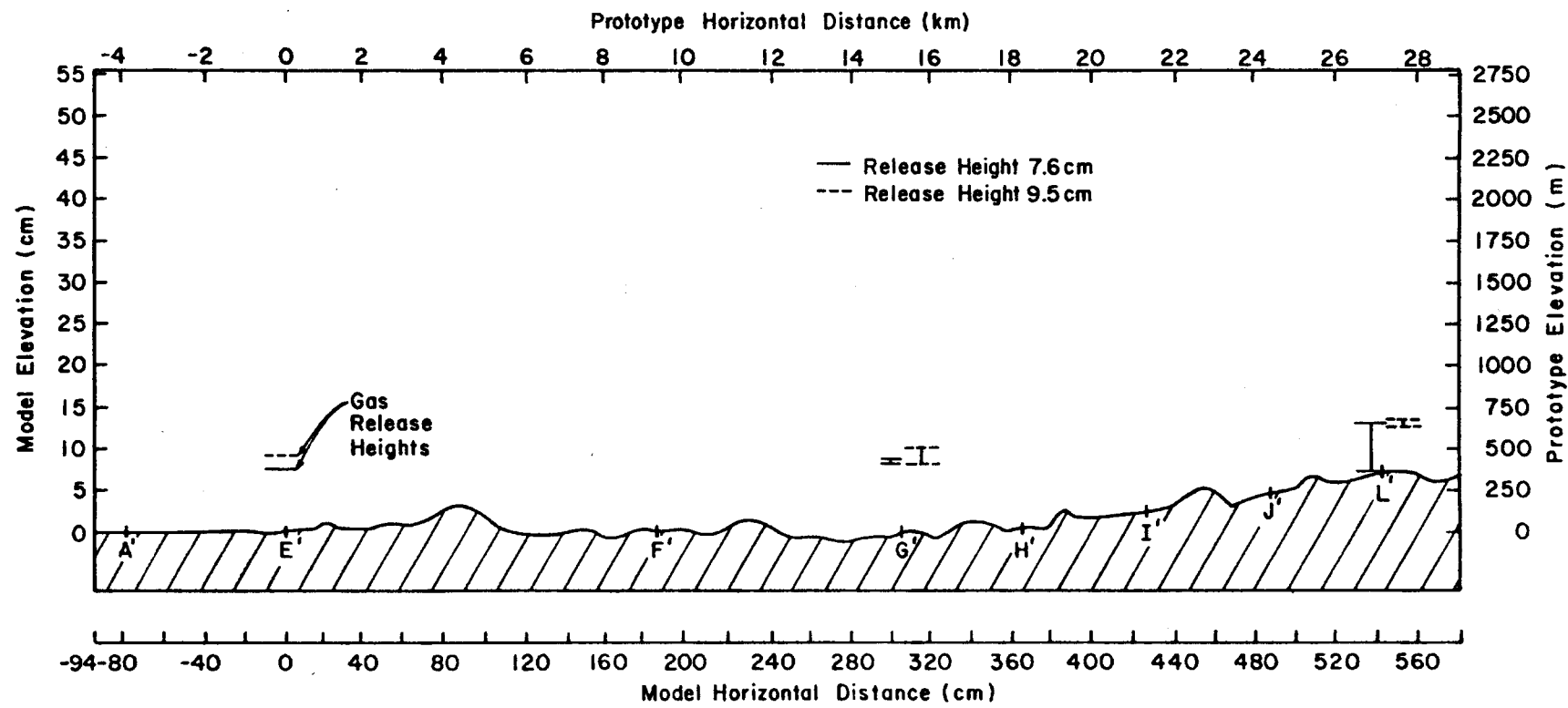


Figure 6.1-12 Plot of Plume Height Range ($\bar{Z} \rightarrow Z_{\max}$) versus Downwind Distance for the 349° Wind Direction and an Fr_T of 6.3

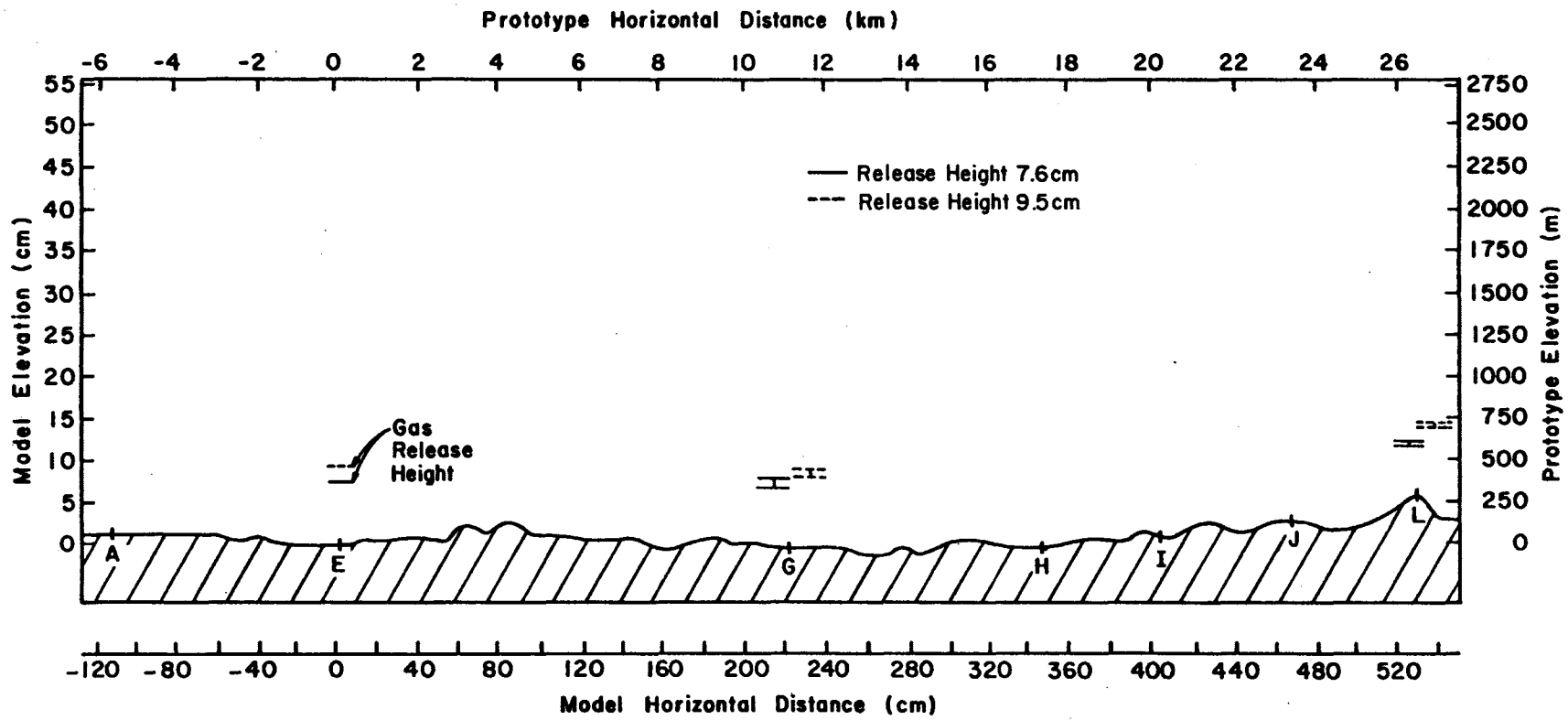


Figure 6.1-13 Plot of Plume Height Range ($Z_{\max} \rightarrow \bar{Z}$) versus downwind Distance for the 325° Wind Direction and an Fr_T of 1.9

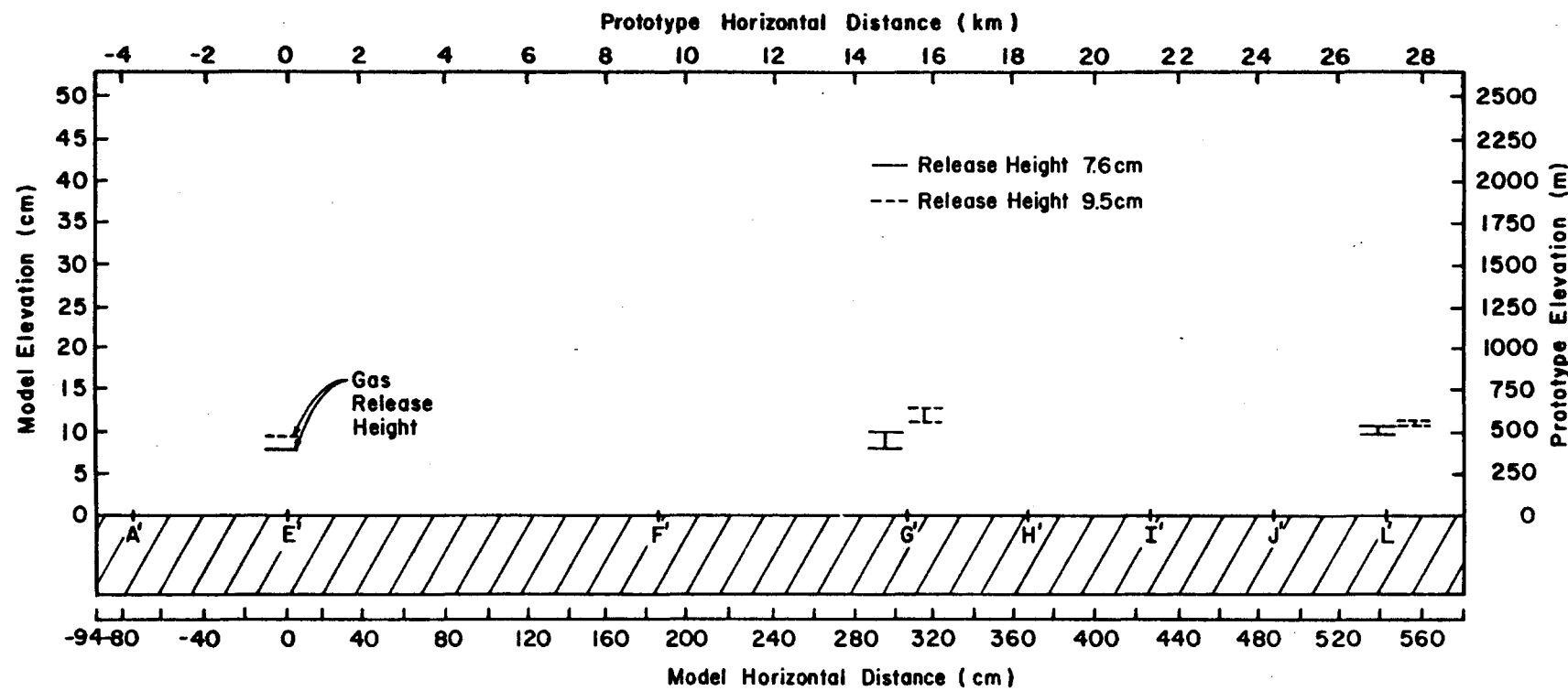


Figure 6.1-14 Plot of Plume Height Range ($\bar{Z} \rightarrow Z_{\max}$) versus Downwind Distance for the Flat Terrain Case with an Fr_T of 1.8

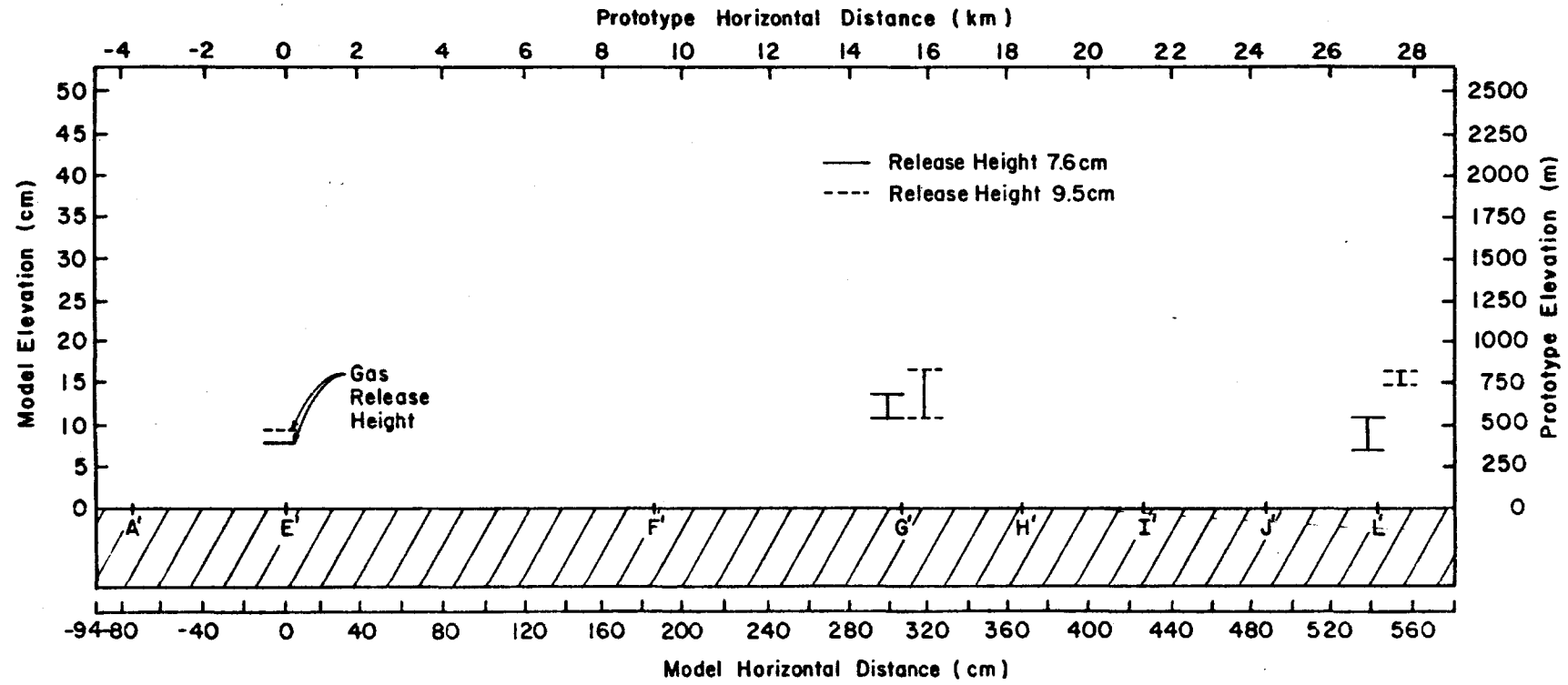


Figure 6.1-15 Plot of Plume Height Range ($\bar{Z} \rightarrow Z_{\max}$) versus Downwind Distance for the Flat Terrain Case with Fr_T of 4.6

Appendix A

Tabulation of Concentration Measurements

Concentration Results for a 325° Wind Direction, 0.076 m Release Height, Location G, Fr = 2.0

DATA FOR ETHANE TRACER GAS BACKGROUND CONC: 8.60 MV-SEC

CAL. FACTOR: .270 (PPM METHANE/MV-SEC) GAS FACTOR (PPM ETHANE/PPM METHANE): 0.533

VELOCITY (M/SEC): .38

SOURCE STRENGTH: .850E+05

STACK DIAMETER: .142E-01

EXIT VELOCITY: .117E+00

128

LOCATION	RAW DATA (MV-SEC)	NON-DIMENSIONAL CONCENTRATION COEFFICIENT (K)	DILUTION FACTOR (C/C ₀)
1	72.1	.126E-01	.108E-03
2	61.7	.106E-01	.900E-04
3	58.4	.990E-02	.840E-04
4	75.7	.133E-01	.114E-03
5	231.1	.442E-01	.377E-03
6	314.1	.607E-01	.517E-03
7	191.7	.364E-01	.310E-03
8	27.0	.366E-02	.310E-04
9	7.4	0	0
10	10.2	.318E-03	.300E-05
11	9.1	.100E-03	.100E-05
12	8.6	0	0
13	28.4	.394E-02	.340E-04
14	306.7	.593E-01	.505E-03
15	810.7	.159E+00	.136E-02
16	478.4	.934E-01	.795E-03
17	12.1	.696E-03	.600E-05
18	173.1	.327E-01	.279E-03
19	161.7	.304E-01	.259E-03
20	809.1	.159E+00	.136E-02
21	53.2	.886E-02	.760E-04
22	11.9	.656E-03	.600E-05
23	11.0	.480E-03	.400E-05
24	9.7	.220E-03	.200E-05

Concentration Results for a 325° Wind Direction, 0.076 m Release Height, Location L, and Fr = 2.0

DATA FOR ETHANE TRACER GAS BACKGROUND CONC: 7.00 MV-SEC
CAL. FACTOR: .270 (PPM METHANE/MV-SEC) GAS FACTOR (PPM ETHANE/PPM METHANE): 0.533

VELOCITY (M/SEC): .38
SOURCE STRENGTH: .850E+05
STACK DIAMETER .142E-01
EXIT VELOCITY: .117E+00

LOCATION	RAW DATA (MV-SEC)	NON-DIMENSIONAL CONCENTRATION COEFFICIENT (K)	DILUTION FACTOR (C/C ₀)
1	158.0	.300E-01	.256E-03
2	281.1	.545E-01	.464E-03
3	590.3	.116E+00	.988E-03
4	530.4	.108E+00	.920E-03
5	248.1	.479E-01	.408E-03
6	59.9	.105E-01	.900E-04
7	18.1	.221E-02	.190E-04
8	12.5	.109E-02	.900E-05
9	7.0	0	0
10	8.9	.380E-03	.300E-05
11	8.5	.300E-03	.300E-05
12	39.7	.650E-02	.103E-04
13	167.1	.318E-01	.271E-03
14	798.4	.157E+00	.134E-02
15	493.6	.967E-01	.824E-03
16	55.9	.972E-02	.830E-04
17	45.9	.773E-02	.660E-04
18	2050.1	.406E+00	.346E-02
19	2194.0	.435E+00	.370E-02
20	1691.8	.335E+00	.285E-02
21	321.6	.625E-01	.533E-03
22	16.3	.185E-02	.160E-04
23	9.2	.440E-03	.400E-05
24	10.5	.700E-03	.600E-05
25	41.1	.678E-02	.580E-04

Concentration Results for a 325° Wind Direction, 0.095 m Release Height, Location G, and Fr = 2.0

DATA FOR ETHANE TRACER GAS BACKGROUND COND: 9.90 MV-SEC

CAL. FACTOR: .270 (PPM METHANE/MV-SEC) GAS FACTOR (PPM ETHANE/PPM METHANE): 0.533

VELOCITY (M/SEC) .40

SOURCE STRENGTH: .850E+05

STACK DIAMETER: .142E-01

EXIT VELOCITY: .117E+00

LOCATION	RAW DATA (MV-SEC)	NON-DIMENSIONAL CONCENTRATION COEFFICIENT (K)	DILUTION FACTOR (C/CO)
1	14.7	.149E-02	.800E-05
2	16.4	.202E-02	.110E-04
3	17.3	.230E-02	.130E-04
4	23.6	.426E-02	.230E-04
5	38.6	.891E-02	.490E-04
6	23.6	.426E-02	.230E-04
7	17.7	.242E-02	.130E-04
8	10.6	.220E-03	.100E-05
9	10.5	.190E-03	.100E-05
10	9.9	0	0
11	10.3	.124E-03	.100E-05
12	10.2	.900E-04	.100E-05
13	351.3	.160E+00	.578E-03
14	2456.8	.760E+00	.414E-02
15	1593.9	.492E+00	.268E-02
16	26.5	.516E-02	.280E-04
17	13.1	.990E-03	.500E-05
18	31.6	.674E-02	.370E-04
19	424.2	.129E+00	.701E-03
20	2996.2	.918E+00	.500E-02
21	848.8	.261E+00	.142E-02
22	32.4	.699E-02	.380E-04
23	12.2	.710E-03	.400E-05
24	13.5	.112E-02	.600E-05

Concentration Results for a 325° Wind Direction, 0.095 m Release Height, Location L, and Fr = 2.0

DATA FOR ETHANE TRACER GAS BACKGROUND CONC: 9.60 MV-SEC
 CAL. FACTOR: .270 (PPM METHANE/MV-SEC) GAS FACTOR (PPM ETHANE/PPM METHANE): 0.533

VELOCITY (M/SEC): .40
 SOURCE STRENGTH: .850E+05
 STACK DIAMETER: .142E-01
 EXIT VELOCITY: .117E+00

LOCATION	RAW DATA (MV-SEC)	NON-DIMENSIONAL CONCENTRATION COEFFICIENT (K)	DILUTION FACTOR (C/C0)
1	21.9	.382E-02	.210E-04
2	15.8	.193E-02	.110E-04
3	30.3	.640E-02	.350E-04
4	19.4	.304E-02	.170E-04
5	13.8	.130E-02	.700E-05
6	10.4	.250E-03	.100E-05
7	10.9	.400E-03	.200E-05
8	9.6	0	0
9	9.9	.900E-04	.100E-05
10	12.9	.102E-02	.600E-05
11	12.3	.840E-03	.500E-05
12	102.8	.289E-01	.158E-03
13	424.7	.129E+00	.703E-03
14	1553.1	.479E+00	.261E-02
15	966.6	.297E+00	.162E-02
16	121.6	.348E-01	.190E-03
17	35.6	.807E-02	.440E-04
18	301.8	.907E-01	.495E-03
19	1552.0	.479E+00	.261E-02
20	1902.6	.588E+00	.321E-02
21	913.1	.281E+00	.153E-02
22	32.7	.717E-02	.390E-04
23	12.5	.900E-03	.500E-05
24	10.4	.250E-03	.100E-05
25	16.4	.217E-02	.120E-04

Concentration Results for a 349° Wind Direction, 0.076 m Release Height, Location M', and Fr = 1.5

CONCENTRATION DATA FOR RUN NO. AC ON NOV. 30 1978 AT 22:22.
 WIND DIRECTION: 349 DEG. UNITS: 1 SCALE FACTOR: 5000
 DATA FOR TRACER GAS NO. 1, ETHANE BACKGROUND CONC. 15.70 MV-SEC.
 CAL. FACTOR: .244 GAS FACTOR (PPM GAS/PPM METHANE): .533

MODEL
 VELOCITY (M/SEC) 32
 SOURCE STRENGTH (PPM) .916E+05
 VOLUME FLOW (CU. M/SEC) .329E-04
 STACK DIAMETER (M) .142E-01
 EXIT VELOCITY (M/SEC) .208E+00

LOCATION	RAW DATA (MV-SEC)	NON-DIMENSIONAL CONCENTRATION COEFFICIENT(K)	DILUTION FACTOR (C/C0)
1	536.5579	.414E-01	.740E-03
2	834.7999	.652E-01	.116E-02
3	1090.8000	.855E-01	.153E-02
4	1187.303	.932E-01	.166E-02
5	1254.911	.986E-01	.176E-02
6	1149.728	.902E-01	.161E-02
7	972.1467	.761E-01	.136E-02
8	240.1737	.179E-01	.319E-03
9	212.3019	.156E-01	.279E-03
10	16.5444	.672E-04	.120E-05
11	18.0226	.185E-03	.330E-05
12	21.0063	.428E-03	.765E-05
13	48.8222	.263E-02	.470E-04
14	253.2883	.189E-01	.337E-03
15	157.1494	.113E-01	.201E-03
16	737.3185	.574E-01	.102E-02
18	2124.498	.169E+00	.300E-02
19	1600.740	.126E+00	.225E-02
20	613.3701	.475E-01	.849E-04
21	55.7901	.319E-02	.569E-04
22	16.6449	.752E-04	.134E-05
23	19.1492	.274E-03	.490E-05
24	15.7154	.122E-05	.218E-07

Concentration Results for a 349° Wind Direction, 0.095 m Release Height, Location G', and Fr = 1.5

CONCENTRATION DATA FOR RUN NO. AE ON DEC. 1 1978 AT 0:15.
 WIND DIRECTION: 349 DEG. UNITS: 2 SCALE FACTOR: 5000.
 DATA FOR TRACER GAS NO. 1, ETHANE BACKGROUND CONC. 15.40 MY-SEC.
 CAL. FACTOR: .244 GAS FACTOR (PPM GAS/PPM METHANE): .533

	MODEL
VELOCITY (M/SEC)	.34
SOURCE STRENGTH (PPM)	.916E+05
VOLUME FLOW (CU M/SEC)	.329E-04
STACK DIAMETER (M)	.142E-01
EXIT VELOCITY (M/SEC)	.208E+00

LOCATION	RAW DATA (MV-SEC)	NON-DIMENSIONAL CONCENTRATION COEFFICIENT(K)	DILUTION FACTOR (C/CD)
1	60.8444	.600E-02	.645E-04
3	62.1080	.617E-02	.663E-04
4	93.9687	.104E-01	.112E-03
5	207.8943	.254E-01	.273E-03
6	160.9822	.192E-01	.207E-03
7	98.6382	.110E-01	.118E-03
8	24.8111	.124E-02	.134E-04
9	19.5269	.545E-03	.586E-05
10	14.8398	.000E+00	.000E+00
11	20.3108	.649E-03	.697E-05
12	17.8623	.325E-03	.350E-05
13	54.7225	.520E-02	.559E-04
14	2228.327	.292E+00	.314E-02
15	1502.783	.197E+00	.211E-02
16	732.9066	.948E-01	.102E-02
17	31.9111	.218E-02	.235E-04
18	153.7930	.183E-01	.197E-03
19	2141.369	.281E+00	.302E-02
20	3355.534	.441E+00	.474E-02
21	843.0760	.109E+00	.118E-02
22	59.2444	.579E-02	.623E-04
23	21.6444	.825E-03	.887E-05
24	19.4000	.529E-03	.568E-05

Concentration Results for a 349° Wind Direction, 0.076 m Release Height, Location G', and Fr = 1.5

CONCENTRATION DATA FOR RUN NO. AF ON DEC. 1 1978 AT 0:56.
 WIND DIRECTION: 349 DEG. UNITS: 1 SCALE FACTOR: 5000.
 DATA FOR TRACER GAS NO. 1, ETHANE BACKGROUND CONC. 15.40 MV-SEC.
 CAL. FACTOR: .244 GAS FACTOR (PPM GAS/PPM METHANE): .533

	MODEL
VELOCITY (M/SEC)	.32
SOURCE STRENGTH (PPM)	.916E+05
VOLUME FLOW (CU. M/SEC)	.329E-04
STACK DIAMETER (M)	.142E-01
EXIT VELOCITY (M/SEC)	.208E+00

LOCATION	RAW DATA (MV-SEC)	NON-DIMENSIONAL CONCENTRATION COEFFICIENT(K)	DILUTION FACTOR (C/C0)
1	850.1334	.664E-01	.119E-02
2	614.1454	.476E-01	.850E-03
3	918.2808	.718E-01	.128E-02
4	1612.618	.127E+00	.227E-02
5	2182.137	.172E+00	.308E-02
6	1577.013	.124E+00	.222E-02
7	965.2043	.756E-01	.135E-02
8	114.5157	.788E-02	.141E-03
9	24.6714	.737E-03	.132E-04
10	17.0896	.134E-03	.240E-05
11	16.0204	.493E-04	.881E-06
12	25.1444	.775E-03	.138E-04
13	74.9676	.474E-02	.846E-04
14	395.0425	.302E-01	.539E-03
15	160.8313	.116E-01	.207E-03
16	145.5221	.104E-01	.185E-03
17	15.4074	.590E-06	.105E-07
18	2053.498	.162E+00	.289E-02
19	6281.012	.498E+00	.890E-02
20	3486.853	.276E+00	.493E-02
21	202.8966	.149E-01	.266E-03
22	23.0775	.611E-03	.109E-04
23	20.2553	.386E-03	.690E-05
24	18.7778	.269E-03	.480E-05

Concentration Results for a 349° Wind Direction, 0.095 m Release Height, Location M', and Fr = 1.5

CONCENTRATION DATA FOR RUN NO. AD ON NOV. 30 1978 AT 23:14
 WIND DIRECTION: 349 DEG UNITS: 2 SCALE FACTOR: 5000.
 DATA FOR TRACER GAS NO. 1: ETHANE BACKGROUND CONC. 15.50 MV-SEC.
 CAL. FACTORY .244 GAS FACTOR (PPM GAS/PPM METHANE): .533

	MODEL
VELOCITY (M/SEC)	.34
SOURCE STRENGTH (PPM)	.916E+05
VOLUME FLOW (CU. M/SEC)	.329E-04
STACK DIAMETER (M)	.142E-01
EXIT VELOCITY (M/SEC)	.208E+00

LOCATION	RAW DATA (MV-SEC)	NON-DIMENSIONAL CONCENTRATION COEFFICIENT(K)	DILUTION FACTOR (C/CO)
1	427.6667	.545E-01	.595E-03
2	584.1865	.751E-01	.808E-03
3	780.7476	.101E+00	.109E-02
4	728.9111	.943E-01	.101E-02
5	585.1429	.753E-01	.809E-03
6	374.3475	.474E-01	.510E-03
7	183.6066	.222E-01	.239E-03
8	49.4556	.449E-02	.482E-04
9	47.9600	.429E-02	.461E-04
10	15.1919	.000E+00	.000E+00
11	19.8314	.572E-03	.615E-05
12	211.2311	.259E-01	.278E-03
13	745.3112	.964E-01	.104E-02
14	1077.262	.140E+00	.151E-02
15	772.6069	.100E+00	.108E-02
16	811.6115	.105E+00	.113E-02
17	86.2390	.935E-02	.100E-03
18	1612.374	.211E+00	.227E-02
19	4097.796	.539E+00	.589E-02
20	3257.838	.428E+00	.461E-02
21	1053.862	.137E+00	.147E-02
22	48.5015	.436E-02	.469E-04
23	15.9096	.541E-04	.582E-06
24	15.5462	.611E-05	.657E-07

Concentration Results for a 349° Wind Direction, 0.076 m Release Height, Location G', and Fr = 3.9

CONCENTRATION DATA FOR RUN NO. BC ON DEC. 2 1978 AT 21:31.
 WIND DIRECTION: 349 DEG. UNITS: 1 SCALE FACTOR: 5000.
 DATA FOR TRACER GAS NO. 1, ETHANE BACKGROUND CONC. 6.10 MV-SEC.
 CAL. FACTOR: .234 GAS FACTOR (PPM GAS/PPM METHANE): .533

	MODEL 71
VELOCITY (M/SEC)	.916E+05
SOURCE STRENGTH (PPM)	
VOLUME FLOW (CU. M/SEC)	.380E-04
STACK DIAMETER (M)	.142E-01
EXIT VELOCITY (M/SEC)	.240E+00

LOCATION	RAW DATA (MV-SEC)	NON-DIMENSIONAL CONCENTRATION COEFFICIENT(K)	DILUTION FACTOR (C/C0)
1	12.2774	.910E-03	.841E-05
2	9.6389	.522E-03	.482E-05
3	16.7660	.157E-02	.145E-04
4	37.5108	.463E-02	.428E-04
5	129.4222	.182E-01	.168E-03
6	132.7111	.216E-01	.200E-03
7	250.8392	.361E-01	.333E-03
8	570.2762	.831E-01	.768E-03
9	997.1453	.146E+00	.135E-02
10	9.6785	.527E-03	.482E-05
11	12.1675	.894E-03	.826E-05
12	162.0889	.230E-01	.212E-03
13	457.9556	.666E-01	.615E-03
14	736.4558	.111E+00	.102E-02
15	338.3445	.490E-01	.453E-03
16	79.1889	.108E-01	.996E-04
17	9.6176	.518E-03	.479E-05
18	256.4427	.369E-01	.341E-03
19	959.5015	.140E+00	.130E-02
20	1352.760	.198E+00	.183E-02
21	688.0916	.101E+00	.929E-03
22	124.0540	.174E-01	.161E-03
23	18.4441	.182E-02	.168E-04
24	6.0893	.000E+00	.000E+00

Concentration Results for a 349° Wind Direction, 0.076 m Release Height, Location M', and Fr = 3.9

CONCENTRATION DATA FOR RUN NO. BB ON DEC. 2 1978 AT 20:35.
 WIND DIRECTION: 349 DEG. UNITS: 1 SCALE FACTOR: 5000.
 DATA FOR TRACER GAS NO. 1, ETHANE BACKGROUND CONC. 10.30 MV-SEC.
 CAL. FACTOR: .234 GAS FACTOR (PPM GAS/PPM METHANE): .533

MODEL
 VELOCITY (M/SEC) 71
 SOURCE STRENGTH (PPM) 916E+05
 VOLUME FLOW (CU. M/SEC) 380E-04
 STACK DIAMETER (M) 142E-01
 EXIT VELOCITY (M/SEC) 240E+00

LOCATION	RAW DATA (MV-SEC)	NON-DIMENSIONAL CONCENTRATION COEFFICIENT(K)	DILUTION FACTOR (C/CO)
1	123.0792	166E-01	154E-03
2	322.5112	475E-01	439E-03
3	627.7933	910E-01	841E-03
4	668.1333	969E-01	896E-03
5	832.3557	121E+00	112E-02
6	902.8728	132E+00	122E-02
7	982.3256	143E+00	132E-02
8	897.4047	131E+00	121E-02
9	487.3044	703E-01	650E-03
10	19.5774	137E-02	126E-04
11	94.6302	124E-01	115E-03
12	189.8531	265E-01	245E-03
13	248.4665	351E-01	324E-03
14	201.7333	282E-01	261E-03
15	138.4001	189E-01	174E-03
16	89.0497	116E-01	107E-03
17	18.8895	127E-02	117E-04
18	694.2930	101E+00	932E-03
19	789.1774	115E+00	106E-02
20	439.7161	633E-01	585E-03
21	200.4538	280E-01	259E-03
22	36.5340	387E-02	357E-04
23	10.2674	000E+00	000E+00

Concentration Results for a 349° Wind Direction, 0.095 m Release Height, Location G', and Fr = 3.9

CONCENTRATION DATA FOR RUN NO. BD ON DEC. 2 1978 AT 22:26
 WIND DIRECTION: 349 DEG. UNITS: 2 SCALE FACTOR: 5000.
 DATA FOR TRACER GAS NO. 1, ETHANE BACKGROUND CONC. 9.70 MV-SEC.
 CAL. FACTOR: .234 GAS FACTOR (PPM GAS/PPM METHANE): .533

MODEL
 VELOCITY (M/SEC) .81
 SOURCE STRENGTH (PPM) .916E+05
 VOLUME FLOW (CU. M/SEC) .380E-04
 STACK DIAMETER (M) .142E-01
 EXIT VELOCITY (M/SEC) .240E+00

LOCATION	RAW DATA (MV-SEC)	NON-DIMENSIONAL CONCENTRATION COEFFICIENT(K)	DILUTION FACTOR (C/CO)
1	16.5444	.180E-02	.932E-05
2	16.5824	.181E-02	.937E-05
3	24.6549	.392E-02	.204E-04
4	52.3519	.112E-01	.581E-04
5	213.5889	.535E-01	.278E-03
6	206.4639	.516E-01	.268E-03
7	223.2572	.560E-01	.291E-03
8	227.2184	.571E-01	.296E-03
9	276.7266	.700E-01	.364E-03
10	9.6667	.000E+00	.000E+00
11	23.0326	.350E-02	.182E-04
12	543.0698	.140E+00	.727E-03
13	1542.203	.402E+00	.209E-02
14	711.7432	.184E+00	.956E-03
15	235.8194	.593E-01	.308E-03
16	17.8602	.214E-02	.111E-04
17	12.2552	.670E-03	.348E-05
18	233.1000	.586E-01	.304E-03
19	1283.730	.334E+00	.174E-02
20	1950.050	.509E+00	.264E-02
21	1447.625	.377E+00	.196E-02
22	370.4039	.946E-01	.491E-03
23	73.9336	.168E-01	.875E-04
24	16.7670	.185E-02	.963E-05

Concentration Results for a 349° Wind Direction, 0.095 m Release Height, Location M', and Fr = 3.9

CONCENTRATION DATA FOR RUN NO. BA ON DEC. 2 1978 AT 19:57
 WIND DIRECTION: 349 DEG. UNITS: 2 SCALE FACTOR: 5000.
 DATA FOR TRACER GAS NO. 1, ETHANE BACKGROUND CONC. 6.70 MV-SEC.
 CAL. FACTOR: .234 GAS FACTOR (PPM GAS/PPM METHANE): .533

	MODEL
VELOCITY (M/SEC)	81
SOURCE STRENGTH (PPM)	.916E+05
VOLUME FLOW (CU. M/SEC)	380E-04
STACK DIAMETER (M)	.142E-01
EXIT VELOCITY (M/SEC)	240E+00

LOCATION	RAW DATA (MV-SEC)	NON-DIMENSIONAL CONCENTRATION COEFFICIENT(K)	DILUTION FACTOR (C/C0)
1	1.46 .9222	.368E-01	.191E-03
2	3.03 .2809	.778E-01	.404E-03
3	4.62 .8629	.120E+00	.621E-03
4	4.68 .7429	.121E+00	.629E-03
5	5.87 .1780	.152E+00	.791E-03
6	5.76 .9303	.150E+00	.777E-03
7	6.11 .5789	.159E+00	.824E-03
8	3.86 .8526	.997E-01	.518E-03
9	1.14 .9450	.276E-01	.143E-03
10	5.1 .1667	.117E-01	.606E-04
11	2.29 .7667	.585E-01	.304E-03
12	3.15 .8169	.811E-01	.421E-03
13	3.46 .6851	.892E-01	.463E-03
14	1.58 .5940	.398E-01	.207E-03
15	7.75 .0938	.179E-01	.932E-04
16	2.4 .9108	.478E-02	.248E-04
17	6 .6733	.000E+00	.000E+00
18	8.20 .5609	.213E+00	.111E-02
19	8.98 .4858	.234E+00	.121E-02
20	4.30 .6796	.111E+00	.578E-03
21	1.88 .9333	.478E-01	.248E-03
22	4.2 .6792	.944E-02	.490E-04
23	7 .1317	.113E-03	.588E-06

Concentration Results for Flat Terrain 0.076 m Release Height, Location G, and Fr = 2.7

CUNCENTRATION DATA FOR RUN NO. FC UN DUL. 22 1978 AT 20:27
 WIND DIRECTION 2 DEG UNITS: 1 SCALE FACTOR: 5000.
 DATA FOR TRACER GAS NO. 1, ETHANE BACKGROUND CONC 8.10 MV-SEC
 CAL FACTOR: .58 GAS FACTOR (PPM GAS/PPM METHANE) 533

VELOCITY (M/SEC) MODEL 58
 SOURCE STRENGTH (PPM) 918E+05
 VOLUME FLOW (CU M/SEC) 278E-04
 STACK DIAMETER (M) 142E-01
 EXIT VELOCITY (M/SEC) 176E+00

LOCATION	RAN DATA MV-SEC)	NON-DIMENSIONAL CONCENTRATION COEFFICIENT(K)	DILUTION FACTOR (C/CD)
1	17.8000	326E-02	274E-04
2	12.507	341E-02	283E-04
3	8.5559	459E-02	591E-04
4	5.9444	713E-02	560E-04
5	4.4701	675E-02	403E-04
6	3.2222	486E-02	420E-04
7	2.3333	506E-02	373E-04
8	1.7778	450E-02	469E-04
9	1.4	565E-02	982E-05
10	1.2222	1065E-02	1.08E-04
11	1.0905	2025E-02	2.12E-03
12	0.9680	3225E-02	2.70E-02
13	0.7314	325E+00	6.03E-04
14	0.7778	227E-02	2.05E-04
15	0.175	247E-02	1.91E-04
16	0.4444	330E-02	1.70E-04
17	0.6000	205E-02	1.72E-04
18	0.9981	319E-02	1.68E-04
19	0.244	262E-02	3.47E-04
20	0.044	102E+00	1.70E-02
21	0.67	105E+00	1.63E-02
22	0.64	590E-02	4.09E-02
23		417E-02	3.46E-02

Concentration Results for Flat Terrain 0.095 m, Location G, and Fr = 2.7

CONCENTRATION DATA FOR RUN NO. FG ON DEC. 22 1978 AT 21:1
 WIND DIRECTION: 2 DEG. HEIGHT: .095 SCALE FACTOR: 5000.
 DATA FOR TRACER GAS NO. 1, ETHANE BACKGROUND CONC. 20.50 MV-SEC.
 CAL. FACTOR: .236 GAS FACTOR (PPM GAS/PPM METHANE): .533

MODEL	
VELOCITY (M/SEC)	.64
SOURCE STRENGTH (PPM)	.917E+05
VOLUME FLOW (CU M/SEC)	.270E-04
STACK DIAMETER (M)	.142E-01
EXIT VELOCITY (M/SEC)	.176E+00

LOCATION	RAW DATA (MV-SEC)	NON-DIMENSIONAL CONCENTRATION COEFFICIENT(K)	DILUTION FACTOR (CC/CD)
1	20.5622	.177E-04	.854E-07
2	16.7394	.000E+00	.000E+00
3	18.6267	.000E+00	.000E+00
4	21.0665	.162E-03	.781E-06
5	24.2101	.106E-02	.509E-05
6	18.4987	.000E+00	.000E+00
7	22.1937	.483E-03	.233E-03
8	16.8866	.000E+00	.000E+00
9	19.4348	.000E+00	.000E+00
10	18.0577	.000E+00	.000E+00
11	22.8553	.672E-03	.323E-03
12	1131.3835	.744E-01	.333E-03
13	1132.0664	.317E+00	.153E-02
14	36.9220	.469E-02	.226E-04
15	19.8892	.000E+00	.000E+00
16	15.0444	.000E+00	.000E+00
17	20.6892	.340E-04	.520E-06
18	24.2591	.107E-02	.516E-05
19	64.4775	.125E-01	.604E-04
20	181.7271	.460E-01	.221E-03
21	466.1352	.122E+00	.612E-03
22	1105.530	.310E+00	.149E-02
23	767.2760	.213E+00	.103E-02
24	201.3427	.516E-01	.248E-03

Concentration Results for Flat Terrain 0.076 m Release Height, Location L, and Fr = 2.7

CONCENTRATION DATA FOR RUN NO. FL ON DEC. 22 1978 AT 19:16.
 WIND DIRECTION: 2 DEG. UNITS: 1 SCALE FACTOR: 5000
 DATA FOR TRACER GAS NO. 1, ETHANE BACKGROUND CONC. 8.10 MV-SEC.
 CAL. FACTOR: .236 GAS FACTOR (PPM GAS/PPM METHANE): .533

	MODEL
VELOCITY (M/SEC)	.58
SOURCE STRENGTH (PPM)	.918E+05
VOLUME FLOW (CU. M/SEC)	.278E-04
STACK DIAMETER (M)	.142E-01
EXIT VELOCITY (M/SEC)	.176E+00

LOCATION	RAW DATA (MV-SEC)	NON-DIMENSIONAL CONCENTRATION COEFFICIENT(K)	DILUTION (C/C00)
1	83.1886	.124E-01	.103E-03
2	262.8991	.421E-01	.349E-03
3	277.7670	.611E-01	.507E-03
4	371.5408	.601E-01	.498E-03
5	312.7631	.503E-01	.418E-03
6			
7	151.4225	.237E-01	.197E-03
8	154.3667	.765E-02	.656E-04
9	101.4000	.286E-01	.203E-03
10	120.0476	.197E-01	.163E-04
11	122.7159	.107E-01	.806E-04
12	323.3445	.521E-01	.472E-03
13	473.6870	.769E-01	.639E-03
14	205.2013	.326E-01	.270E-03
15	111.1783	.170E-01	.141E-03
16	119.9064	.195E-02	.162E-04
17	222.1788	.233E-02	.193E-04
18	813.2203	.133E+00	.110E-02
19	659.2108	.108E+00	.894E-03
20	449.5601	.730E-01	.605E-03
21	345.6896	.558E-01	.463E-03
22	220.6545	.361E-01	.292E-03
23	114.4907	.176E-01	.146E-03
24	42.0670	.561E-02	.466E-04

Concentration Results for Flat Terrain 0.095 m Release Height, Location L, and Fr = 2.7

CONCENTRATION DATA FOR RUN NO. FL ON DEC. 22 1978 AT 18:45
 WIND DIRECTION: 2 DEG. UNITS: 2 SCALE FACTOR: 5000.
 DATA FOR TRACER GAS NO. 1, ETHANE BACKGROUND CONC. 8.10 MV-SEC.
 CAL. FACTOR: .236 GAS FACTOR (PPM GAS/PPM METHANE): .533

MODEL	
VELOCITY (M/SEC)	.64
SOURCE STRENGTH (PPM)	.910E+05
VOLUME FLOW (CCU. M/SEC)	.278E-04
STACK DIAMETER (M)	.142E-01
EXIT VELOCITY (M/SEC)	.176E+00

LOCATION	RAW DATA (MV-SEC)	NON-DIMENSIONAL CONCENTRATION COEFFICIENT(K)	DILUTION FACTOR (C/CD)
1	30.1730	.629E-02	.303E-04
2	51.8447	.125E-01	.600E-04
3	63.6667	.158E-01	.762E-04
4	54.3201	.132E-01	.634E-04
5	51.7396	.124E-01	.598E-04
6	27.3333	.548E-02	.264E-04
7	34.7450	.759E-03	.365E-04
8	28.8225	.590E-02	.284E-04
9	42.1160	.969E-02	.467E-04
10	21.6048	.385E-02	.105E-04
11	95.8111	.250E-01	.120E-03
12	416.9256	.116E+00	.561E-03
13	566.8024	.189E+00	.766E-03
14	207.8114	.569E-01	.274E-03
15	79.7903	.204E-01	.903E-04
16	25.4124	.493E-02	.237E-04
17	27.7444	.580E-02	.269E-04
18	251.9803	.695E-01	.334E-03
19	327.1729	.909E-01	.438E-03
20	409.0368	.114E+00	.550E-03
21	440.8539	.123E+00	.593E-03
22	248.0639	.684E-01	.329E-03
23	358.8298	.999E-02	.481E-03
24	173.7558	.472E-02	.227E-03

Concentration Results for Flat Terrain 0.076 m Release Height, Location G, and Fr = 2.2

CONCENTRATION DATA FOR RUN NO. LG ON DEC. 23 1978 AT 21:44.
 WIND DIRECTION: 0 DEG. UNITS: 1 SCALE FACTOR: 5000.
 DATA FOR TRACER GAS NO. 1, ETHANE BACKGROUND CONC. 4.10 MV-SEC.
 CAL. FACTOR= .236 PPM⁴ GAS FACTOR (PPM GAS/PPM METHANE) .533

MODEL	
VELOCITY (M/SEC)	.49
SOURCE STRENGTH (PPM)	.918E+05
VOLUME FLOW (CU. M/SEC)	.278E-04
STACK DIAMETER (M)	.142E-01
EXIT VELOCITY (M/SEC)	.176E+00

LOCATION	RAW DATA (MV-SEC)	NON-DIMENSIONAL CONCENTRATION COEFFICIENT(K)	DILUTION FACTOR (G/CD)
2	24.2599	.281E-02	.276E-04
3	26.4241	.312E-02	.306E-04
4	42.7317	.539E-02	.530E-04
5	88.3365	.118E-01	.116E-03
6	97.1659	.130E-01	.128E-03
7	129.2239	.175E-01	.172E-03
8	106.8320	.143E-01	.141E-03
9	51.2103	.658E-02	.646E-04
11	4.0679	.000E+00	.000E+00
12	102.0882	.137E-01	.134E-03
13	1122.493	.156E+00	.153E-02
14	2114.931	.295E+00	.289E-02
15	336.8192	.465E-01	.456E-03
16	18.3226	.199E-02	.195E-04
17	14.5107	.145E-02	.143E-04
18	97.9992	.131E-01	.129E-03
19	1711.702	.238E+00	.234E-02
20	3581.885	.500E+00	.491E-02
21	2755.866	.384E+00	.377E-02
22	402.4545	.556E-01	.546E-03
23	36.2724	.449E-02	.441E-04
24	37.6333	.468E-02	.460E-04

Concentration Results for Flat Terrain 0.076 m Release Height, Location L, and Fr = 2.2

CONCENTRATION DATA FOR RUN NO. LL ON DEC. 23 1978 AT 21:4
 WIND DIRECTION: 0 DEG. UNITS: 1 SCALE FACTOR: 5000.
 DATA FOR TRACER GAS NO. 1, ETHANE BACKGROUND CONC. 4.10 MV-SEC.
 CAL. FACTOR: .236 GAS FACTOR (PPM GAS/PPM METHANE): .533

	MODEL
VELOCITY (M/SEC)	.49
SOURCE STRENGTH (PPM)	.918E+05
VOLUME FLOW (CU. M/SEC)	.278E-04
STACK DIAMETER (M)	.142E-01
EXIT VELOCITY (M/SEC)	.176E+00

LOCATION	RAW	NON-DIMENSIONAL	DILUTION
	DATA	CONCENTRATION	FACTOR
	(MV-SEC)	COEFFICIENT(K)	(C/CD)
1	13.2205	.127E-02	.125E-04
1	47.6128	.608E-02	.597E-04
2	66.0207	.865E-02	.849E-04
3	132.6136	.129E-01	.176E-03
4	172.8120	.236E-01	.231E-03
5	343.2153	.473E-01	.465E-03
6	415.5967	.675E-01	.564E-03
7	506.9724	.702E-01	.690E-03
8	384.9971	.532E-01	.522E-03
9	408.1017	.564E-01	.554E-03
10	27.2862	.324E-02	.318E-04
11	153.5753	.209E-01	.205E-03
12	2314.855	.323E+00	.317E-02
13	1500.404	.209E+00	.205E-02
14	269.3320	.370E-01	.364E-03
15	38.8871	.486E-02	.477E-04
16	440.5016	.609E-01	.598E-03
17	626.7839	.869E-01	.854E-03
18	945.4236	.131E+00	.129E-02
19	1575.842	.219E+00	.216E-02
20	333.9376	.461E-01	.452E-03
21	21.4059	.242E-02	.237E-04
22	10.8777	.946E-03	.930E-05

Concentration Results for Flat Terrain 0.095 m Release Height, Location G, and Fr = 2.2

CONCENTRATION DATA FOR RUN NO. HG ON DEC. 23 1978 AT 22:29
 WIND DIRECTION: 0 DEG UNITS: 2 SCALE FACTOR: 5000.
 DATA FOR TRACER GAS NO. 1, ETHANE BACKGROUND CONC. 4.10 MV-SEC.
 CAL. FACTOR: .236 GAS FACTOR (PPM GAS/PPM METHANE): .533

	MODEL
VELOCITY (M/SEC)	.57
SOURCE STRENGTH (PPM)	.918E+05
VOLUME FLOW (CU. M/SEC)	.278E-04
STACK DIAMETER (M)	.142E-01
EXIT VELOCITY (M/SEC)	.176E+00

LOCATION	RAW DATA (M/SEC)	NON-DIMENSIONAL CONCENTRATION COEFFICIENT(K)	DILUTION FACTOR (C/C0)
1	17.6850	.345E-02	.196E-04
3	4.8800	.198E-03	.107E-05
5	-9.0052	.000E+00	.000E+00
6	-1.1810	.000E+00	.000E+00
6	-3.9407	.000E+00	.000E+00
7	11.8867	.198E-02	.107E-04
7	21.7519	.448E-02	.242E-04
8	20.4522	.415E-02	.224E-04
12	126.9953	.312E-01	.169E-03
13	1600.069	.407E+00	.220E-02
14	768.4954	.194E+00	.105E-02
15	86.2148	.208E-01	.113E-03
16	64.32	.000E+00	.000E+00
19	251.2486	.627E-01	.339E-03
20	1914.397	.485E+00	.262E-02
21	2629.250	.666E+00	.360E-02
22	1275.620	.323E+00	.174E-02
23	300.5181	.752E-01	.407E-03
24	309.8865	.776E-01	.419E-03

Concentration Results for Flat Terrain 0.095 m Release Height, Location L, and Fr = 2.2

CONCENTRATION DATA FOR RUN NO. HL ON DEC. 23 1978 AT 20:15.
 WIND DIRECTION: 0 DEG. UNITS: 2 SCALE FACTOR: 5000.
 DATA FOR TRACER GAS NO. 1, ETHANE BACKGROUND CONC. 4.10 MV-SEC.
 CAL. FACTOR: .236 GAS FACTOR (PPM GAS/PPM METHANE): .533

MODEL	
VELOCITY (M/SEC)	.57
SOURCE STRENGTH (PPM)	.918E+05
VOLUME FLOW (CU. M/SEC)	.278E-04
STACK DIAMETER (M)	.142E-01
EXIT VELOCITY (M/SEC)	.176E+00

LOCATION	RAW DATA (MV-SEC)	NON-DIMENSIONAL CONCENTRATION COEFFICIENT(K)	DILUTION FACTOR (C/C0)
1	17.1192	.330E-02	.179E-04
2	19.1484	.382E-02	.206E-04
3	55.4845	.130E-01	.705E-04
4	75.00*	.19E-01	.972E-04
5	147.9683	.365E-01	.197E-03
6	105.00*	.26E-01	.138E-03
7	137.4969	.339E-01	.183E-03
8	124.8394	.306E-01	.166E-03
9	110.8418	.271E-01	.146E-03
10	4.6285	.134E-03	.725E-06
12	158.8829	.393E-01	.212E-03
13	641.9349	.162E+00	.875E-03
14	1410.734	.357E+00	.193E-02
15	999.1783	.253E+00	.136E-02
16	110.00*	.27E-01	.145E-03
17	9.3102	.132E-02	.715E-05
18	160.0654	.396E-01	.214E-03
19	252.8780	.631E-01	.341E-03
20	576.9083	.145E+00	.786E-03
21	1389.791	.352E+00	.190E-02
22	474.1799	.119E+00	.645E-03
23	55.0544	.129E-01	.699E-04

Note: Reconstructed from strip chart.

Appendix B

Error Analysis

Error Analysis

This appendix includes the basic equations and calculations of uncertainty intervals for the experimental data using the technique outlined in Kline and McClintock (1953). The basic theorem for calculating uncertainty intervals, w_R is

"If R is a linear function of n independent variables each of which is normally distributed, then the relation between the interval for the variables w_i , and the interval for the result w_R , which gives the same odds for each of the variables and for the result is

$$w_R = \left[\left(\frac{\partial R}{\partial v_1} w_1 \right)^2 + \left(\frac{\partial R}{\partial v_2} w_2 \right)^2 + \dots \left(\frac{\partial R}{\partial v_n} w_n \right)^2 \right]^{1/2}.$$

This equation will be used to calculate uncertainty intervals for the relevant measured and calculated quantities.

- Velocity Measurements

Consider the calibration equation for velocity

$$u = \left[\frac{E^2}{R_H(R_H - R_a) - A} \right]^{1/2} = [Y]^{1/2}$$

where A , B and n are the calibration constants discussed in section 4.5, E is the voltage output from the anemometer and R_H and R_a are the hot and cold (at ambient temperature) resistance of the wire. The error equation for u can be derived to be the following

$$\begin{aligned} \frac{w_u}{u} = \frac{1}{nY} & \left[\left(\frac{2E w_E}{R_H(R_H - R_a)} \right)^2 + \left(\frac{w_A}{B} \right)^2 + \left(\frac{w_B}{B} Y \right)^2 + \left(\frac{Y \ln Y}{n} w_n \right)^2 \right. \\ & \left. + \left(\frac{w_{R_a} E^2}{R_H B (R_H - R_a)^2} \right)^2 \right]^{1/2} \end{aligned}$$

The average constants and estimated errors based on four calibrations of the same wire are as follows:

$$R_H = 8.9975 \Omega$$

$$R_a = 5.9975 \pm 0.01 \Omega$$

$$A = 0.1499 \pm 0.0013$$

$$B = 0.06369 \pm 0.0012$$

$$n = 0.556 \pm 0.006.$$

The errors in A, B and n were estimated by taking half of the root-mean-square error between the different calibration runs. The error in R_a is based on the accuracy R_a can be measured on the anemometer. The W_E value represents the resolution of the analog to digital converter used to process the data.

Substituting the above values into the equation gives the following relative error as a function of velocity

$u(\text{m/s})$	W_u/u
0.05	0.26
0.10	0.18
0.20	0.13
0.40	0.09
1.00	0.06

The above results show that at low speeds the errors become very large whereas at free stream conditions the error is on the order of six percent. It is anticipated that the error in turbulence intensity is of the same order as u .

- Nondimensional Concentration

The following equation defines a nondimensional concentration K as used to display the data in this report

$$K = \frac{(x - x_{BG}) u H^2}{x_0 V}$$

where

x = measured concentration

x_{BG} = background concentration

u = wind speed

x_0 = source strength

V = volume flow rate

H = height of release probe.

The error equation for K is

$$\frac{w_K}{K} = \left[\left(\frac{w_x}{x - x_{BG}} \right)^2 + \left(\frac{w_{x_{BG}}}{x - x_{BG}} \right)^2 + \left(\frac{w_{x_0}}{x_0} \right)^2 + \left(\frac{w_u}{u} \right)^2 + \left(\frac{w_V}{V} \right)^2 \right]^{1/2}$$

The scatter in calibration constants for calculating x and the measured source strength was on the order of three percent, or

$$\frac{w_x}{x} = 0.03$$

$$\frac{w_{x_0}}{x_0} = 0.03 .$$

The average background concentration was observed to be 1.27 ppm ethane with a root-mean-square variation of 0.62 ppm, or

$$\frac{w_{x_{BG}}}{x_{BG}} = 0.49 .$$

The flowmeter used for regulating the volume flow was calibrated with a soap bubble technique; hence, the largest errors are associated with the setting of the float reading. The estimated error for V is

$$w_V = \pm 1.6 \text{ cc/s} .$$

Using the operating conditions for Run #3 ($u = 0.38 \text{ m/s}$, $V = 18.5 \text{ cc/s}$) the following equation results

$$\frac{w_K}{K} = \left[\left(\frac{0.03}{1 - \frac{x_{BG}}{x}} \right)^2 + \left(\frac{.49}{\frac{x}{x_{BG}} - 1} \right)^2 + (0.03)^2 + (0.09)^2 + (0.09)^2 \right]$$

When $x \gg x_{BG}$ this reduces to

$$\frac{w_K}{K} = 0.13.$$

However, if $x = 2 x_{BG}$

$$\frac{w_K}{K} = 0.51$$

Hence concentrations close to the background value can have large errors whereas concentrations much larger than the background have a maximum error of 13 percent.

- Richardson Number

The defining equation for the Richardson number is

$$Ri = \frac{\frac{g}{T} (T_2 - T_1)(z_2 - z_1)}{(u_2 - u_1)^2}$$

Assuming that the temperature and velocity are the major error contributors, the following equation results

$$\frac{w_{Ri}}{Ri} = \left[\left(\frac{w_{T_2}}{T_2 - T_1} \right)^2 + \left(\frac{w_{T_1}}{T_2 - T_1} \right)^2 + \left(\frac{2w_{u_2}}{\Delta u} \right)^2 + \left(\frac{2w_{u_1}}{\Delta u} \right)^2 \right]$$

Consider a typical case with

$$T_2 = 293.5 \pm 0.1$$

$$T_1 = 291.0 \pm 0.1$$

$$u_1 = 0.229 \pm 0.030$$

$$u_2 = 0.160 \pm 0.024 .$$

Substituting gives the following error for R_i

$$\frac{w_{R_i}}{R_i} = 1.12.$$

Thus it is evident large errors in R_i can be expected at low speeds where Δu is on the same order as w_u .

- Froude Number

The defining equation for Froude number is

$$Fr = \frac{u(z)}{z \sqrt{\frac{g}{T} \frac{(T_2 - T_1)}{z}}} .$$

Again assume u and T are the parameters contributing the significant error. The error equation for Fr becomes

$$\frac{w_{Fr}}{Fr} = \left[\left(\frac{w_u}{u} \right)^2 + \left(\frac{1}{2} \frac{w_{T_2}}{T_2 - T_1} \right)^2 + \left(\frac{1}{2} \frac{w_{T_1}}{T_2 - T_1} \right)^2 \right]^{1/2}$$

Using the same parameters as above with $z = u_2$ gives the following error

$$\frac{w_{Fr}}{Fr} = 0.15 .$$

Hence for evaluating stability Fr is a more useful quantity since the expected error is significantly less than the error for R_i .

Appendix C
Valley Model Computer Outputs
(To be included in final report)

RELOCATE 2/3 INCH UP-/- 0.0

0.0 **0.0**

0.0 0.0 0.0

0.0 **0.0** **0.0** **0.0** **0.0** **0.0** **0.0**

UNITS I-IV (24 HR. ESTIMATES) MAR 4, 1976

0.0 0.0 0.0 0.0
HLIFE= 24.00 HRS. CONCTR CORRCTD TO STD COND VIA FACTOR 1.000. MAX TOWARD 159. DEC. NORTH TOWARD TCP. PLOT 190.872
0.0 0.0

0.0 0.

0.0 0.0 0.0

MULTIPLY PRINTED VALUES BY

1.0E-01 TO GET CONC. IN ug/l43

* 460,60* SOR ELEV COORDX COORDY STK HT QIGM/SEC1 FIXD DH

0.0 ***** 0.0 3245.FT 460.00 60.00 211.M 1.9200E 02 *****

0.0 0.0 0.0 0.0 BRIG.E BRIG.F DMIX DMNI STAR F WIDTH

0.0 310.***** 1200. 100. 1.00 0.

0.0 0.0 0.0 BRIGEN STACKS SEP

0.0 0.0 3330. 2 82.

0.0 . . .
0.0 . . .

MEAN WIND SPEED MPH 0.0
2.50000 3.80000 5.30000 7.80000 11.20000 0.0

0.0 0.0 0.0 0.0

0.0 0.0 AIR T GAS T DIAM GAS V FLOW

257. 361. 7.3 30.31 276.8

0.0 180.0

0.0 190.0

1 **0.0**

0.0

0.0

0 KM 8.125KM 16.250KM 24.375KM 32.500KM 40.625KM 48.750KM

BUR1 - LONG-TERM MODE. 0.0 0.0 ____RELOCATE 2/3 INCH DOWN
0.0 ---/ 0.1 SLOPING TERRAIN CONCEPT.

0.0 /-- 0.0
RELOCATE 2/3 INCH UP-/ 0.0

0.0 0.0
0.0 0.0

0.0 0.0
0.0 0.0

COLSTRIP UNITS III - IV

COLSTRIP POWER PLTS

UNITS I-IV (24 HR. ESTIMATES) OCT 29, 1976

0.0 0.0 0.0 0.0
HLIFE= 24.00 HRS. CONCTR CORRCTD TO STD COND VIA FACTOR 1.000. MAX TOWARD 180. DEG. NORTH TOWARD TOP. PLOT 226.430
0.0

0.0 0.0 0.0 0.0
0.0 0.0 0.0 0.0

0.0 0.0 0.0 0.0
0.0 0.0 0.0 0.0

0.0 * ***** 0.0
* COORD * 0.0 0.0 0.0 0.0 0.0 0.0 0.0 0.0 0.0
* 460,60* SDR ELEV COORDX COORDY STK HT Q(1GM/SEC) FIXD DH
0.0 * ***** 0.0 3245.FT 460.00 60.00 211.M 1.9200E 02 *****

0.0 0.0 0.0 0.0 0.0 BRIG.E BRIG.F DMIX DMNI STAR F WIDTH
0.0 0.0 0.0 0.0 0.0 179.***** 1200. 100. 1.00 0.
0.0 0.0 0.0 0.0 0.0

0.0 0.0 0.0 0.0 0.0 BRIGUN STACKS SEP
0.0 0.0 0.0 0.0 0.0 2821. 2 83.

0.0 0.0 0.0 0.0 0.0
0.0 VV MEAN WIND SPD(S(MPS)) VV 0.0
0.0 5.30000 2.50000 3.80000 5.30000 7.80000 11.20000 0.0

0.0 0.0 0.0 0.0 0.0
0.0 0.0 0.0 0.0 0.0 AIR T GAS T DIAM GAS V FLOW
0.0 0.0 0.0 0.0 0.0 282. 361. 7.3 30.31276.8

0.0 0.0 0.0 0.0 0.0
0.0 0.0 0.0 0.0 0.0
0.0 0.0 0.0 0.0 0.0

0.0 0.0 0.0 0.0 0.0
0.0 0.0 0.0 0.0 0.0
0.0 0.0 0.0 0.0 0.0

0.0 0.0 0.0 0.0 0.0
0.0 KM 8.125KM 16.250KM 24.375KM 32.500KM 40.625KM 48.750KM
83.0 --RELOCATE 2/3 INCH DOWN

BURL, LCNG-TERM MODE. 0.0 20.2--/ 0.0 SLOPING TERRAIN CONCEPT.

0.0 /-- 0.0
RELOCATE 2/3 INCH UP-/ 0

0.0

0.0	0.0	0.0	0.0
0.0	0.0	0.0	0.0
0.0	0.0	0.0	0.0
0.0	0.0	0.0	0.0
0.0	0.0	0.0	0.0

COLSTRIP UNITS III - IV

0.0 0.0 0.0 0.0
HLIFE= 24.00 HRS. CONCTR CORRCTD TO STD COND VIA FACTOR 1.000. MAX TOWARD 180. DEG. NORTH TOWARD TOP. PLOT 210.202
0.0

COLSTRIP POWER PLTS
OCT 29, 1976

UNITS I-IV (24 HR. ESTIMATES)

0.0	0.0	0.0	0.0
0.0	0.0	0.0	0.0
0.0	0.0	0.0	0.0
0.0	0.0	0.0	0.0
0.0	0.0	0.0	0.0

0.0	0.0	0.0	0.0
0.0	0.0	0.0	0.0
0.0	0.0	0.0	0.0
0.0	0.0	0.0	0.0
0.0	0.0	0.0	0.0

MULTIPLY PRINTED VALUES BY
1.0E-01 TO GET CONC. IN UG/M³

* COORD * SDR ELEV COORDX COORDY STK HT Q(GM/SEC) FIXD DH
* 460,60* 3245.FT. 460.00 60.00 211.M 1.9200E 02 *****
***** 0.0 0.0 0.0

0.0	0.0	0.0	0.0
0.0	0.0	0.0	0.0
0.0	0.0	0.0	0.0
0.0	0.0	0.0	0.0
0.0	0.0	0.0	0.0

BRIG.E BRIG.F DMIX DMNI STAR F WDTHTH
174.***** 1200. 100. 1.00 0.

0.0	0.0	0.0	0.0
0.0	0.0	0.0	0.0
0.0	0.0	0.0	0.0
0.0	0.0	0.0	0.0
0.0	0.0	0.0	0.0

BRIGUN STACKS SEP
2821. 2 83.

0.0	0.0	0.0	0.0
0.0	0.0	0.0	0.0
0.0	0.0	0.0	0.0
0.0	0.0	0.0	0.0
0.0	0.0	0.0	0.0

0.0	0.0	0.0	0.0
0.0	0.0	0.0	0.0
0.0	0.0	0.0	0.0
0.0	0.0	0.0	0.0
0.0	0.0	0.0	0.0

AIR T GAS T DIAM GAS V FLOW
282. 361. 7.3 30.31276.8

0.0	0.0	0.0	0.0
0.0	0.0	0.0	0.0
0.0	0.0	0.0	0.0
0.0	0.0	0.0	0.0
0.0	0.0	0.0	0.0

0.0	0.0	0.0	0.0
0.0	0.0	0.0	0.0
0.0	0.0	0.0	0.0
0.0	0.0	0.0	0.0
0.0	0.0	0.0	0.0

0 KM 8.125KM 16.250KM 24.375KM 32.500KM 40.625KM 48.750KM
....+....+....+....+....+....+....
79.6 RELOCATE 2/3 INCH DOWN
20.0--/ 0.0 SLOPING TERRAIN CONCEPT.

RURL, LONG-TERM MODE

0.0 /-- .0.0
RELOCATE 2/3 INCH UP-/ 0.0

0.0

0.0
0.0 0.0
0.0 0.0
0.0 0.0

COLSTRIP UNITS III - IV

COLSTRIP POWER PLTS
UNITS I-IV (24 HR. ESTIMATES) (APRIL 1, 1977)

0.0 0.0 0.0 0.0
HLIFE= 24.00 HRS. CONCTR CORRCTD TO STD COND VIA FACTOR 1.000. MAX TOWARD 158. DEG. NORTH TOWARD TOP. PLOT 190.863
0.0 0.0

0.0 0.0 0.0 0.0 0.0
0.0 0.0 0.0 0.0 0.0
0.0 0.0 0.0 0.0 0.0
0.0 0.0 0.0 0.0 0.0

MULTIPLY PRINTED VALUES BY
1.0E-01 TO GET CONC. IN UG/M³

0.0 0.0 0.0 0.0 0.0 * -+ * 0.0 0.0 0.0 0.0 0.0 0.0 0.0 0.0
 * 460,60* SOR ELEV COORDX COORDY STK HT Q(GM/SEC) FIXD OH
 0.0 ***** 0.0 3245.FT 460.00 60.00 211.M 1.9200E 02 *****
 0.0 0.0
 0.0 0.0 0.0 0.0 BRIG.E BRIG.F DMIX DMNI STAR F WIDTH
 0.0 185.***** 1200. 100. 1.00 0.
 0.0 0.0
 0.0 0.0 0.0 0.0 0.0 BRIGUN STACKS SEP
 0.0 0.0 0.0 0.0 0.0 3032. 2 83.

0.0 0.0 0.0
0.0 5.30000 2.50000 3.80000 5.30000 7.80000 11.20000 0.0

0.0 0.0 0.0 0.5 0.0 0.0 AIR T GAS T DIAM GAS V FLOW

0.0 0.0 190.9 0.0 272. 361. 7.3 30.31276.8

0.0 0.0 0.0

0.0 0.0 1.6 0.0

0.0 0.5

0.0 0.5
0 KM 8.125KM 16.250KM 24.375KM 32.500KM 40.625KM 48.750KM

RURL, LONG-TERM MODE. 0.0 0.0 - RELOCATE 2/3 INCH DOWN
0.0--/ 0.6 SLOPING TERRAIN CONCEPT.

KURE, LONG-TERM MODE. 0.0 0.0--> 0.0 SLOPING TERRAIN CONCEPT.

0.0 /-- 0.0
RELOCATE 2/3 INCH UP-/ 0.0

0.0 . 0.0

9-9 **9-9**

0.0 0.0 0.0 COLSTRIP_UNITS_ITT = IV

COLSTRIP POWER PLTS.
UNITS (-IV 124 HR. ESTIMATES) AUG 6-1977

0.0 0.0 0.0 0.0 0.0 0.0
HLIFE= 24.00 HRS. CONCTR CORRCTD TO STD COND VIA FACTOR 1.000. MAX TOWARD 158. DEG. NORTH TOWARD TOP. PLOT 214.016

0.0 0.0 0.0 0.0 0.0 0.0 0.0

0.0 0.0
0.0 ***** 0.0 * COORD * MULTIPLY PRINTED VALUES BY
1.0E-01 TO GET CONC. IN UG/M3

0.0 0.0 0.0 0.0 BRIG.E BRIG.F DMIX DMNI STAR F WIDTH
0.0 321.***** 1200. 100. 1.00 0

0.0 0.0 0.0 0.0 0.0 0.0 BRIGUN STACKS SEP
0.0 0.0 0.0 0.0 0.0 2689. 2 83.

0.0 0.0 VV MEAN WIND SPD(S(HPS)) VV 0.0
0.0 1.00000 2.50000 3.80000 5.30000 7.80000 11.20000

AIR T	GAS T	DIAM	GAS V	FLOW
288.	361.	7.3	30.31276.8	

214.0 0.0

0.0 0.1 0.0

0.0

KM 8.125KM 16.250KM 24.375KM 32.500KM 40.625KM 48.750KM

RURL, LONG-TERM MODE. 0.0 0.0 --RELOCATE 2/3 INCH DOWN-- 0.0--/ 0.1 SLOPING TERRAIN CONCEPT

0.0 /-- 0.0
RELOCATE 2/3 INCH UP-/

0.0

0.0	0.0	0.0	0.0
0.0	0.0	0.0	0.0
0.0	0.0	0.0	0.0
0.0	0.0	0.0	0.0

COLSTRIP UNITS III - IV

0.0 0.0 0.0 0.0
HLIFE= 24.00 HRS. CONCTR CORRCTD TO STD COND VIA FACTOR 1.000. MAX TOWARD 180, DEG. NORTH TOWARD TOP. PLOT 227.063
0.0

COLSTRIP POWER PLTS

UNITS I-IV (24 HR. ESTIMATES) SEPT 23, 1977

0.0	0.0	0.0	0.0	0.0
0.0	0.0	0.0	0.0	0.0
0.0	0.0	0.0	0.0	0.0
0.0	0.0	0.0	0.0	0.0

0.0 0.0 0.0 0.0 0.0
0.0 ***** 0.0
0.0 * COORD * 1.0E-01 TO GET CONC. IN UG/M3

* 40.60* SOR ELEV CCCPDX COCRDY STK HT Q(GM/SEC) FIXD DH
0.0 ***** 0.0 3245.FT 460.00 60.00 211.M 1.9200E 02 *****

0.0 0.0 0.0 BRIG.E BRIG.F DMIX DMNT STAR F WIDTH
0.0 178.***** 1200. 100. 1.00 0.

0.0 0.0 0.0 0.0 0.0 BRIGUN STACKS SEP
0.0 2778. 2 83.

0.0 0.0 0.0 0.0 0.0
0.0 VV MEAN WIND SPD\$ (MPS) VV 0.0
0.0 5.30000 2.50000 3.80000 5.30000 7.80000 11.20000 0.0

0.0 0.0 0.0 0.0 0.0 AIR T GAS T DIAM GAS V FLOW
0.0 284. 361. 7.3 30.31276.8

0.0 0.0 0.0 0.0 0.0
0.0 227.1 0.0 0.0

0.0 0.0 0.0 0.0 0.0
0.0 131.9 0.0 0.0

0.0 0.0 0.0 0.0 0.0
0.0 0 KM 8.125KM 16.250KM 24.375KM 32.500KM 40.625KM 48.750KM

83.8 RELOCATE 2/3 INCH DOWN
20.5--/ 0.0 SLOPING TERRAIN CONCEPT.

RURL, LONG-TERM MODE.

